

NORTHEASTERN TULAROSA BASIN REGIONAL HYDROGEOLOGY STUDY, NEW MEXICO

Final Technical Report
Prepared for Otero Soil and Water Conservation District

June 2014

Open-file Report 562

New Mexico Bureau
of Geology and
Mineral Resources



Ethan A. Mamer,
B. Talon Newton, Daniel J. Koning,
Stacy S. Timmons, and Shari A. Kelley



The views and conclusions are those of the authors, and should not be interpreted as necessarily representing the official policies, either expressed or implied, of the State of New Mexico.



New Mexico Bureau of Geology and Mineral Resources
A division of New Mexico Institute of Mining and Technology

Socorro, NM 87801
(575) 835-5490
Fax (575) 835-6333
www.geoinfo.nmt.edu

NORTHEASTERN TULAROSA BASIN REGIONAL HYDROGEOLOGY STUDY, NEW MEXICO

Final Technical Report
Prepared for Otero Soil and Water Conservation District

June 2014

Open-file Report 562

Ethan A. Mamer,
B. Talon Newton, Daniel J. Koning,
Stacy S. Timmons, and
Shari A. Kelley



New Mexico Bureau of Geology and Mineral Resources

PROJECT FUNDING

Funded by the New Mexico State Legislature through
Otero Soil and Water Conservation District,
the New Mexico Bureau of Geology and Mineral Resources—Aquifer Mapping Program,
and the National Cooperative Geologic Mapping Program (STATEMAP).

TABLE OF CONTENTS

EXECUTIVE SUMMARY	1	PROJECT PERSONNEL AND ACKNOWLEDGMENTS	66
I. INTRODUCTION	4	REFERENCES	67
Significance	4	FIGURES	
Description of study area	4	Figure 1–Location of the study area	5
Study area regions	6	Figure 2–Topographic features of the study area	6
Purpose and scope	7	Figure 3–Published 1:24,000-scale geologic maps	11
II. PREVIOUS WORK	8	Figure 4–Site inventory map	12 & 13
Geology	8	Figure 5–Regional geology of the study area	16
Hydrogeology and hydrology	9	Figure 6–Geologic map of the study area.....	17 & 18
Previous recharge estimates	9	Figure 7–Average annual precipitation versus elevation.....	20
III. METHODS	10	Figure 8–Location of sampled surface water	21
Data description	10	Figure 9–Geologic cross sections	23 & 24
Geologic data	10	Figure 10–Schematic stratigraphic section	25
Geologic maps and cross sections	10	Photographs of hydrostratigraphic units	
Location of sites	11	Figure 11–San Andres Formation	27
Water-level data	11	Figure 12–Grayburg, Moenkopi, and Dakota Sandstone Formations	28
Geochemical methods	13	Figure 13–Mancos Shale	28
IV. RESULTS	15	Figure 14–Gallup Sandstone and lower Crevasse Canyon Formation	29
Geology	15	Figure 15–Gallup Sandstone and lower Crevasse Canyon Formation	30
Regional geology	15	Figure 16–Lava flows and volcanoclastic rocks of the Sierra Blanca volcanic field	31
Rio Grande rift	15	Figure 17–Intrusions of the Sierra Blanca volcanic field	32
Sierra Blanca Basin	15	Figure 18–Volcanic dikes	33
Capitan lineament	19	Figure 19–Basin-fill hydrostratigraphic unit that are relevant to groundwater flow	34
Geologic structure	19	Figure 20–Location of springs	35
Hydrology	19	Figure 21–Percentage of total springs inventoried for study by topographic location	36
Precipitation	19	Figure 22–Water level elevation contour maps	38 & 39
Streams and drainage basins	21	Figure 23–Water table in the Three Rivers drainage	40
Groundwater	22	Figure 24–Bar graph showing the percent of each hydrograph trend by topographic location	41
Springs.....	35	Figure 25–Location map of wells that were used in the hydrograph analysis	42
Primary aquifers.....	36	Figure 26–Hydrograph with recharge, pumping, decline, and no change trends	43
Water-level changes and hydrographs	40	Figure 27–Comparison of the water levels with the atmospheric pressure	43
Water chemistry	44	Figure 28–Map of specific conductivity measurements from field sampling locations	45
Field measurements	45		
Major ion chemistry and water type	45		
Controls on water chemistry	46		
Stable isotopes of hydrogen and oxygen	51		
Groundwater age and residence time	53		
V. CONCLUSIONS	59		
Estimating Darcy calculation values	59		
Recharge Estimates	60		
Location and Mechanisms Controlling Recharge	62		
Groundwater-Surface Water Interactions	64		
Implications and Future Work	64		

Figure 29–Map showing locations and results of sampled water chemistry using Stiff diagrams	46
Figure 30–Piper diagram shows percentage of ion content in spring, well and stream samples	47
Figure 31–Map of A. sulfate, B. calcium and C. silica concentrations from springs and wells	48
Figure 32–Map showing locations of the molar ratios of bicarbonate/silica	49
Figure 33–Water chemistry bivariate plots	49
Figure 34–Assessment of sodium and chloride molar ratios	50
Figure 35–Locations of precipitation collection sites	51
Figure 36–Local meteoric water line developed from stable isotope data for precipitation samples	52
Figure 37–Stable isotopic compositions of water samples collected from wells, springs, and streams in the southern portion of the study area	53
Figure 38–Stable isotopic compositions of water samples collected from wells, springs, and streams in the northern portion of the study area	53
Figure 39–Tritium values for well, spring, and stream samples	54
Figure 40–Tritium concentrations in well and spring samples as a function of elevation	55
Figure 42–CFC113/CFC12 ratio ages as a function of CFC12 ages	56
Figure 43–CFC12 apparent age as a function of the proportion of young CFC-bearing water	57
Figure 44–Tritium concentrations as a function of the proportion of young water	57
Figure 45–Spatial distribution of young groundwater	58
Figure 46–Cross sections used to estimate area of available aquifer for darcy flow calculation	60
Figure 47–Estimated flow paths	64

TABLES

Table 1–NOAA weather stations	20
Table 2–Number of wells and springs located in each hydrostratigraphic unit	35
Table 3–Number of wells with distinct hydrograph trend in each hydrostratigraphic unit	41
Table 4–Statistical summary for chemical parameters for springs, wells and streams	44
Table 5–Site elevations and periods of precipitation collection	51
Table 6–Groundwater age	57
Table 7–Flow volume estimates	61

APPENDICES

Appendix 1–Site inventory
Appendix 2–NMOSE well records
Appendix 3–Pressure transducer data
Appendix 4–Water level measurements
Appendix 5–Water level trends
Appendix 6–Water chemistry, isotopes and age data

EXECUTIVE SUMMARY

In 2005, the New Mexico Bureau of Geology and Mineral Resources initiated a hydrogeology study in the southern Sacramento Mountains. In 2009, upon completion of data collection for the Sacramento Mountains hydrogeology study, efforts were moved to the adjacent Tularosa Basin region. As with the Sacramento Mountains study, the northeastern Tularosa Basin regional hydrogeologic study was supported with funding from the Otero Soil and Water Conservation District, through legislative appropriations.

Water issues in the lower elevation regions west of the Sacramento Mountains, in the Tularosa Basin region, have been significant. With few perennial streams in this closed basin, water is sparse. The population centers in Alamogordo, Carrizozo, La Luz, and numerous other small communities, are largely supported by groundwater resources. Fresh water resources are limited, and recharge to these areas originates within the high elevation watersheds in the Sacramento Mountains, as precipitation, stream and spring flow. In recent years, water users across the region have noted declines in water levels, diminished water quality, reduced spring flow, and significant changes in precipitation frequency and amounts. This study has been an effort to help address some of these concerns.

The work presented in this report covers the northeastern region of the Tularosa Basin, along the western mountain front of the Sierra Blanca and Sacramento Mountains, approximately from Carrizozo to northern Alamogordo. This study's goal was to improve understanding of the groundwater resources in this region by identifying recharge areas and quantities, determining

groundwater flow rates and direction, and to interpret the groundwater/surface water interactions that exist in the region. Methods used in this effort included geologic mapping, groundwater level measurements, and geochemical analyses of the groundwater, springs and streams.

The detailed geologic mapping from this study reveals a very complicated geologic framework, with an equally complex aquifer system. In the northeastern region, north of Three Rivers, the geology of the Sierra Blanca Mountains is dominated by volcanic rocks, volcanoclastic sediments, and igneous intrusions. These rocks make up a network of fractured aquifers, crisscrossed by sills and dikes that act as barriers to groundwater flow. As result, this area has an abundance of springs.

Moving down the mountain front, into the Carrizozo area, there are several permeable sedimentary units composed of interbedded sandstone channel-fills and lower permeability floodplain deposits, which collectively make productive aquifers. These units have a relatively high hydraulic conductivity based on the high proportion of channel-fill sediments, thick intervals of weak cementation, and the relative abundance of springs.

East of Alamogordo and the steep escarpment of the southern Sacramento Mountains, the geology is composed of a very different group of rock units. Made up of sedimentary Permian and Pennsylvanian age rocks, the Sacramento Mountains are primarily composed of fractured carbonates, as well as conglomerates, sandstones, and siltstones, that dip to the east. Groundwater flows preferentially through these rocks

primarily due to the karst processes that result in solution enlarged fractures and conduits that easily transmit water.

Along the eastern border of the Tularosa Basin is the Alamogordo Fault, which is responsible for the down dropped basin, and the high topographic relief of the Sacramento Mountains. On the western down dropped side of the Alamogordo Fault, there is 3000 to 4000 feet of weakly cemented basin-fill deposits in the Tularosa area. These sediments have a high hydraulic conductivity and are the primary aquifer in the basin.

Using water-level measurements collected between 2009 and 2011, we were able to determine zones where aquifers are recharging, being pumped, declining, or not changing. Wells that showed recharge trends are generally found at high elevations, screened in the fractured volcanic rocks, as well as the permeable sedimentary units east of Carrizozo. The water levels in these wells are relatively shallow. Recharge enters the aquifers as winter snowmelt in the high mountains, and as monsoon precipitation at lower elevations. Hydrographs that show a pumping trend were found primarily in the basin-fill deposits at low elevations. These records closely follow the agricultural cycle of the area. Wells that show steady declines to the water table of more than 1 ft per year are scattered throughout the study area. The highest density is in the north, around the Nogal drainage. Hydrographs that demonstrated less than 1 ft of fluctuation per year were classified as “no change.” This trend made up about 30% of the wells that were monitored, and are primarily located in less permeable sandstones, near Carrizozo.

The geochemical analyses of the groundwater, springs and streams served to emphasize the complex hydrogeologic system of the mountain front. The observations of spatial trends in water chemistry are highly correlated to the geology and the flow path that the groundwater follows through the subsurface. Water chemistry reveals weathering of carbonates is dominant, but silicate

weathering is more common in some of the northern regions where volcanic materials are more prevalent.

The stable isotopic compositions of well and spring samples collected in the study area was used to help identify recharge areas, assess recharge mechanisms, and characterize groundwater flow paths. We found most water undergoes evaporation, either in the shallow soil or mountain streams before recharging the groundwater system. Further analysis of stable isotopes shows the majority of the groundwater recharge occurs as result of summer monsoon rain; however, several springs located at high elevations near Sierra Blanca are isotopically light, suggesting their source is winter precipitation.

Groundwater age (or residence time) indicates that although much of the groundwater is very old, there is young water that makes its way into the system and mixes with the older water. There is no obvious correlation between the occurrence of this young water and topography. It should be noted that the mixing of young and old waters likely occurs by groundwater mixing due to spatial variations in the flow velocity of groundwater along a flow path. The tortuous flow paths through different lithologies and structures in this mountain hydrologic system likely result in a large range of velocities that cause the mixing of waters of different ages. Our results also suggest within the different drainages, water enters the system at different points along a flow path, thereby mixing younger water with older water. The high spatial variability in the groundwater ages is consistent with stable isotope results. This suggests that flow paths in different areas are isolated from each other.

To quantify the total mean annual volume of recharge entering the basin we conducted Darcy Flow calculations along cross sections parallel to the mountain front. This calculation determined approximately 68,000 AFY of water enters the basin in this area. The Darcy Flow calculations were then

compared with other recharge approximations from previous studies to determine the approximate volume entering the system via the different recharge mechanisms: mountain-block recharge (MBR) and mountain-front recharge (MFR). MFR describes runoff from ephemeral and perennial mountain streams infiltrating into adjacent basin sediments. A previous study approximated streamflow from the mountain front. MBR estimates the volume of water that recharges in the high mountains, slowly flows down gradient through the aquifers present in the mountain block, before entering the basin-fill aquifer. By subtracting the estimated streamflow from the Darcy Flow calculation, we are left with the MBR amount. We found that sixty-six percent of recharge is from MFR, and the remaining thirty-three percent is from MBR.

The results of this study have significantly increased our knowledge about the hydrologic system responsible for recharging the northeastern Tularosa Basin region from the east. With added pressures of population growth, local communities and agricultural needs are increasingly utilizing groundwater. Continued water level monitoring will be crucial to monitor potential groundwater depletion. With increased dependence on local groundwater, community education related to water conservation is highly encouraged.

I. INTRODUCTION

SIGNIFICANCE

This report presents the results of a hydrogeologic investigation along the western Sacramento Mountains and the northeastern region of the Tularosa Basin. The principal objective of this study is to develop a better understanding of the water chemistry, physical hydrology and geologic framework that controls the occurrence and movement of groundwater in the region.

Numerous small, rural population centers, including Carrizozo, Nogal, Oscuro, Three Rivers, Tularosa, and La Luz, are located in the study area. These communities rely on high elevation watersheds in the Sacramento Mountains that serve as sources of recharge to local aquifers.

These high elevation watersheds also feed the stream systems that drain into the Tularosa Basin. In recent years, water managers and users across the region have observed changes in precipitation patterns, climate variability, and declines in water levels and spring flow. In response to these stresses on the hydrologic system related to population growth, economic development, and water use changes, water resource managers are interested in understanding their groundwater system better, allowing them to make informed decisions regarding land and water resource management.

Hydrologic study of the Tularosa Basin dates back to the early 1900s based on work by Meinzer and Hare (1915). This initial research, as well as more recent studies conducted in the past 50 years, has emphasized the role that precipitation, which falls on the adjacent Sacramento Mountains, plays on recharge entering the Tularosa Basin. Although the present study focuses primarily on the northeastern region of the Tularosa Basin, it adds to the understanding of the regional hydrogeology and provides evidence of the importance of high mountain precipitation in recharging adjacent

regional aquifers. The results of this work includes identification of recharge areas, quantification of recharge to groundwater, determination of groundwater flow directions and flow rates, and it furthers the understanding of groundwater/surface water interactions in this area.

DESCRIPTION OF STUDY AREA

Spanning the northeastern Tularosa Basin and the Sacramento Mountains, the study area exhibits a diverse array of landscapes ranging from scrubland deserts to alpine mountain slopes. The area of investigation extends from the town of Carrizozo in the north to Alamogordo in the south (Fig. 1). The high peaks of Sierra Blanca and Carrizo Mountain lie along the northeastern study area boundary, with the southern Sacramento Mountains on the southeast boundary. Many small communities in the study area include High Rolls, Tularosa, La Luz, Bent, Oscuro, Three Rivers, and Nogal (Fig. 1). Highway 54 gently curves from northwest to northeast (in a northward direction) near the western study area boundary. Highway 380 goes northwest-southeast through Carrizozo in the northern study area. To the south Highway 70 connects Ruidoso and Alamogordo. The western boundary of the study area coincides with the eastern boundary of the White Sands Missile Range.

Ranging in elevation from 1200 to 3649 m (4000 to 11,973 ft), the study area exhibits a variety of climates. Across this broad range of topography most of the precipitation accumulates during monsoonal storms in July, August, and September and only 26–27% falls in the cooler months of November through March. Average summer temperatures vary from 43–94°F and average winter temperatures of 18–64°F (<http://www.wrcc.dri.edu/summary/climsmnm.html>).

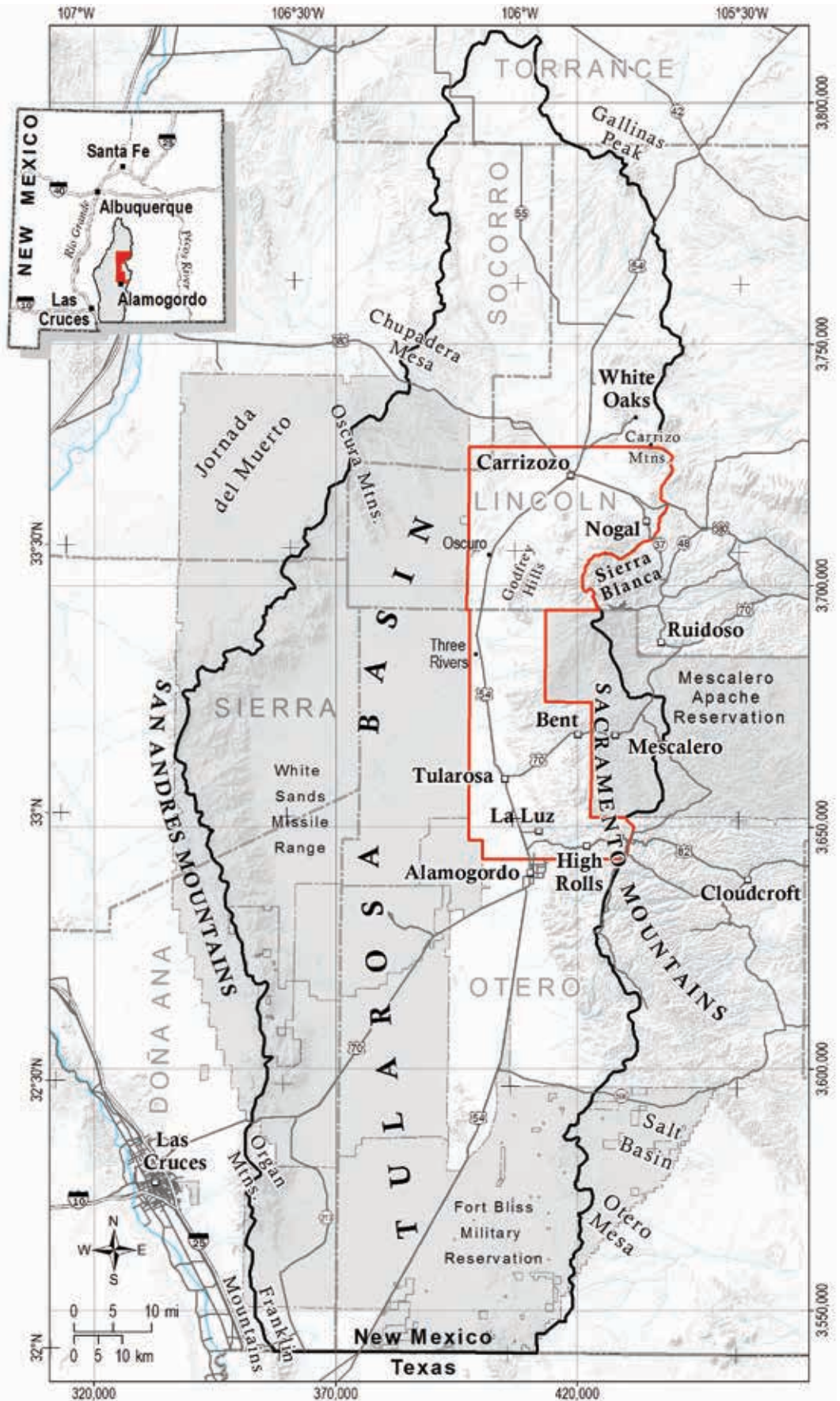


Figure 1—Location of the study area. The red line depicts the hydrogeologic study area. The black line is the boundary of the hydrologic closed basin in southern New Mexico.

For the purposes of this report, we have divided the study area into the following subregions: 1) Tularosa Basin (TB), 2) Carrizozo hilly plain (CHP), 3) northern high mountains (NHM), and 4) southern high mountains (SHM) (Fig. 2). These zones were identified using topographic and geologic characteristics. More detail on the

physiography, topography, and geography of the study area is available in Koning et al. (2014) and Kelley et al. (2014). Data presented in this report for the SHM region are from the western escarpment of the SHM region, in contrast to work done by Newton et al. (2012) which described studies in the eastern high mountain region.

Study Area Regions

Tularosa Basin (TB)

Well-known for its gypsum sand dunes (the White Sands) and the Carrizozo lava flow (commonly called the Malpais), the fault-bounded Tularosa Basin extends ~85 km (~53 mi) north-south and 30–34 km (18–21 mi) west-east. The study area encompasses parts of this basin (Fig. 2), where elevation ranges from 1200–1520 m (4000–5000 ft). The basin's eastern bounding fault, called the Alamogordo fault, is an important structure in the study area and we discuss it in more detail in the geologic structure section. Near Three Rivers and to the south, the landscape is characterized by west-sloping alluvial fans that coalesce westward into a gently west-sloping desert plain. The vegetation of this arid landscape is primarily Chihuahuan scrubland with sparse grass. Major shrubs include creosote, mesquite, and saltbrush—the latter two becoming more abundant to the west and southwest. In the northwest corner of the study area, the floor of the basin is occupied by the extremely rough Carrizozo lava flow, which locally exhibits up to 15 m (50 ft) of topographic relief.

Carrizozo Hilly Plain (CHP)

The “Carrizozo hilly plain” refers to the low-relief terrain lying between the Alamogordo fault and the mountainous area of Sierra Blanca and Carrizo Mountain (Fig. 2). Although many hills and small mountains are present in this region, gently sloping piedmonts constitute the dominant landform. The piedmonts include alluvial fans adjacent to mountains that coalesce down slope to the west. Piedmont elevations range from 1390 to 2130 m (4550–7000 ft) and the surface is variably dissected. The various hills and mountains reach elevations of

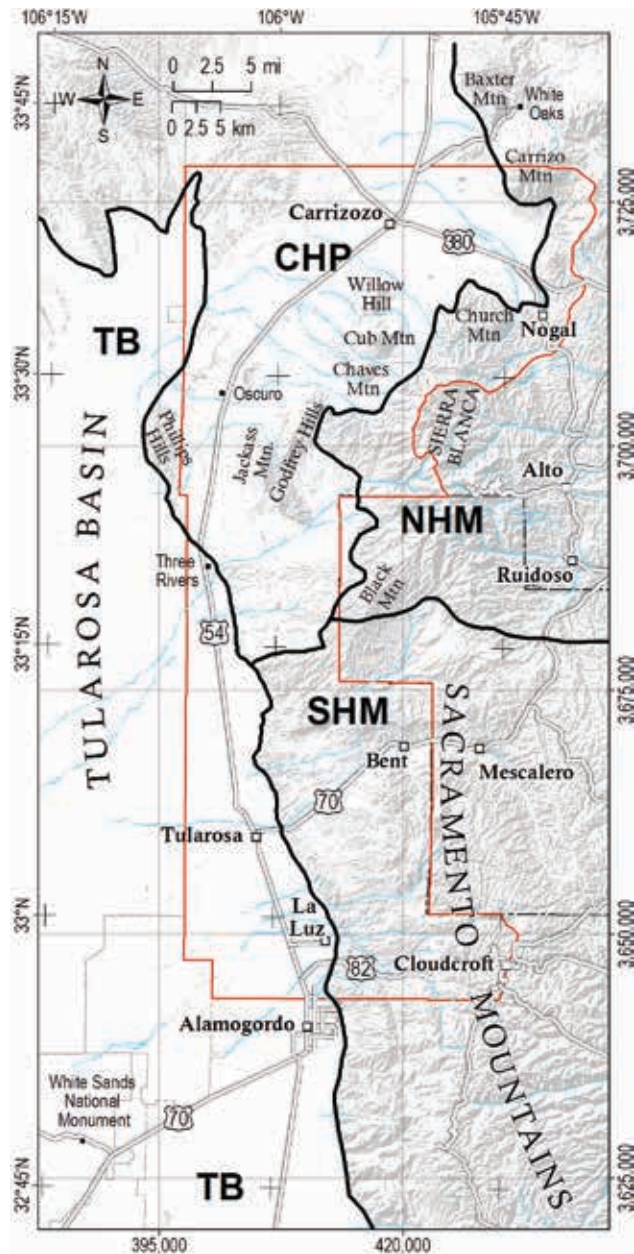


Figure 2—Topographic features of the study area. This area consists of the relatively flat Tularosa Basin to the west (TB), high mountains on the east (Northern = NHM; Southern = SHM) that include the Sierra Blanca mountains and the northern Sacramento Mountains, and the Carrizozo hilly plain in-between (CHP). The black lines demarcate the boundaries of these topographic regions. Study area shown in red.

1950–2440 m (6400–8000 ft). South of Oscuro, the vegetation of this region is characterized by desert scrub dominated by creosote, mesquite, and saltbrush. Grass cover here is slightly denser than in the Tularosa Basin to the west. In a zone extending ~13 km (~8 mi) north of Oscuro, this scrubland transitions northward into grassy plains containing scattered soaptree yucca and very sparse mesquite. These grassy plains extend from Carrizozo eastward toward Nogal (Fig. 2).

Northern High Mountains (NHM)

The northern high mountains include Carrizo Mountain and Sierra Blanca (Fig. 2). In these mountains, piñon and juniper trees dominate between 1800 and 2700 m (6000 and 9000 ft), locally with stands of ponderosa pine near ~2400 m (~8000 ft). Spruce and aspen trees may be found above ~2400 m (8,000 ft). Patches of scrub oak may occur between 2100 m and 3050 m (7000 and 10,000 ft).

Carrizo Mountain lies northeast of Carrizozo and the Sierra Blanca highland extends north of Black Mountain, the later being located 28 km (17 mi) northeast of Tularosa (Fig. 2). Sierra Blanca consists of a broad ridge that gradually decreases in elevation northwards, from 3649 m (11,973 ft; the elevation of the highest point, Sierra Blanca Peak) to 2440–2680 m (8000–8800 ft) near Church Mountain and Diamond Peak (Fig. 2). The western and northern flanks of the Sierra Blanca highland boast the highest topographic relief in New Mexico and the flanks of Carrizo Mountain are also impressively steep.

Southern High Mountains (SHM)

High-elevation ridges extend south of Black Mountain and merge into the southern Sacramento Mountains in the vicinity of Bent (Fig. 2). In the study area, the north-trending crest of the Sacramento Mountains generally lies at an elevation of 2400–2700 m (8000–9000 ft). These mountains are capped by spruce and ponderosa forests. Pinon-juniper interspersed with scrub oak patches extends from the crest down to ~1800 m (6000 ft) elevation, and Chihuahuan desert scrubs grow on the lower slopes.

PURPOSE AND SCOPE

The purpose of this project is to provide fundamental geologic data, hydrologic data, and interpretations on the northeastern region of the Tularosa Basin, from Carrizozo to Nogal, south to Alamogordo and High Rolls (Fig. 1). The primary objectives include:

- Identification of the recharge areas for this region
- Quantifying the groundwater recharge
- Assessing the flow directions and rates of groundwater movement
- Examining the interactions between different aquifers, as well as groundwater-surface water interactions

II. PREVIOUS WORK

Over the past 100 years, there have been numerous geological and hydrogeological studies in the Tularosa Basin. O. E. Meinzer, credited as the father of modern hydrogeology, did some of his first work in the field of hydrogeology studying the Tularosa Basin (Meinzer and Hare, 1915). In this section we will cover major conclusions of previous work done in this region.

GEOLOGY

The earliest publications germane to the study area pertained to the Carrizozo lava flow (Harrington, 1885; Tarr, 1891) and the general structure of the Tularosa Basin. Four workers inferred that the Carrizozo lava flow covered an old riverbed or that an underground stream flowed southward in channels carved beneath the lavas (Harrington, 1885; Herrick, 1900; Tight, 1905; MacBride, 1905). Herrick (1904), and MacBride (1905) also recognized that the Tularosa Basin represented a large block of the Earth's crust that was down-dropped between basin-bounding faults.

Several early 20th century studies focused on various mining districts in the compilation area or analyzed the geology for petroleum potential. Koning et al. (2014) expound upon the numerous studies between the years of 1900 and 2000 on the mining districts. These studies will not be enumerated here. Targeting an audience of oil geologists, Darton (1922) undertook an ambitious effort to summarize the stratigraphy and geologic structure of New Mexico. He described the igneous rocks of Sierra Blanca as “an older porphyry and a thick succession of late Paleogene fragmental and effusive sheets, dikes, and stocks of various kinds” (Darton, 1922, p. 223). He also interpreted Carrizo Mountain as a stock and the Phillips Hills as a non-faulted anticline on the east side of a synclinal Tularosa Basin.

Several detailed geologic investigations and mapping efforts, conducted in the late 1950s through the early 1990s, advanced our understanding of the stratigraphy and geologic structure in the study area. Foremost among these was geologic mapping by Lloyd Pray in the southern Sacramento Mountains (Pray, 1952, 1961). Although his work did not extend into the study area, the stratigraphy he developed laid the groundwork for future sedimentologic and stratigraphic studies in the Sacramento Mountains. Otte (1959) mapped the Sacramento Mountains between Alamogordo and 10 km (6 mi) north of Tularosa. Robert Weber (1964) made the first detailed geologic map of the area around and southeast of Carrizozo. Structural characterization of the Sierra Blanca Basin as a north-trending, synclinal depression was first made by Wegemann (1914), an interpretation confirmed by Bodine (1956), Weber (1964), and Kelley and Thompson (1964). Under the tutelage of Vincent Kelley, Tommy Thompson investigated the Sierra Blanca volcanic field and established an initial stratigraphy for the rocks there (Thompson, 1966, 1972, 1973, 1974). Stratigraphic, sedimentologic, and paleontologic work on Cretaceous and Eocene strata southwest of Carrizozo was accomplished by Thompson (1973), Arkell (1983), Lucas et al. (1989), and Cather (1991).

Additional research was conducted in the Sierra Blanca and surrounding mountains around 1990. This effort resulted in two geologic maps of the Mescalero Apache Reservation in the southern part of the Sierra Blanca volcanic field (Moore et al., 1988a, b). New data and ideas regarding the structure and igneous rocks of this area were presented in Moore et al. (1991). Studies by Allen and Foord (1991) and Pertl and Cepeda (1991) focused on the intrusions of the northern study area, with the former summarizing several radiometric ages (including those from Weber, 1971).

HYDROGEOLOGY AND HYDROLOGY

The most significant and comprehensive previous study of the Tularosa Basin is Meinzer and Hare (1915). They investigated both the geology and groundwater of the Tularosa Basin, describing the physiography, geomorphology, bedrock and basin-fill geology, hydrology and precipitation trends. Specifically, Meinzer and Hare (1915) describe the spatial and temporal variability of precipitation showing that precipitation varies with altitude, that most of it occurs in the months of June-September, and that precipitation increases somewhat to the north. The geologically young Carrizozo lava flows are very permeable according to Meinzer and Hare (1915). They also divide aquifers of the region into groups including: a) valley fill, b) Cretaceous-age rocks and overlying units (on the east wall of the Alamogordo fault), and c) Carboniferous rocks (i.e., Permian and Pennsylvanian age layers).

A regional water table map is included in Meinzer and Hare (1915). They suggest that infiltration of precipitation mostly occurs along proximal fans, with little to no infiltration (recharge) in the middle to distal fan locations. A more recent regional water table map, constructed by Embid and Finch (2011), shows similar trends to those shown in the map of Meinzer and Hare (1915).

Most of the study area described in this report lies along the eastern and northeastern margin of the Tularosa Basin. The Tularosa Basin's groundwater is dominantly saline (total dissolved solids (TDS) >1000 mg/L) with a large proportion of brines (TDS >35,000 mg/L) and less than 0.2% of the saturated deposits contain fresh water (McLean, 1970). Orr and Meyers (1986) estimated that 85% of the saturated deposits in the basin may contain saline water with TDS values greater than 3000 mg/L. Fresh water is primarily located in alluvial fan deposits on the eastern and western margins of the basin (Orr and Myers, 1986). In general, water quality decreases with depth and toward the center of the basin.

Previous Recharge Estimates

Previous research has attempted to quantify recharge to the Tularosa Basin. Here we will summarize this research and later will analyze how it compares with our findings. Rau (1986) estimated recharge entering the basin along a cross section at the mouth of the Nogal drainage. This research used a Darcy Flow approximation based on several aquifer tests conducted in the basin-fill.

Waltemeyer (2001) assumed the sole source of recharge to the basin was via runoff. To estimate recharge, the study area was delineated into 12 separate drainage basins. The Basin-Climatic Characteristic Method was applied to each drainage basin to estimate streamflow (Waltemeyer, 2001). This method takes into account the area of each drainage basin and the average precipitation. It is very rough approximation and does not account for numerous important factors, such as rock type, slope, and vegetation. It is not as precise as a streamflow-gauging system. That said, the Basin-Climatic Characteristic Method is a simple approximation that can be conducted via computer entirely from existing data.

Research conducted in 2006 by Livingston and Shomaker for the "40-year water development plan" used an alternative method to estimate recharge called the Surplus Precipitation Method. Similar to the work by Waltemeyer, the mountain front was delineated into individual drainage basins. The analysis of watershed yield is based on finding the elevation at which precipitation exceeds potential evaporation, plant transpiration, and interception. Then, by finding the area of each watershed above that elevation, surplus precipitation (or recharge) can be calculated. This method accounts for all recharge entering the system and not only runoff. Like the Basin-Climatic Characteristic Method, this is a simple approximation that can be conducted on a computer with existing data. There is a great deal of uncertainty associated with both of these methods.

III. METHODS

DATA DESCRIPTION

Existing and previously reported data used in this study include published geologic maps, subsurface geologic data from well records and lithologic logs, hydrologic consultants' reports, weather station data, and historical depth-to-water and water quality data from published and unpublished sources.

New data collected by the NMBGMR, contractors and students from 2009 to 2012 includes:

- Geologic mapping at 1:24,000-scale with cross sections
- Subsurface geologic unit identification from well logs
- Accurate measurements of field site locations
- Characterization the geologic setting of spring and well sites
- One-time and repeated depth-to-water measurements in wells
- One-time and repeated geochemical, isotopic, and environmental tracer sampling from wells, springs, streams, and precipitation

Water-level measurements can provide insight about the occurrence and direction of groundwater flow. Repeated water-level measurements and/or continuous measurements provide information about daily, monthly and seasonal fluctuations that occur in an aquifer system.

Details about the new data collected for this study are described and interpreted in this report. Details about water sampling procedures, analysis methods and systematics are described in Timmons et al. (2013).

GEOLOGIC DATA

Geologic Maps and Cross Sections

Geologic mapping at a scale of 1:24,000 was conducted August 2007 through July 2011 (Fig. 3). These 1:24,000-scale quadrangles were then compiled in two 1:50,000-scale geologic maps (Kelley et al., 2014; Koning et al., 2014).

The general method for mapping the 1:24,000-scale quadrangles entailed field traverses and interpretations of aerial photography. Initial work involved reconnaissance inspection and/or mapping of representative parts of a quadrangle with a hand-held GPS unit and U.S. Geological Survey topographic maps. This preliminary map was then utilized in identifying and mapping units using aerial photography. On four of these quadrangles (Tularosa, Tularosa NE, Three Rivers, and Oscuro), Daniel Koning mapped contacts and identified units from aerial photographs using the PG-2 plotter at the U.S. Geological Survey in Denver. Line work from the aerial photograph-based mapping was then field-checked during subsequent field visits to a quadrangle. After 2012, further air photograph mapping and contact refinements were accomplished on the Three Rivers, western Oscuro, and northern Godfrey Hills quadrangles using the Stereo Analyst extension for ArcGIS 10.1 and related 3-D viewing hardware.

The compilation phase of the project spanned from July 2011 through June of 2014. The major tasks of this phase included developing a map unit nomenclature applicable for the entire study area, writing unit descriptions for these regional map units, edge-matching the geology along the quadrangle boundaries, field checking geology in certain areas (such as along quadrangle boundaries), and constructing 14 cross sections. Given the large area and

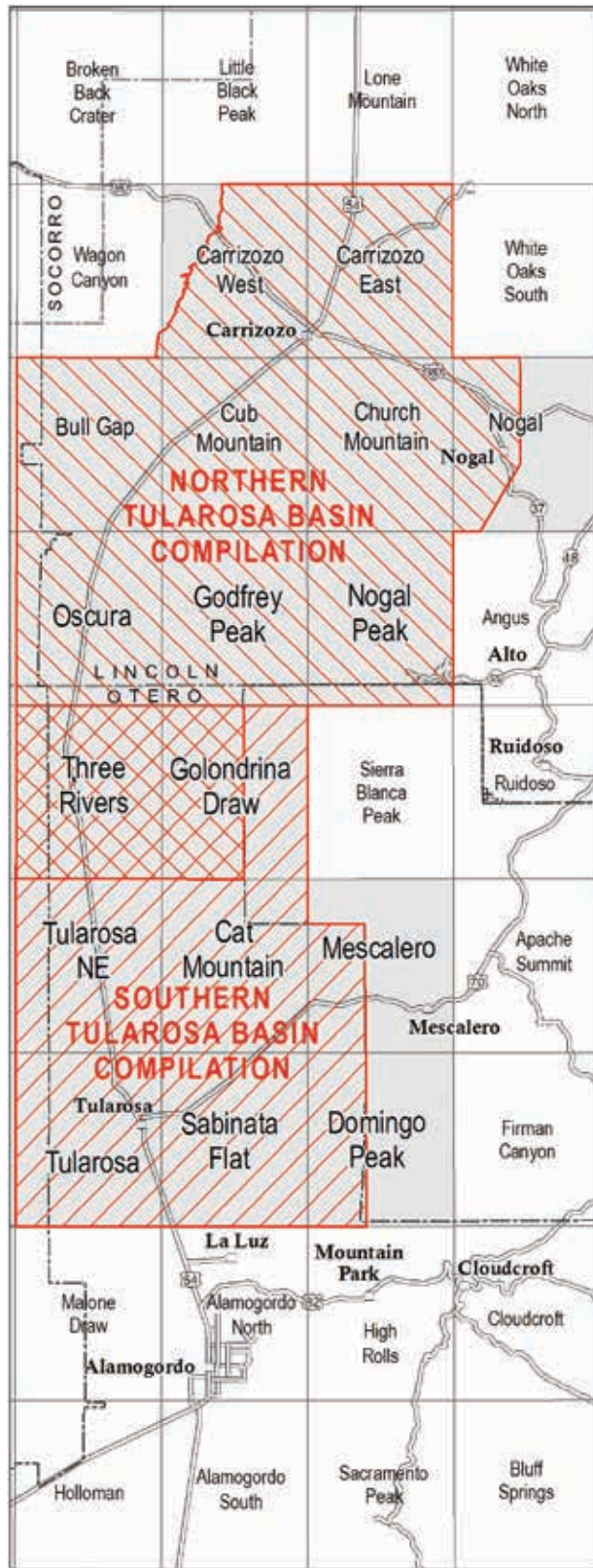


Figure 3—Published 1:24,000-scale geologic maps (shown in gray) completed for this study. The red lines represent the boundaries Tularosa Basin geologic compilation maps. Note that there is overlap between the two geologic compilation maps in the Three Rivers area.

the desired scale of 1:50,000, two compilation maps were constructed (Fig. 3). One compilation map covers the northern half of the study area (Koning et al., 2014) and the other encompasses the southern half of the study area (Kelley et al., 2014), with two quadrangles in the middle included in both (Three Rivers and the western half of the Golondrina Draw quadrangle).

LOCATION OF SITES

All sample and measurement sites (wells, springs, streams, precipitation collectors) were located using a hand-held Garmin 76 or 76S global positioning system (GPS) and were assigned a study identification number (TB-####) (Fig. 4). The elevations of the sites were derived in ArcGIS from a 10-meter horizontal resolution digital elevation model. All spring sites were characterized in the field in terms of the physical characteristics of the discharge point and site conditions. Wells used in this study were inventoried in detail to describe the type of well, its construction, and a description of the measuring point used for water-level measurements (Appendix 1).

WATER-LEVEL DATA

For this study, water-level measurements were obtained from numerous private wells (Fig. 4). Attempts were made to identify the well record associated with each well from the New Mexico Office of the State Engineer. The well records provide details about the drilling and construction of the well, in addition to the geologic units encountered while drilling (Appendix 2).

Water-level measurements in most wells were made on a monthly to bimonthly basis between fall 2009 and summer 2011 (Appendix 3). From a specific measuring point on each well, depth to water measurements were made by staff of the Bureau using one of several different techniques. To insure accuracy, water levels measured with a steel tape were repeated until the measurement was within 0.02 feet of an earlier measurement. In wells with no dedicated pump equipment, water levels were measured with an electronic

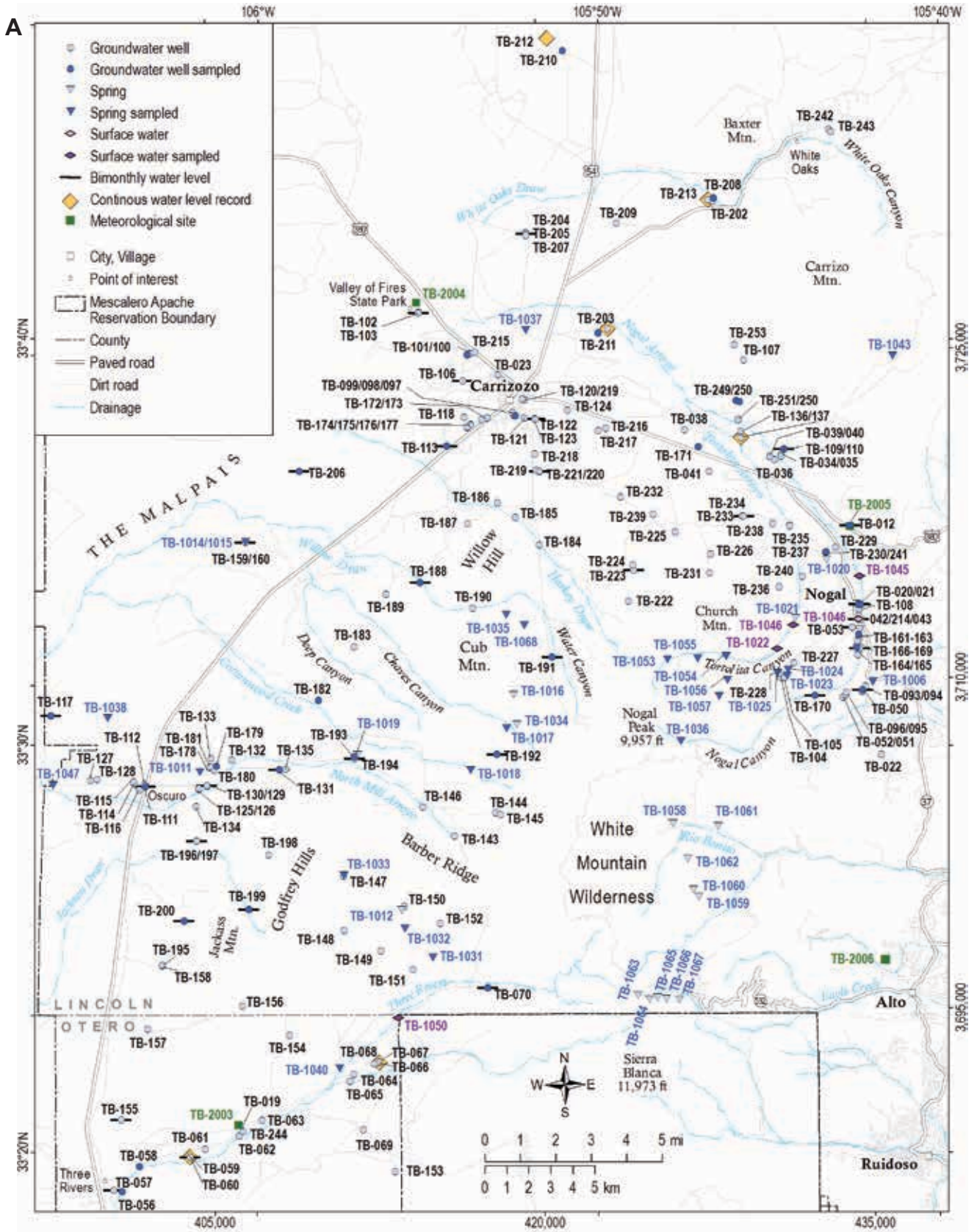


Figure 4A—Site inventory map of the northern portion of the study area. Points on map indicate locations of all inventoried wells, springs, streams, and precipitation stations, as well as which sites were sampled.

B

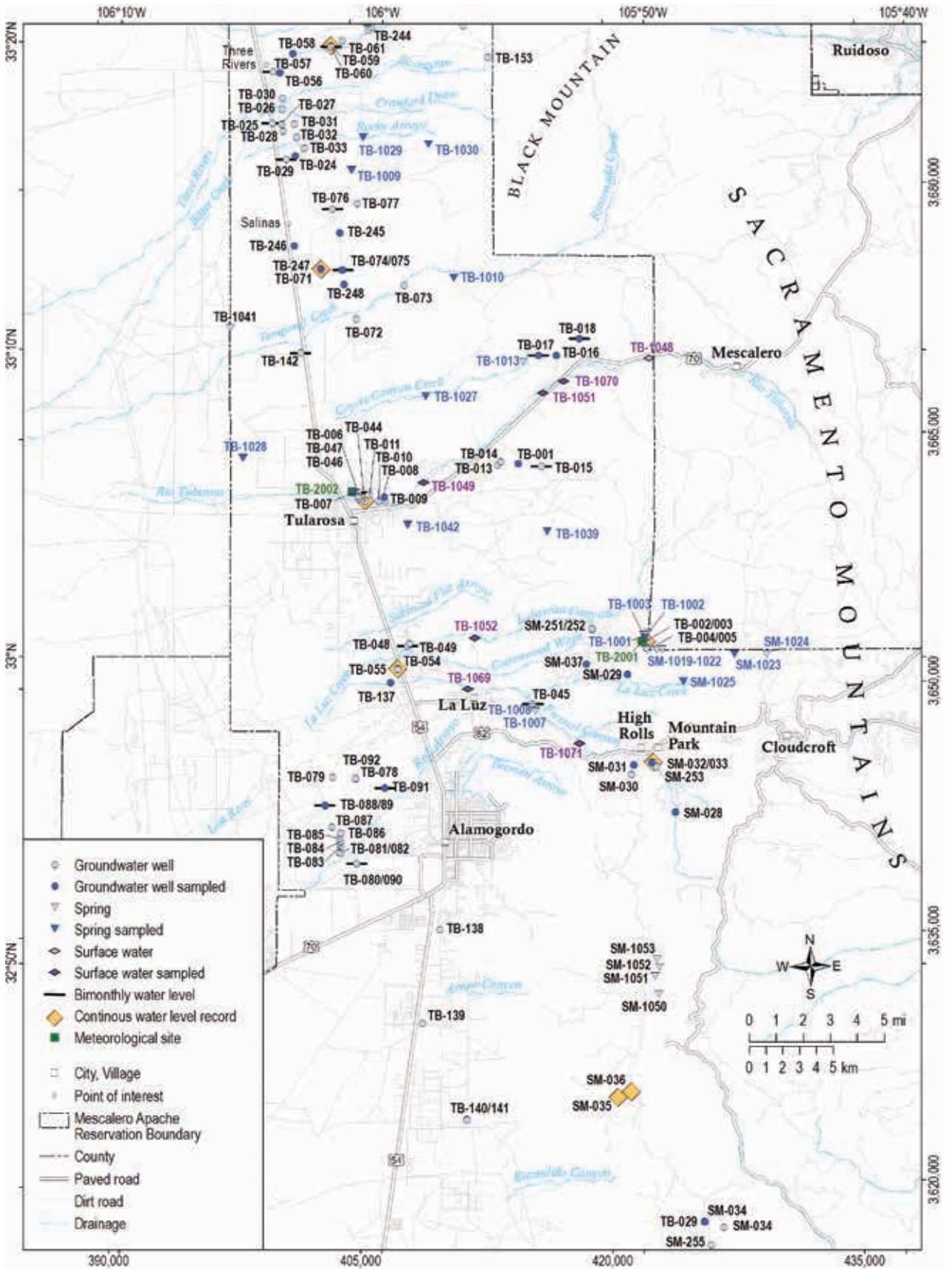


Figure 4B—Site inventory map of the southern portion of the study area. Points on map indicate locations of all inventoried wells, springs, streams, and precipitation stations, as well as which sites were sampled.

sounder. A sonic water-level meter was also used to determine approximate depths to water.

Eleven wells were monitored with continuous water-level recorders for various time intervals ranging from a few months to several years (Fig. 4). These were programmed to record water level and temperature at hourly intervals for the duration of the study. Water-level recorders were checked and downloaded every three to four months, and water levels were measured manually at those times (Appendix 4).

GEOCHEMICAL METHODS

Chemical and isotopic analysis of precipitation, streams, springs, and well waters provide insight into the flow path of groundwater, where it is recharged, and its residence time in the subsurface. For this study, water was sampled for a number of analyses including major ion chemistry, trace metal chemistry, stable isotopes of oxygen and hydrogen, and several naturally occurring environmental tracers which provide estimates of groundwater age. Major ion chemistry and trace metals can provide information about the “life” of the water and the flow path it has traveled from recharge to discharge location, and various other influences within the hydrologic cycle. Stable isotopes of hydrogen and oxygen are useful tools for tracking precipitation through a hydrologic system, and determine what time of year water recharged the aquifer (i.e. monsoon precipitation or snowmelt). Tritium is an environmental tracer that can help determine the relative age of groundwater less than fifty years old. Another environmental tracer that we used to help determine the age of the groundwater was carbon-14. Chlorofluorocarbons (CFC) sampling can provide very accurate groundwater age dating. A more complete summary of sampling and analytical methods are described in detail in Timmons et al. (2013).

IV. RESULTS

GEOLOGY

Regional Geology

Tectonic forces associated with the Rio Grande rift, combined with extensive erosion over the past 25 million years, are largely responsible for the present-day landscape of the study area (Figs. 5, 6). The Sierra Blanca Basin is an important structure between Carrizozo and Ruidoso that began forming prior to rifting. Carrizo Mountain represents one of many intrusions along the Capitan lineament. Below, we expound on these three regional geologic features.

Rio Grande Rift

The Rio Grande rift is characterized by fault-bounded basins and mountains. This tectonic feature extends from southern Colorado south to the Las Cruces-El Paso area, where it merges with the larger Basin and Range extensional province. In southern New Mexico, the rift is 150–160 km (90–100 mi) wide and there are commonly 3–4 extensional basins along a given latitude.

The Tularosa Basin exemplifies a fault-bounded basin in the southern Rio Grande rift. This basin is internally drained and has extensive deposits of salts, mainly gypsum, in the topographically lowest area of the basin (southwest of the study area and west of White Sands National Monument). Structurally, the Tularosa Basin consists of two half-grabens tilted in opposite directions (Lozinsky and Bauer, 1991). The eastern half-graben is 25–30 km (15–20 mi) wide, tilted to the east, and is bounded on the east by the west-down Alamogordo fault zone. Rift basin-fill, called the Santa Fe Group, thickens eastward in this eastern half graben. Maximum basin-fill thickness estimates range

from 900 to 2400 m (3000–8000 ft) based on data in Healy et al. (1978), Orr and Myers (1986), and modeling of Peterson and Roy (2005). Along the Alamogordo fault, basin-fill is probably deepest south of Alamogordo and shallower to the north (Koning, 1999). In the Tularosa area, researchers (Peterson and Roy, 2005; Healy et al., 1978; Orr and Myers, 1986) estimate a maximum basin-fill thickness of 900–1200 m (3000–4000 ft).

Rift-related, west-down displacement along the Alamogordo fault created the western face of the southern Sacramento Mountains, which have been tilted eastward. The Sacramento Mountains are underlain mainly by sedimentary rocks of Pennsylvanian to Permian age. East of the town of Tularosa, the lower mountain-front profile exhibits a bench-like geomorphic feature that generally overlies the Permian-age Abo Formation (Fig. 5). There is 750–850 m (2460–2800 ft) of topographic relief between this bench and the crest of the Sacramento Mountains. This higher escarpment is underlain by the Yeso Formation capped by the San Andres Formation (Fig. 6; Newton et al., 2012; Rawling, 2012).

Sierra Blanca Basin

Although the Sierra Blanca mountains are topographically high, the volcanic and intrusive igneous rocks that compose these mountains actually fill a large depression in the Earth's crust called the Sierra Blanca Basin. This structural depression extends between Three Rivers and Ruidoso and is identified on regional New Mexico geology maps by northeast-elongated exposures of Mesozoic rocks surrounded by Paleozoic rocks (Fig. 5). Near and north of Ruidoso, the eastern margin of the Sierra Blanca Basin coincides with west-down, north- to northeast-trending faults within a 4–12 km (2.5–7.5mi) wide zone. This zone of faults

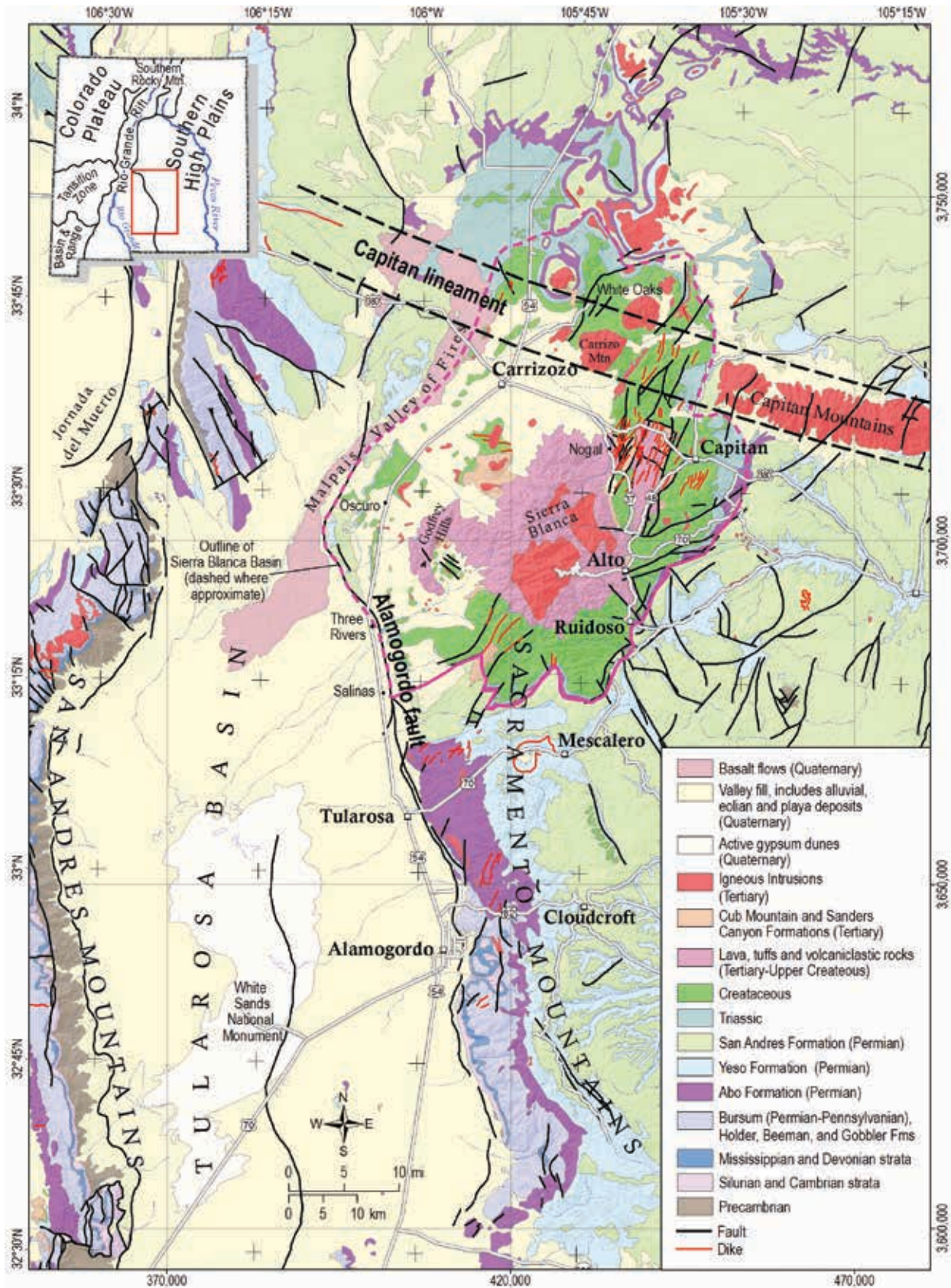


Figure 5—Map illustrating the generalized regional geology of the study area (Geologic Map of New Mexico, 1:500,000, P. Scholle, New Mexico Bureau of Geology and Mineral Resources, 2003).

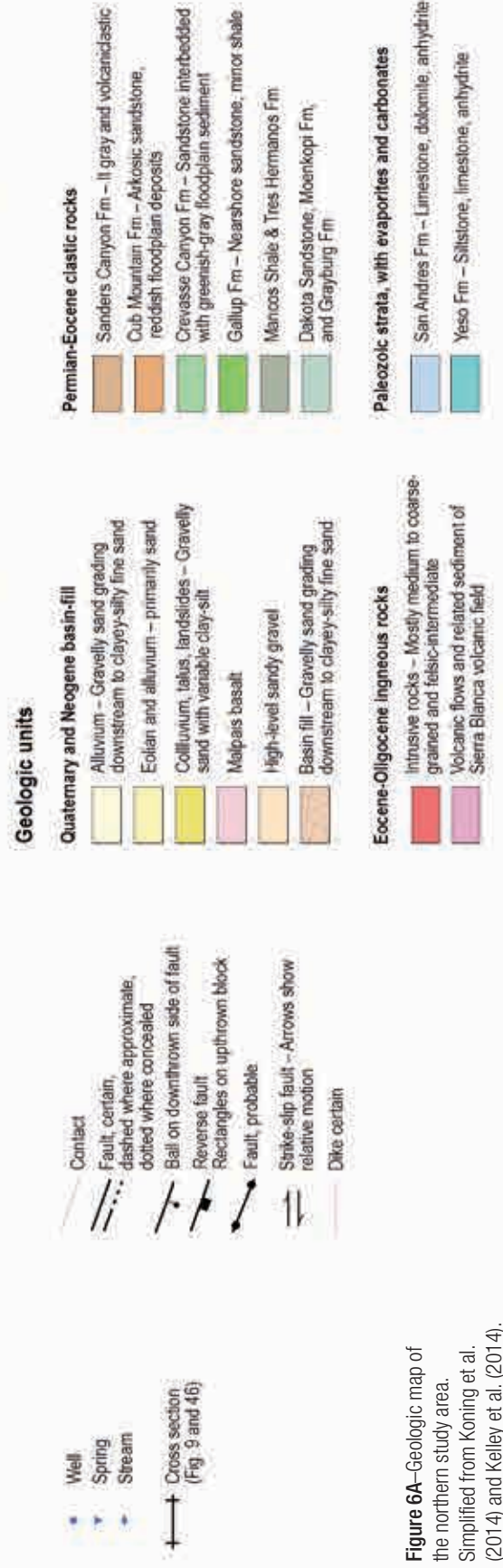
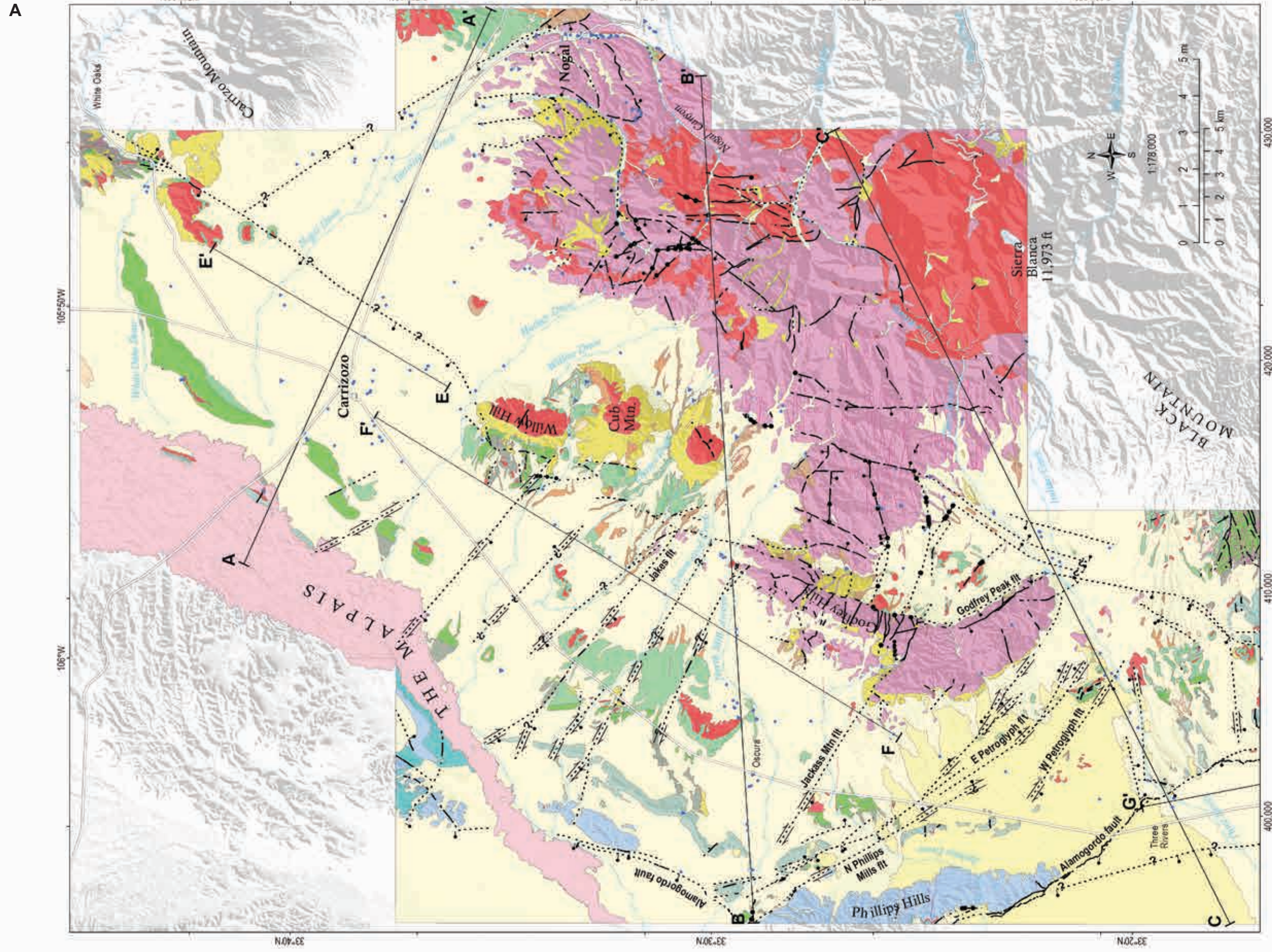


Figure 6A-Geologic map of the northern study area. Simplified from Koning et al. (2014) and Kelley et al. (2014).

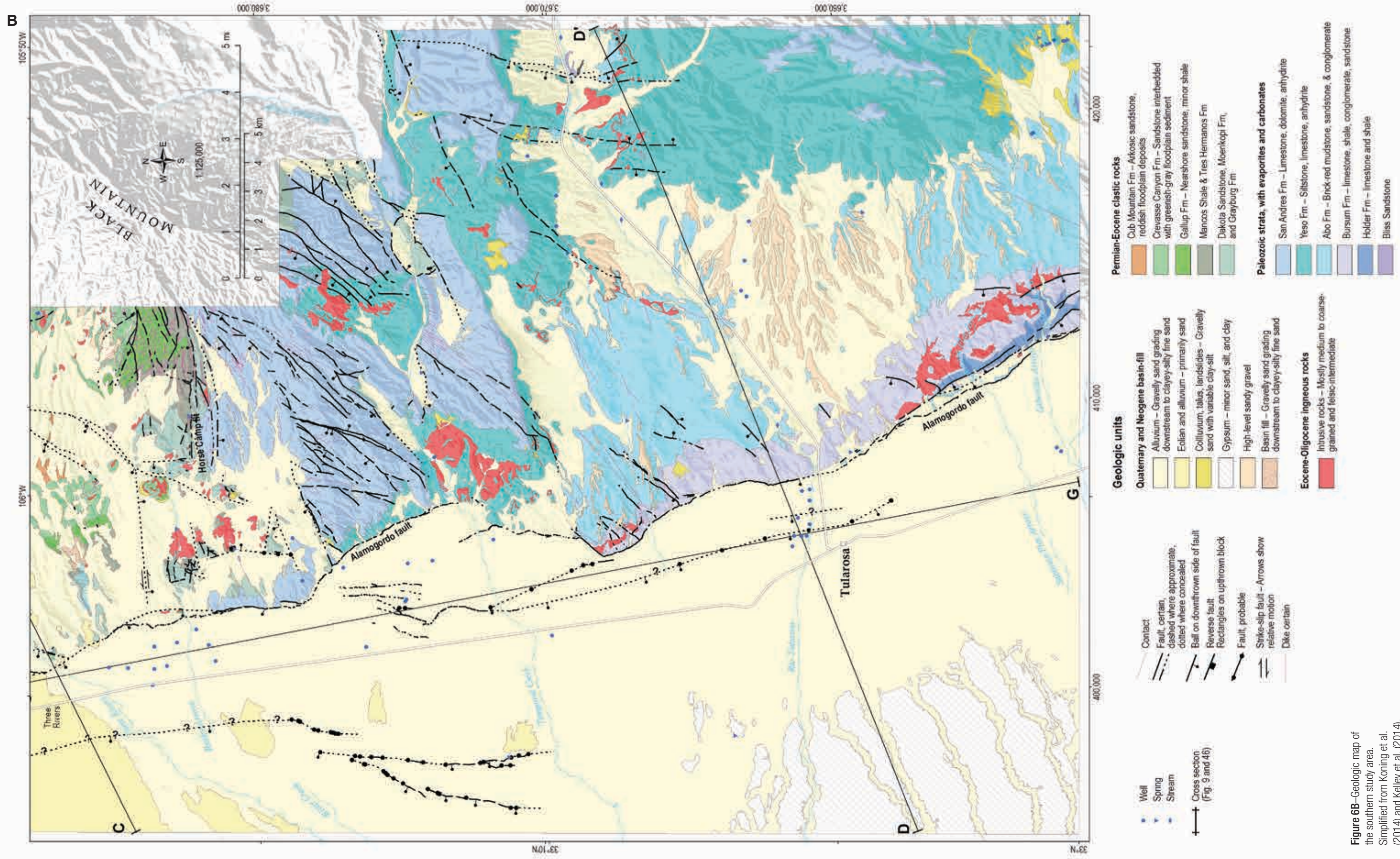


Figure 6B—Geologic map of the southern study area. Simplified from Koning et al. (2014) and Kelley et al. (2014).

contains a relatively dense network of similarly trending dikes (Rawling, 2009, 2011). The southern margin of the Sierra Blanca Basin is cut by at least four east- to northeast-striking, north-down faults with 200–250 m (650–820 ft) of vertical offset.

Capitan Lineament

A regional, west- to northwest-trending lineament of igneous intrusions is found near the northern boundary of the study area (Fig. 5). A lineament, in geologic terms, refers to a linear feature in a landscape which is an expression of an underlying geologic structure, in this case, a band of volcanic intrusions. These intrusions are generally of granitic composition (e.g., Carrizo Mountain and Capitan Mountains). However, the source of the basaltic Carrizozo lava flow, Little Black Peak, also lies along this lineament.

Geologic Structure

The geologic structure in the study area is generally a result of crustal blocks tilting between normal faults. Except for the eastern margin of the Sierra Blanca Basin, folding is relatively minor and generally related to either drag folding along normal faults or, to older tectonic events.

Faults can influence groundwater flow and thus are important to consider in a hydrogeologic study. Offset along faults may juxtapose a high-permeability unit, such as porous sandstone, against a low-permeability unit like mudstone—thereby creating fault barriers and potentially blocking groundwater flow. Faults in bedrock create a fracture network that may enhance permeability and direct groundwater flow parallel to the fault. Some springs in the study area, such as Aguilar Spring (TB-1029) and Maxwell Spring (TB-1010), are associated with bedrock fault zones. Faulting in basin-fill commonly results in low-permeability fault damage zones and clayey fault cores, which may create local groundwater barriers. A more complete discussion of faults is given in Koning et al. (2014) and Kelley et al. (2014).

HYDROLOGY

Precipitation

Groundwater recharge to the Tularosa Basin comes in the form of precipitation. It is important, therefore, to understand regional climatic and geographic controls on the spatial and temporal variability of precipitation in the area. In this section we discuss important regional weather patterns and analyze existing local precipitation data.

Precipitation Patterns

The primary source of precipitation in the Tularosa Basin and surrounding mountains is associated with the North American Monsoon. This northward migration of moist air from the eastern Pacific and the Gulf of California, as well as the Gulf of Mexico, results in intense afternoon thunderstorms in July, August and September. These rains account for more than half of the annual precipitation. Conversely, November through April is usually the driest period, with April typically the driest month (Malm, 2003). The spatial variability of precipitation is usually related to surface elevation. As air is forced up and over topographic features such as mountains, moisture within the air condenses and falls as precipitation. Therefore, areas of high elevation usually receive more precipitation than those at lower elevations (Liebmann et al., 2008, Stensrud et al., 1995, Gochis and Higgins, 2007, Ritchie et al., 2007, Ritchie and Szenasi, 2006, National Weather Service, n.d. a, National Weather Service, n.d. b, National Weather Service Southern Region Headquarters, 2006, National Weather Service Climate Prediction Center, 2003).

There are several climate disturbances that can impact the precipitation received by the area. Tropical storms originating in the Gulf of Mexico or eastern Pacific can also add significant amounts of rain to the southwestern U.S. These storms generally occur at the end of the monsoon season (National Weather Service Climate Prediction Center, 2003; Ritchie et al., 2007; Ritchie and Szenasi, 2006). During the winter, frontal storms are the primary source

of precipitation in the state. Finally, large-scale fluctuations in heating and cooling of the Pacific Ocean can also alter the prevailing storm track. This cycle is known as the El Niño, and La Niña. La Niña winters typically produce only half to one-third of the precipitation dropped during El Niño winters in the southwest (Ahrens, 2003). For a more detailed analysis of the precipitation patterns throughout the region, please refer to Newton et al. (2012).

Historic Precipitation

Daily precipitation amounts have been recorded in the Tularosa Basin and vicinity for most of the past century, with some records dating back to 1895. These detailed records are available from the Western Regional Climate Center, National Oceanic and Atmospheric Administration (NOAA) (see <http://www.wrcc.dri.edu/summary/climsmnm.html>). Portions of this record have been compiled to show general trends in annual and seasonal precipitation in the study area. Average annual precipitation ranges from 66 cm/year (26.0 in/year) in Cloudcroft to 26 cm/year (10.2 in/year) in Tularosa. Figure 7 shows a linear regression for average annual precipitation reported at weather stations listed in Table 1, as a function of elevation. Correlation

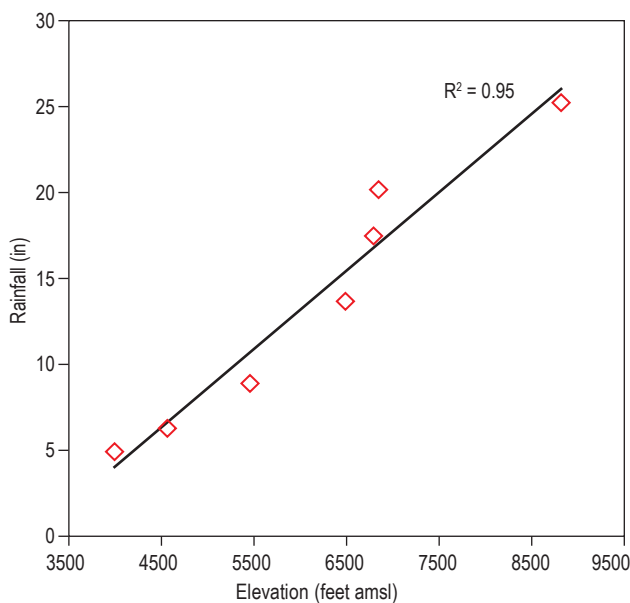


Figure 7– Average annual precipitation versus elevation. The total annual precipitation at weather stations listed in Table 1 increases linearly with elevation, indicating that there is more precipitation at higher elevation than at lower elevations.

with elevation is good with an R² value of 0.95, indicating that elevation is a strong predictor of average annual rainfall in the study area.

Using precipitation data collected at seven different weather stations in the area, we compared the historical climate record with the time frame over which the study was conducted (Table 1). The previous study in this area, which focused on the eastern side of the Sacramento Mountains, was conducted from 2005–2009 (Newton et al., 2012). During this study period precipitation values were quite high, exceeding the average by 18%. The 2005–2009 period was unique in that it saw the wettest month on record, July 2008, and the third wettest year on record, 2006 (Newton et al., 2012).

Water-level measurements from the western side of the Sacramento Mountains and Tularosa Basin were collected between 2009 and 2011. Whereas the three previous years had above average rainfall, 2009 received 17% less precipitation than average throughout the study area. 2010 saw a slight increase in precipitation receiving 5% more precipitation than average (Table 1). The 2009 monsoon season was one of the driest on record, with only 8.5 inches of precipitation at Cloudcroft, compared with the 13 inch annual average. The 2009 to 2010 winter, however, saw nearly 11.5 inches of equivalent precipitation, compared with 6.5 inch average.

Table 1–NOAA weather stations within the region used for examination of historical precipitation, as well as an analysis of the 2009 and 2010 precipitation.

Parameter	Station #	Elevation (ft)	Average Annual Precipitation (in)	2009 deviation from average	2010 deviation from average
White Sands	299686	3990	9.01	-35.85%	+28.52%
Tularosa	299165	4540	10.27	-7.89%	-3.80%
Carrizozo	291515	5440	12.50	-25.12%	+2.40%
Capitan	291440	6470	16.49	-33.17%	-8.67%
Mountain Park	295960	6790	19.57	+5.47%	+2.71%
Ruidoso	297649	6860	21.86	-10.84%	+5.63%
Cloudcroft	292931	8810	26.00	-14.76%	+10.05%
				-17.45%	+5.26%

The 2010 to 2011 period saw an entirely opposite record, receiving above average precipitation (20.9 inches) during the 2010 monsoon, and only 2.1 inches of precipitation during the winter of 2010 to 2011.

Streams and Drainage Basins

Previous research conducted in the area suggests streamflow plays a major role in recharging the Tularosa Basin aquifers (Garza and McLean, 1977; Orr and Myers, 1986; Waltemeyer, 2001; Huff, 2004; Livingston and Shomaker, 2006). It is therefore important to analyze streamflow and its contributing factors. Surface water that flows from the Sacramento Mountains generally originates from springs and seasonal runoff.

A study conducted by the USGS focused on major drainages and watersheds along the edges of the Tularosa Basin (Waltemeyer, 2001). The range front was delineated into 12 drainage basins, ranging from 0.87–157 mi². Waltemeyer (2001) used a Basin-Climatic Characteristics Method that attempts to estimate annual stream flow by taking into account the drainage basin area, the average precipitation, and evaporation. Precipitation estimates were determined based on the average elevation of each drainage basin. These elevations were plotted on the trend line created by the annual precipitation vs. elevation graph (e.g., Fig. 7) to estimate an average annual precipitation value for each drainage basin. This method estimates 45,300 acre-feet/year (AFY) of streamflow, on average, enters the basin (about 6% of the annual mean precipitation).

There are three main streams that drain the northern, central, and southern mountains; Nogal Creek, Three Rivers, and the Tularosa River (Fig. 8). Nogal Creek is an ephemeral stream whose headwaters are located on the eastern flank of Nogal Peak in the northern high mountains. As it descends from the mountain it curves north around Church Mountain and finally west before it discharges into the Carrizozo hilly plains. Several springs are located along the margins of the stream as it passes through the town of Nogal. Unfortunately, there is no stream gauge record to measure flow, though total flow is estimated to be approximately

4300 acre-feet/year using the same method used by Waltemeyer (2001).

Three Rivers is an ephemeral stream that flows southwest from the western slopes of Sierra Blanca in the central region. At its headwaters are several springs which discharge from Sierra Blanca volcanic rocks. Three Rivers drains

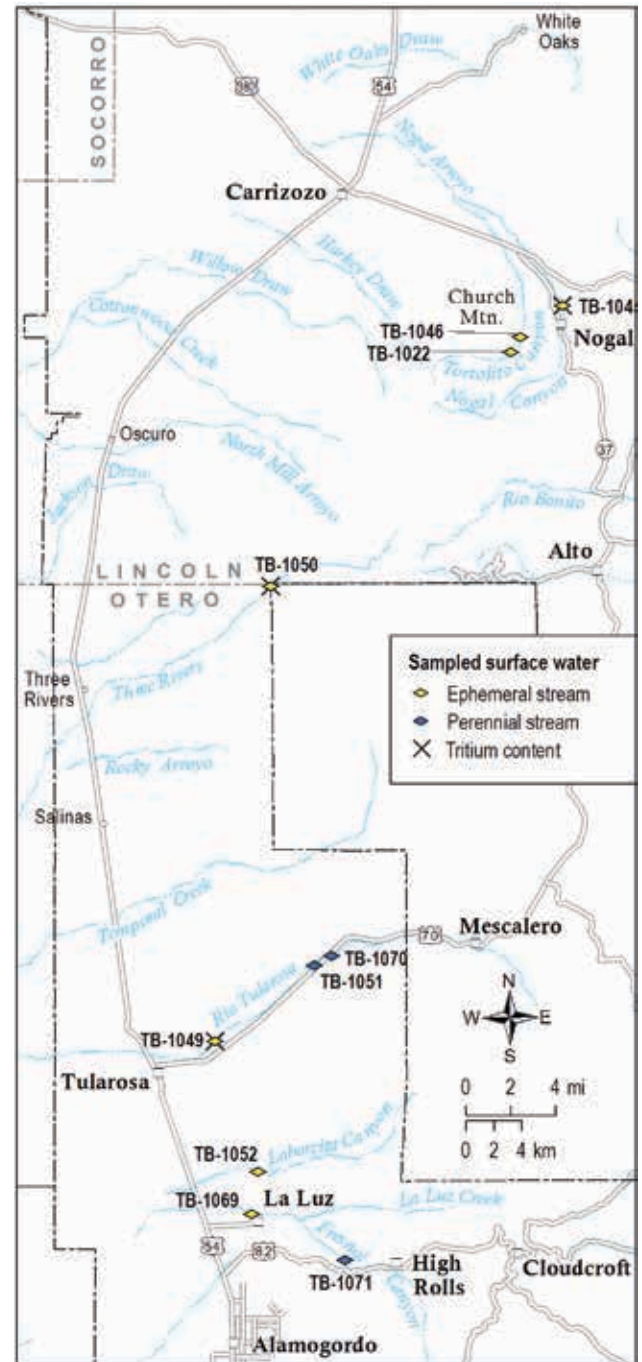


Figure 8— Location of sampled surface water, denoting ephemeral and perennial streams.

at the margin of all four topographical regions (NHM, SHM, CHP, TB). The only streamflow data pertaining to Three Rivers was collected from 1956 to 1977 by the USGS and only recorded peak flow (Livingston and Shomaker, 2006). Waltemeyer (2001) estimated 8300 AFY of total streamflow.

The largest perennially flowing stream in the area is the Tularosa River. The Tularosa River flows southwest down the southern mountain front and through the town of Tularosa before infiltrating into the alluvial-basin aquifers. The headwaters of the stream originate in the canyons on the Mescalero Apache Indian Reservation in the northern Sacramento Mountains. Spring flow, derived largely from snowmelt, contributes a large part of the total flow (Garza and McLean, 1977). Several of the smaller tributaries contribute to the streamflow via runoff from monsoon rains.

The Tularosa River is the only stream in the area with a currently functioning stream gauge. Discharge measurements have been recorded since 1932. While the river flows year round at an average of 13.5 cubic feet per second (CFS) (9800 AFY), during monsoon rains the river has flooded to over 100 CFS (72,400 AFY). Streamflow is historically lowest in June, averaging 11.0 CFS (8000 AFY). In August stream flow spikes to an average of 15.1 CFS (10,900 AFY) from monsoon runoff. A second, more sustained peak occurs in the winter between January and February as snowmelt and springs feed the river, averaging 14.6 CFS (10,600 AFY).

Averaged discharge has fluctuated quite significantly throughout its 81 year record. From 1932–1947 the average flow was around 10,000 AFY. Between 1948 and 1977 flow was significantly lower, around 7000 AFY. Flow increased dramatically between 1978–1995, discharging approximately 16,000 AFY. From 1996 to present the river has been flowing on average around 10,000 AFY. Curiously, Waltemeyer's (2001) calculation of annual streamflow is significantly higher, estimating 17,500 AFY of streamflow from the Tularosa River drainage basin. This inconsistency with measured vs. approximated flow highlights the rudimentary and rough estimation of the Basin-Climatic Characteristics Method.

Two other ephemeral streams in the area, which Waltemeyer (2001) identified as providing significant streamflow to the Tularosa Basin are Temporal Creek and La Luz Creek. Temporal Creek, which flows from Rinconada Canyon is located between Three Rivers and the Tularosa River, is estimated to discharge 9200 AFY. La Luz Creek, located just south of the Tularosa River, is estimated to discharge at 5300 AFY.

Groundwater

Hydrogeologic Cross Sections

A useful visual representation of the geologic structure of the study area is given in the cross sections of Figure 9, which represent a subset of the cross sections presented in Kelley et al. (2014) and Koning et al. (2014). These cross sections show the stratigraphic units that are discussed below.

Hydrostratigraphic Units

The study area contains a diverse array of sedimentary and igneous rock units. Sedimentary units include carbonates (limestone and dolomite), evaporites (gypsum and anhydrite), and clastic sedimentary rocks (conglomerate, sandstone, siltstone, claystone) or their non-lithified, weakly consolidated counterparts (gravel, sand, silt, clay). Carbonates and evaporites are restricted to older marine rocks of the Paleozoic. Igneous rock units consist of lava flows and intrusions. Intrusions take the form of dikes, sills, and stocks.

Below, we describe the rock units from oldest to youngest, with emphasis on properties that may control groundwater storage and flow. The rock units are grouped according to common lithologic properties that may affect groundwater flow. A schematic stratigraphic section that illustrate Paleozoic, Mesozoic, and early Cenozoic strata is given in Figure 10. Please refer to Kelley et al. (2014) and Koning et al. (2014) for more detailed descriptions and genetic interpretations of the rock units. Of particular note is the refinement to the volcanic stratigraphy of the Sierra Blanca Basin (Kelley et al., in press; Kelley et al., 2014.; Koning et al., 2014). Koning et al. (2014) presents figures and glossaries explaining

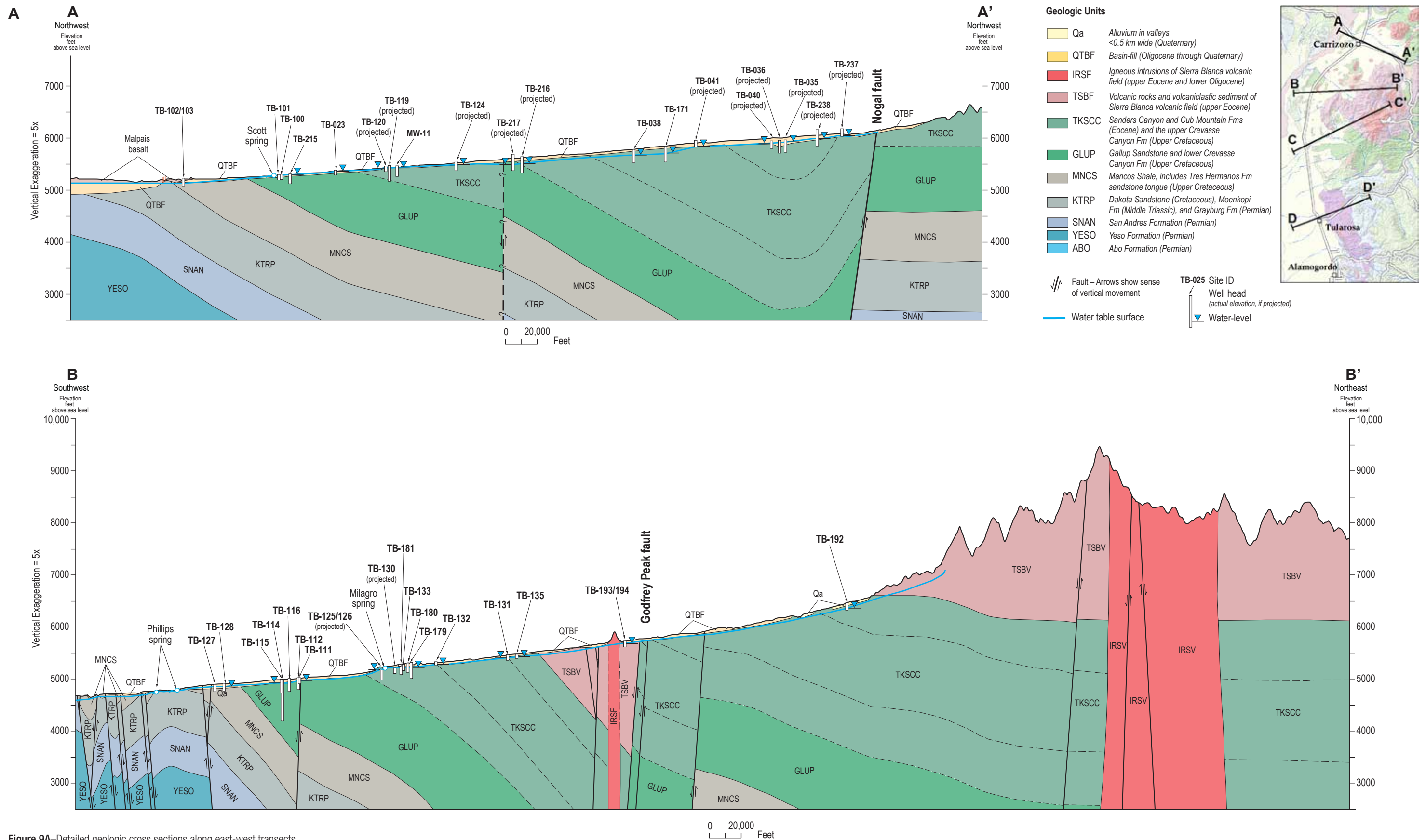
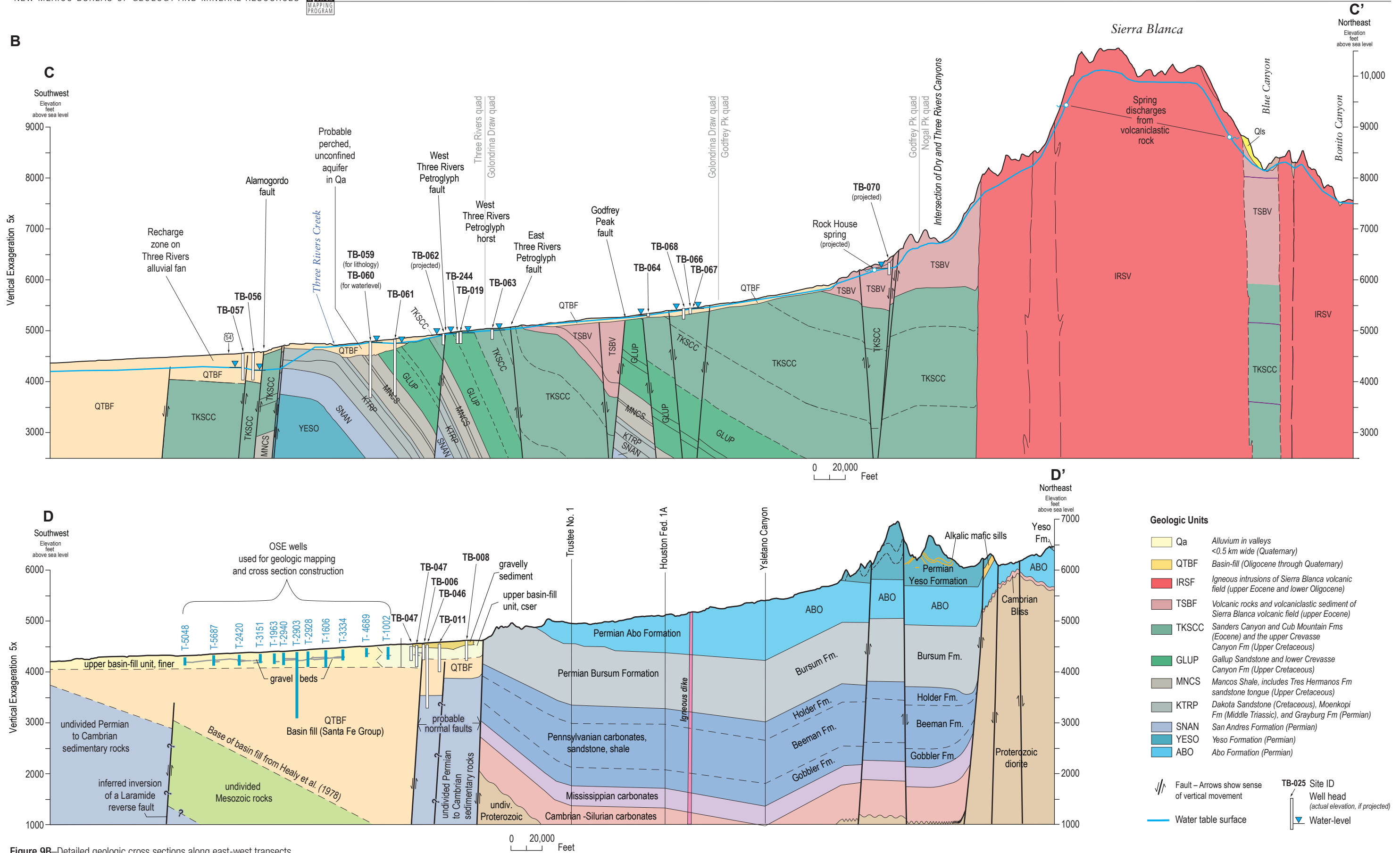


Figure 9A—Detailed geologic cross sections along east-west transects



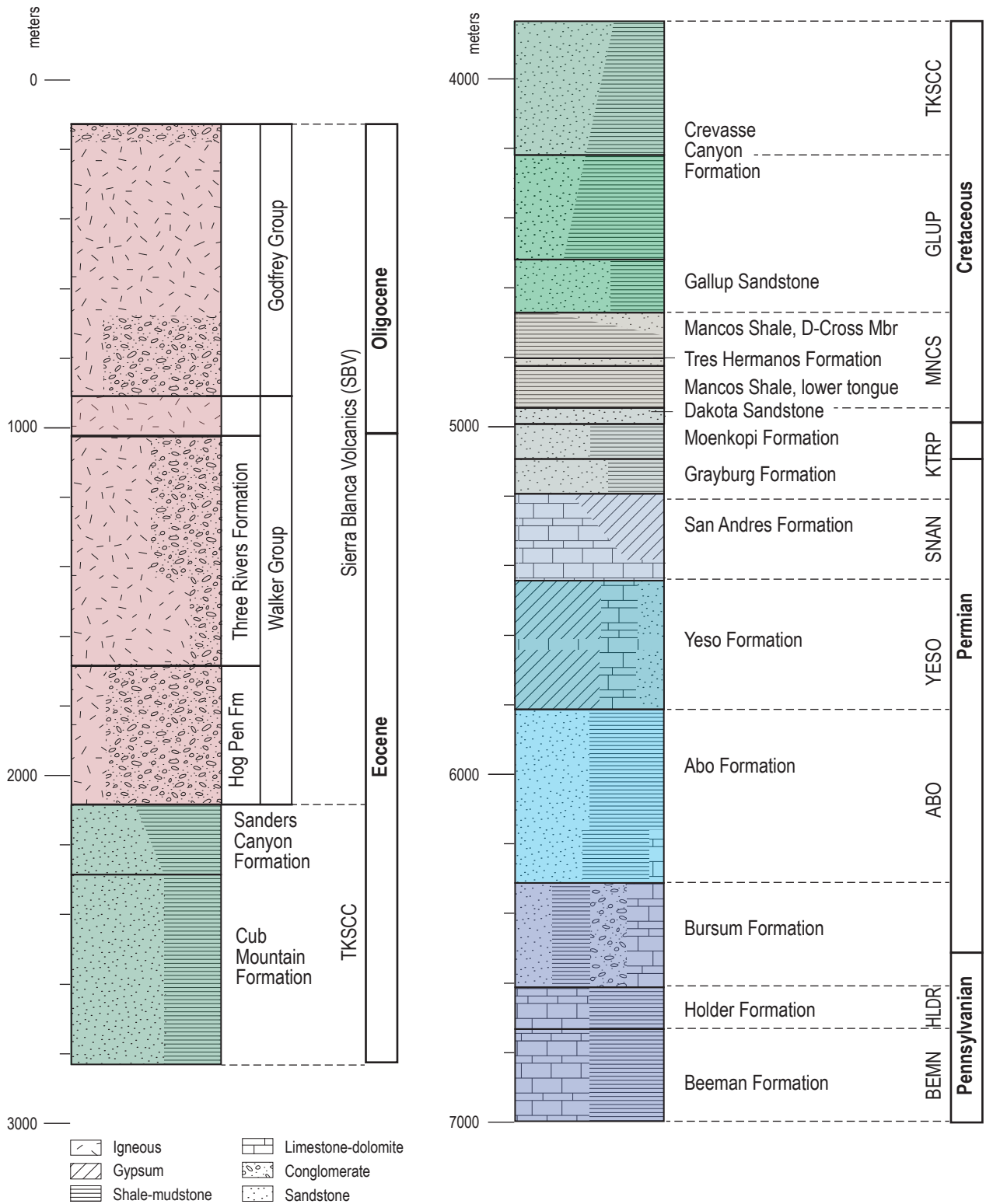


Figure 10—Schematic stratigraphic section illustrating all of the rock units found in the study area.

geologic terms or concepts (e.g., stratigraphy and geologic time) that may be unfamiliar to some readers. Aquifer names are abbreviated in section headers and are referred to on maps and later in the text.

Beeman (BEMN) and Holder (HLDR) Formations (Pennsylvanian Period)—The grayish Holder and underlying Beeman Formations are composed of shale and fossiliferous limestone with sparse beds of sandstone, mudstone, and limestone conglomerate (Fig. 10). These formations generally make poor aquifers, except where fractured. The combined thickness of these formations is approximately 230 to 425 m (750–1400 ft) (Otte, 1959).

Bursum Formation (Pennsylvanian and Permian Periods)—The gray to red Bursum Formation contains conglomerates interbedded with sandstone, fossiliferous limestone and shale (Fig. 10). Some of the discontinuous beds of sandstone, conglomerate and fossiliferous limestone could be potential aquifers east and northeast of Tularosa. The Bursum Formation east of Tularosa is 170 to 300 m (560–1000 ft) thick, thickening from south to north (Otte, 1959).

Abo Formation (Permian Period)—The brick-red Abo Formation is dominated by mudstone (50%) together with sandstone and conglomerate (40%) (Fig. 10). Fossiliferous limestone and carbonate (10%) are primarily found in the basal 150 m (500 ft) of the unit (Otte, 1959). The discontinuous sandstones and conglomerates in the Abo Formation form localized aquifers east and northeast of Tularosa. The Abo is 430 to 550 m (1400–1800 ft) thick near Tularosa (Otte, 1959; Speer, 1983) and 530 to 630 m (1740–2070 ft) thick farther north in the subsurface near Three Rivers.

Yeso Formation (Permian Period)—The Yeso Formation can be divided into three parts in the study area. The exposed lower part consists of red and yellow siltstone, gray limestone, and thinly bedded gypsum (Fig. 10). A 30 m (100 ft) thick limestone is observed in the middle portion of the formation. Rocks of the upper part of the Yeso Formation include gypsum, limestone, and yellow to red siltstone. Fractured limestones

serve as aquifers in the Yeso Formation. Dissolution of gypsum locally creates sinkholes and deforms overlying rock units. The maximum thickness of this unit is 372 m (1200 ft) east-northeast of Tularosa, but it thickens to 610 m (2000 ft) near Three Rivers.

San Andres Formation (SNAN) (Permian Period)—The San Andres Formation in the study area includes the Rio Bonito and Fourmile Draw Members (nomenclature adapted from the tripartite subdivision of the San Andres from Kelley, 1971) (Figs. 10, 11). The lower unit, the Rio Bonito Member, is 40–60 m (150–200 ft) thick and consists largely of dark-gray limestone (Figs. 10, 11). The overlying Fourmile Draw Member is 177–183 m (580–600 ft) thick and composed of brownish gray, interbedded dolomite, limestone, and gypsum or anhydrite (Figs. 10, 11). The Glorieta Sandstone, which constitutes a good aquifer in central New Mexico, is not seen in the southern study area but to the north is present as one or two relatively thin beds, each <3 m (10 ft) thick, in the Rio Bonito Member. This sandstone is absent in the vicinity of Bent and is a single bed northeast of Tularosa. Based on surface exposures on the east flank of the Sacramento Mountains, the predominance of groundwater flow in the San Andres Formation is via fractures enlarged by dissolution. Maxwell Spring (TB-1010) in Temporal Canyon is associated with faulted San Andres limestone (Fig. 12).

Clastic Rocks (KTRP) (Permian, Triassic, and Cretaceous Periods)—The Grayburg Formation is an easily eroded unit that consists of orangish-red, moderately cemented, fine-grained sandstone, silty to clayey very fine- to fine-grained sandstone, and subordinate siltstone and shale (Fig. 12). In the southern compilation map area, thick gypsum or anhydrite beds are interbedded in these deposits. The Grayburg is about 105–110 m (~350–360 ft) thick. No springs discharge from the Grayburg Formation and groundwater is inferred to flow interstitially or via fractures.

The Moenkopi Formation in the study area is about 85–105 m (290–345 ft) thick (maximum thickness from Lucas, 1991) and consists of reddish-brown, fine- to coarse-grained sandstone, mudstone, and 1–5% pebble-conglomerate. Channel-fill sandstones in the

Moenkopi are well-cemented and groundwater flow is probably through fractures. No springs discharge from the Moenkopi Formation and its well-cemented sandstones and clayey floodplain deposits may impede groundwater flow.

The Dakota Sandstone is relatively thin (30–50 m (100–170 ft) thick), generally composed of fine- to very coarse-grained sandstone, and is very well cemented (Fig. 12). Up-section, beds of siltstone, very fine-grained to fine-grained sandstone, and shale-mudstone become increasingly common. Because of its well-cemented nature, there is likely minimal interstitial (between sand grains) groundwater flow in the Dakota Sandstone. Rather, flow is probably through fractures/joints or via bedding planes, as seems to be the case for the spring at Bull

Gap (TB-1038) (K. Zeigler, pers. commun., 2011). West of Oscuro, the western spring associated with Phillips Springs (TB-1047) discharges from the Dakota Sandstone.

Marine Shales (MNCS) (Late Cretaceous Period)—This succession of shale-dominated rocks thickens to the north. The unit includes two tongues of the gray to yellow Mancos Shale, the lower being 100–120 m (330–380 ft) thick and the upper being 90–140 m (310–450 ft) thick. The two shale tongues are separated by a 20–30 m-thick (70–100 ft-thick) tongue of sandstone-dominated strata (the Tres Hermanos Formation) (Fig. 10). Very fine- to fine-grained sandstone and siltstone interbeds are found near the base of the Mancos Shale and become

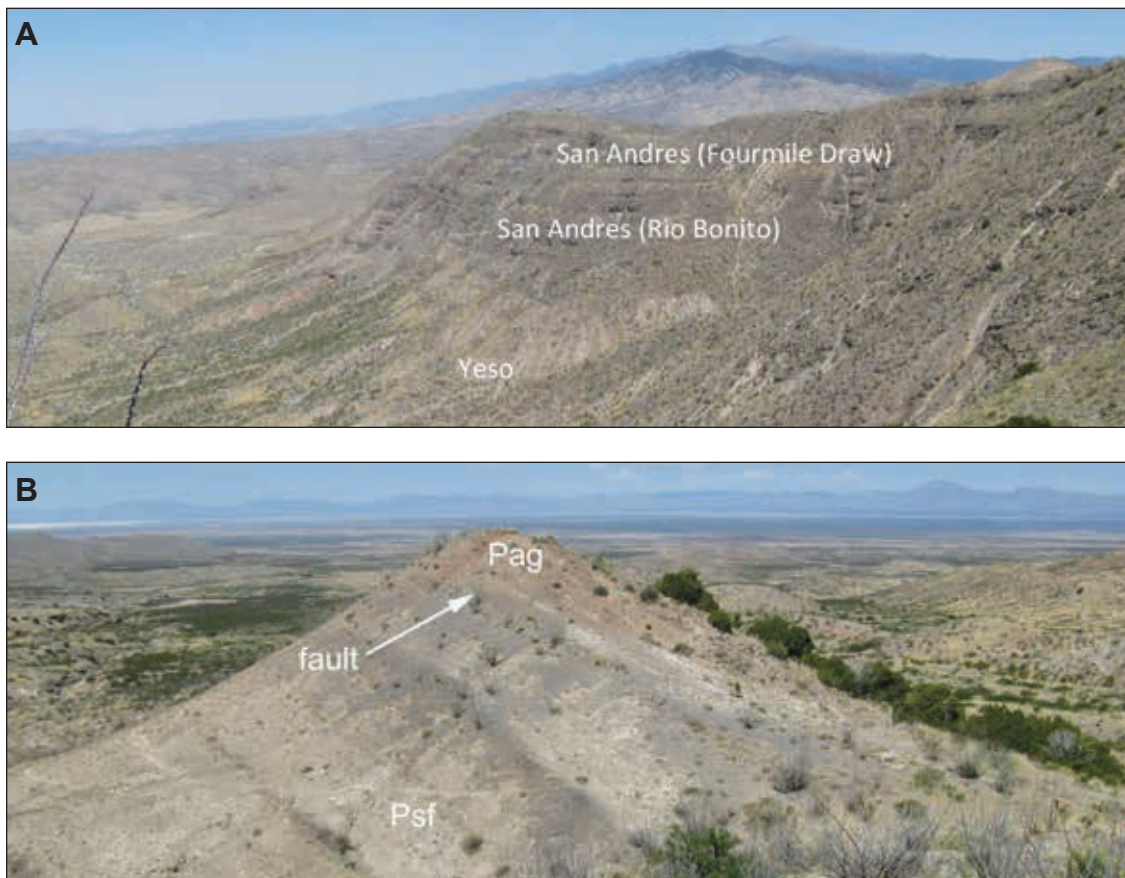


Figure 11—Photographs of the San Andres Formation. **A.** The two mappable members of the San Andres Formation (Fourmile Draw and Rio Bonito) are well exposed on this steep slope 1.8 km (1.1 mi) in the Temporal Creek drainage. Note their gray color and ledge-forming outcrop character. Where seen here, both of the members are mostly composed of carbonate rocks (with the Rio Bonito predominately composed of limestone), but the Fourmile Draw Member contains interbedded gypsum or anhydrite beds as well. Below lies the Yeso Formation, which is more of a slope-former than the San Andres Formation. **B.** A faulted contact between the Fourmile Draw Member of the San Andres Formation (Psf) and the Grayburg Formation of the Artesia Group (Pag); photo taken 14.5 km (9 mi) southeast of Three Rivers. The light tan strata in the Fourmile Draw Member consist of gypsum and the darker bands are composed of dolomite or limestone



Figure 12—Photographs displaying the hydrostratigraphic unit that includes the Grayburg, Moenkopi, and Dakota Sandstone Formations. **A.** Reddish orange, silty very fine-grained sandstone cut by a fault. Blue backpack for scale. Two fault planes are present as indicated at white arrows. The left one has a 4–5 cm gouge zone composed of finely brecciated Grayburg sandstone. The right fault contains 0.5–1.0 cm-thick, gypsiferous gouge. Preferential reduction has occurred along both faults. Photo taken 440 m west of Kitty Spring (TB-1009). **B.** Unconformable contact between the Moenkopi and Grayburg Formations (labeled TRm and Pag, respectively). **C.** Cross-stratification related to paleo-river sand bars in the Dakota Formation. Photo taken from outcrops 4.5 mi (7.3 km) west of Carrizozo. **D.** Another photograph of cross-stratified sandstone of the Dakota; photo taken 8.9 mi (14.3 km) north-east of Carrizozo. Note the intense varnishing that commonly occurs when this unit is subject to prolonged subaerial exposure.



Figure 13—Photograph of Mancos Shale, taken in an arroyo exposure at north end of the Phillips Hills. Hammer for scale. Strata are light gray to pale yellow, silty mudstone that is horizontal planar-laminated and fissile. Correlated to the upper tongue of the Mancos Shale.

increasingly common in the upper half of the upper tongue (Fig. 12). Because of its clay-rich lithology, the Mancos Shale hosts relatively few springs and likely functions as an aquitard. One spring in the Mancos Shale is Aguilar Spring (TB-1029), which discharges from a fault 7.5 km (4.7 mi) southeast of Three Rivers. A spring (now dry) once discharged from the Tres Hermanos Formation at a location 5.8 km (3.6 mi) southwest of the Carrizozo airport. The existence of this spring is noteworthy as it indicates that the Tres Hermanos Sandstone can act as a confined aquifer within the adjoining Mancos aquitard.

Gallup Sandstone and Lower Crevasse Canyon Formation (GLUP) (Late Cretaceous Period)—We combine the Gallup Sandstone and lower Crevasse Canyon Formation into one hydro-



Figure 14—Photographs of the hydrostratigraphic unit comprised of the Gallup Sandstone and lower Crevasse Canyon Formation. **A.** Near intrusions, the Gallup Sandstone commonly is well-cemented and makes bold cliffs. Shown here is the upper tongue of the Gallup Sandstone, which tends to be the thickest, outcropping on the lower western flank of Willow Hill. **B.** Cross-stratification in the Gallup Sandstone. **C.** Not all of the Gallup is sandstone, about 1/3 of it consists of tongues of shale or muddy sandstone. Shown here is low permeability sandstone and muddy sandstone that were probably deposited in a lagoonal setting. **D.** Lower half of the Crevasse Canyon Formation, exposed in upper Deep Canyon (Fig 4A). **E.** Sandstone channel-fill of the lower Crevasse Canyon Fm, exposure is on the west face of Willow Hill (Fig 4A). **F.** Coal seam in the lower Crevasse Canyon Formation, upper Deep Canyon.

stratigraphic unit because of laterally extensive, several meter-thick shale tongues in the former and the fact that the latter is mostly composed of low-permeability, fine-grained flood-plain deposits (Fig. 14). Collectively, these fine-grained deposits likely act to retard groundwater flow and may result in low hydraulic conductivity values for this unit. The Gallup Sandstone consists of laterally extensive tongues of white to yellow sandstone separated by subordinate gray shale. The sandstone is weakly to well cemented, with cemented intervals common near large volcanic intrusions (e.g., White Oaks area and west side of Willow Hills) (Fig. 14). The Gallup Sandstone is 105–195 m thick (350–640 ft thick), being thickest in the White Oaks area.

Springs discharging from the Gallup Sandstone are limited to the Carrizozo area and west

of Black Mountain. These include Scotts Spring, alongside Highway 380 west of Carrizozo, and Anchor Spring, located 1.2 mi (2 km) west of the Carrizozo airport. A line of seeps extends 490 m (1600 ft) north of Anchor Spring, parallel to bedding strike, and the northern seeps discharge ~15 stratigraphic meters (~50 ft) below outcrops of Gallup Sandstone, indicating a strong component of interstitial flow or bedding plane flow in confined, stratal conditions. Several springs occur in narrow canyons incised deeply into the Gallup Sandstone 7 km (4.5 km) southeast of Three Rivers, at the western foot of Black Mountain.

The entire Crevasse Canyon Formation is 530–760 m (1750–2500 ft) thick, the lower half of which is included in this lower-permeability unit. The basal 30–90 m (100–300 ft) of the Crevasse Canyon Formation is transitional

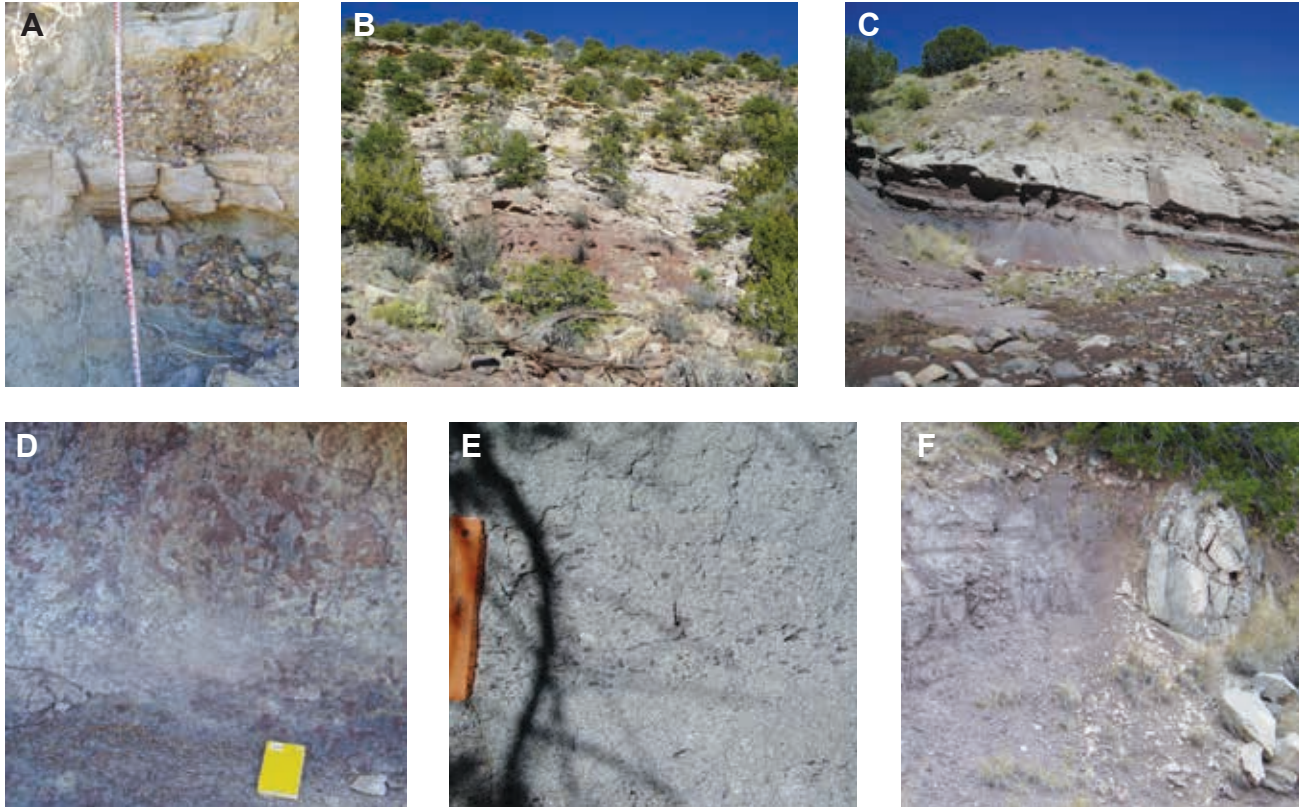


Figure 15—Photographs of the hydrostratigraphic unit comprised of the upper Crevasse Canyon Formation, Cub Mountain Formation, and the Sanders Canyon Formation. **A.** The upper 30–60 m (100–200 ft) of the Crevasse Canyon Formation contains abundant gravel and conglomerate interbeds, as shown here from an exposure in Deep Canyon. **B.** Outcrops of Cub Mountain Formation on the western slopes of Cub Mountain. **C.** Sandstone channel-fill overlying reddish floodplain deposits of Cub Mountain Formation. **D.** Mottling and bioturbation in reddish, silty very fine- to fine-grained sandstone of Cub Mountain Formation. Black and white segments on the measuring tape to the right are 12 inches long. **E.** Clay rip-ups in grayish, medium- to very coarse-grained sandstone of a channel-fill in the Sanders Canyon Formation. The sandstone of this unit generally has 15–30% volcanic lithic grains. **F.** Like the Cub Mountain Formation, the Sanders Canyon Formation contains reddish to purplish floodplain deposits. Here, fine sandstone floodplain deposits are intruded by a trachyte dike. Photographs C through D are taken in Chaves Canyon; photographs E and F are taken in lower Sanders Canyon.

with the underlying Gallup Sandstone. In the lower Crevasse Canyon Formation, the sandstone is generally yellow, very fine- to medium-grained, and commonly deposited within former river channels. Floodplain sediment between the sandy channel-fills is characterized by mudstone or clayey-silty very fine- to fine-grained sandstone. Coal or carbonaceous mudstone beds may be found as interbeds in swamp- or floodplain-mudstone in the lower half of the Crevasse Canyon Formation (Fig. 14). Lower Coyote Spring (TB-1027) and Bloom Spring discharge from the lower Crevasse Canyon Formation, ~3 km (~2 mi) southwest of the Carrizozo airport, and outcrop observations suggest stratal-controlled discharge from sandstone under confined conditions (Fig. 12).

Clastic rocks (TKSCC) (Late Cretaceous Period and Eocene Epoch)—These units include the upper Crevasse Canyon, Cub Mountain, and Sanders Canyon Formations. The thickness of the hydrostratigraphic unit ranges from 800 to 1160 m (2600 to 3800 ft) (Fig. 10). A 3–8 m-thick (10–26 ft-thick) zone of strong cementation lies at the boundary between the Crevasse Canyon and Cub Mountain Formations, coinciding with a paleosol. Strata are characterized by interbedded sandstone channel-fills and lower permeability floodplain deposits composed of mudstone and very fine- to fine-grained sandstone (Fig. 15). Floodplain deposits are subequal to or subordinate to sandstone channel-fills, which are fine- to coarse-grained and locally contain pebble beds (Fig. 15). The sandstone channel-fills may be stacked upon one



Figure 16—Photographs exhibiting lava flows and volcaniclastic rocks of the Sierra Blanca volcanic field. **A.** Conglomerate in the Hog Pen Formation near the head of Chaves Canyon. **B.** Typical flow of the Hog Pen Formation, exhibiting large pyroxene phenocrysts, taken in Water Canyon. **C.** Flow breccia in the Hog Pen Formation, taken in Water Canyon. **D.** Plagioclase-phyric lavas along the ridge north of Three Rivers Canyon. **E.** Clayey-gravelly, red sandstone commonly found interbedded with trachybasalts in the lower-middle part of the Three Rivers Formation. **F.** Trachybasalt flows, located 0.8 mi (1.2 km) southwest of Jackass Mountain (Fig 4A).

another (amalgamated) to form 1–10 m-thick sandstone packages. These rock units are weakly to well-cemented, with the upper 100–300 m (300–1000 ft) generally weakly cemented. Springs are common in sandstone intervals (e.g., Milagro (TB-1011), Jakes, and Shady Springs (TB-1034)) and outcrop observations indicate bedding plane, fracture, and interstitial groundwater flow (Koning et al., 2014). We infer a relatively high hydraulic conductivity value for this unit based on the high proportion of channel-fills, thick intervals of weak cementation, and the relative abundance of springs.

Sierra Blanca Volcanic Field (SBV) (late Paleogene Period)—Because igneous rocks underlie high topography in the Sierra Blanca highland and Carrizo Mountain, groundwater recharge in the northern study area occurs in these rock types and thus their hydrologic properties are

important to consider (Figs. 6a, 10, 16). Except for the White Oaks area and Carrizo Mountain, practically all the igneous rocks in the study area relate to the Sierra Blanca volcanic field.

Sierra Blanca volcanic rocks and volcaniclastic sediment—Up to 1400 m (4600 ft) of interbedded volcanic sedimentary rocks composed of volcanic detritus are preserved in the deepest part of the Sierra Blanca basin (i.e., beneath the Sierra Blanca highland). Recent geologic mapping has greatly refined the volcanic stratigraphy and has differentiated the Walker Group of Thompson (1966, 1972) into the Hog Pen and Three Rivers Formations (Fig. 10)(Kelley et al., 2014; Koning et al., 2014; Kelley et al., in press). For the purposes of this investigation, however, the volcanic lithologic units are treated as a single hydrostratigraphic unit. The volcanic rocks are mostly alkalic andesite lavas, with minor alkalic basalt, dacite, and rhyolite flows.

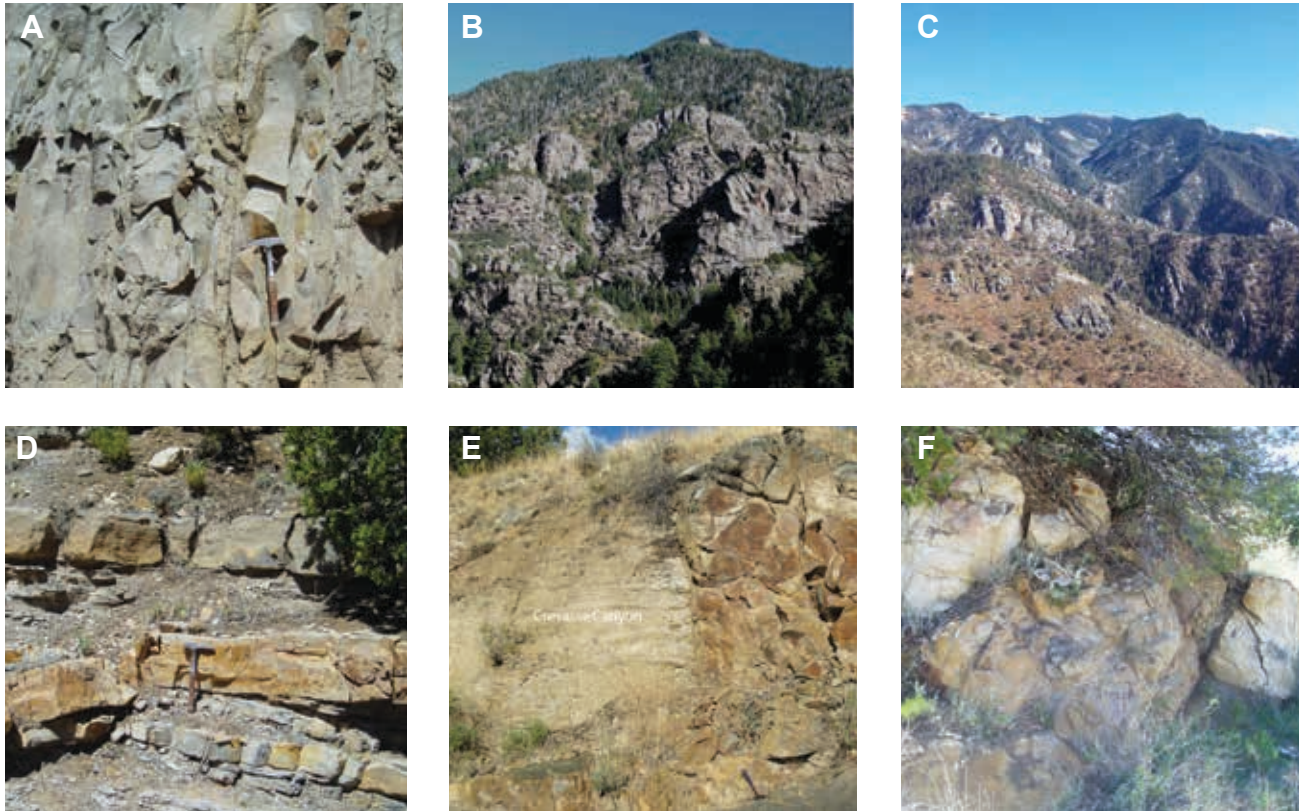


Figure 17—Photographs displaying intrusions of the Sierra Blanca volcanic field. **A.** Close-up photo of the syenite sill capping Willow Hill; rock hammer for scale. **B.** and **C.** The fractured Three Rivers stock, as exposed in Three Rivers Canyon area. **D.** Thin trachyte sill cutting across limestone beds in the Mancos Shale; exposure lies on the southern slopes of Baxter Mountain, west of White Oaks. **E.** Basaltic dike intruding sandstone of the Crevasse Canyon Formation. **F.** Altered dike cross-cutting a felsic sill on the southern slopes of Baxter Mountain.

These rocks commonly have flow breccias at the tops and bottoms of individual lava flows. The sedimentary rocks consist of gray to red, well-cemented sandy conglomerate and clayey-pebbly sandstone derived from eroded lava flows (Fig. 16).

Springs are common in volcanic rocks in the Sierra Blanca high country and feed perennial streams in the Ruidoso area. Springs are locally found in canyons that drain the lower western slopes. Spring locations in the Sierra Blanca highland commonly coincide with flow breccias at the bottoms or tops of lava flows (Fig. 16). The flows themselves are variably fractured, although the degree of jointing is commonly masked by weathering- or root-induced fracturing and heavy vegetation. Fracture density of volcanic rocks increases along fault zones. This inference is based on the observation that fault zones typically coincide with canyons; presumably, the high degree of fracturing along fault zones facilitates localized erosion and canyon

incision. Fracture zones alongside faults may be an important pathway in transporting high-mountain recharge into sub-volcanic, Eocene and Cretaceous, sedimentary strata.

Sierra Blanca igneous intrusions—A variety of igneous intrusions are found in the Sierra Blanca volcanic field (Fig. 17). Intrusions decrease in abundance outward from Sierra Blanca and include large bodies (stocks) of crystalline rocks and sills. This volcanic field also contains thousands of igneous dikes that extend outward from former volcanoes. Because the volcanoes were clustered in what is now the Sierra Blanca highland, the regional dike trend forms a radiating pattern away from Sierra Blanca. Large intrusive bodies are generally felsic (syenite to granite); dikes and sills are composed of basaltic, andesitic, and felsic igneous rocks.

The physical properties and extent of intrusions in the study area are important for

understanding groundwater flow. Fractures in large intrusive bodies, such as those underlying Sierra Blanca Peak, appear to extend at least hundreds of meters (>1000 ft) in some areas and probably facilitate deep recharge. Meinzer and Hare (1915) noted that sills in the Carrizozo area acted as groundwater aquitards, with the groundwater table forming step-like geometries (in a profile view) over a given sill.

Field observations from recent geologic mapping efforts indicate a less simplistic view of the roles of sills and dikes in groundwater flow (Koning et al., 2014). Fractured dikes and sills may act as preferential groundwater pathways when surrounding strata is of relatively low permeability, such as in the Mancos Shale. An example is Kitty Spring (TB-1009), which flows directly out of fractures in a >50 m- (>160 ft)-thick sill that intruded Mancos Shale (Fig. 18).

However, dikes and sills appear to act as groundwater barriers or aquitards where hosted by hydrostratigraphic units with higher hydraulic conductivities. This is seen at Milagro Springs (TB-1011), which flows out of the upper Crevasse Canyon Formation immediately up-gradient of a sill-dike complex (Koning et al., 2014). In addition, the northern limit of seeps associated with Anchor Spring, located 4 km west of Carrizozo, is clearly controlled by the presence of a northwest-trending dike (Koning et al., 2014).

Basin-fill (QTBF) (late Paleogene through Quaternary Periods)—The basin-fill unit includes weakly to well consolidated, non-to strongly cemented sediment that fills the Tularosa Basin and underlies most of the Carrizozo hilly plain region (Fig. 14). Basin-fill is thickest in the Tularosa Basin, where it is likely as old as late Oligocene at depth. Basin-fill is 900–1200 m (3000–4000 ft) thick in the Tularosa area (Peterson and Roy, 2005; Healy et al., 1978; Orr and Myers, 1986) but likely thins northward. Inspection of well data in the Tularosa and Alamogordo areas indicates that the basin-fill contains an upper, 30–140 m-thick (100–450 ft-thick), coarser subunit that overlies a somewhat finer-grained subunit (Fig. 9).

Both the lower and upper subunits become finer-grained with increasing distance from the mountain front (Fig. 9). Sand and gravel dominate within 1–2 km (0.6–1.2 mi) of the mountain front. Westward, tongues of sand and gravel (amalgamated channel-fills) occur within clayey-silty fine sand and the extent and number of these tongues likely decrease in a basinward direction. Groundwater preferentially flows in these coarse-grained tongues and they have greater groundwater yields (Shomaker, 2005, unpublished consultant report on the La Luz well field). High permeability, eolian sand units are likely in the subsurface in the Three Rivers area and west of Tularosa. Eolian sand



Figure 18—Illustration of how dikes can preferentially conduct groundwater if the surrounding strata are less permeable. In the two photographs depicted here, the less permeable strata surrounding the dikes consist of Mancos Shale. The dikes originally consisted of hornblende- and biotite-bearing trachyte but have been significantly altered by hot water after their emplacement (hence the orange oxidation colors). Note how the hydrothermal waters did not notably alter the Mancos Shale, which still retains its gray color. Rather, the flow of the hydrothermal waters, and resulting alteration, appears to have been restricted to the dikes because the dikes were more permeable than the Mancos Shale.



Figure 19—Photographs illustrating various features of the basin-fill hydrostratigraphic unit that are relevant to groundwater flow. **A.** Gravelly alluvium deposited by Three Rivers drainage. High-permeability gravel intervals increase towards the mountain front and extend farther away from the mountain-front where they are associated with large drainages (e.g., Three Rivers and Tularosa Creek). **B.** Gray gravel of a channel-fill complex (arrows) inset into older, slightly clayey-silty, light orange sand. The gravelly sediment would be expected to have higher permeability than the silty-clayey sand, but the inset relations would result in highly directional, anisotropic horizontal flow. Measuring tape is 2 m long. **C.** Gray gravel of Pleistocene basin-fill overlying a clayey bed; this illustrates the lithologic variability in the basin-fill that would result in anisotropic vertical flow. **D.** The basin fill fines away from the mountain front. This photograph illustrates fine-grained basin-fill 7–8 km (4.3–5.0 mi) northwest of Tularosa, on the north bank of the present-day channel of Tularosa Creek. Measuring tape is 2 m (6.6 ft) long. **E.** Strongly developed calcic-gypsic soil horizons on the north bank of Jackson Draw, overlain by a soil horizon of illuviated clay. Such strongly developed soils would affect flow in the vadose and saturated zones. **F.** Cave likely created by dissolution of buried gypsum layers (solution channels). Such caves and sinkholes are abundant on the Tularosa alluvial fan >6 km (>3.5 mi) southwest of downtown Tularosa. The solution channels may be partly filled by porous material (Meinzer and Hare, 1915, p. 102), would result in relatively high groundwater flow velocities, and may feed springs to the west of the study area (e.g., Lost River).

in the latter is largely composed of gypsum; dissolution of this gypsum has created caves (possibly subjected to post-dissolution sedimentation) and sinkholes that may result in highly directional, relatively rapid groundwater pathways. In the Tularosa Basin, deep subsurface bedrock strata likely dip towards the Alamogordo fault and dip magnitudes likely increase with depth. This dip would influence groundwater flow and in the center of the basin may facilitate spring discharge from confined, east-dipping beds.

On top of the younger, coarser subunit lies <10 m of Holocene sediment, including

Holocene-age alluvium, eolian and sheetflood-slopewash sediment. Except for sandy eolian deposits, Holocene sediment is generally finer-grained and browner than older, Pleistocene units, into which it is commonly inset. Holocene deposits are generally unsaturated and not described in detail here (see Koning et al., 2014).

Valley-fill (QUAL) (Quaternary)—This hydrostratigraphic unit correlates to the younger, coarser basin-fill unit described above. It is differentiated from basin-fill where it underlies the floors of relatively narrow, <0.5 km (0.3 mi) wide valleys.

Springs

Springs are the primary source of water for many streams in the area that drain into the Tularosa Basin. Seventy springs were inventoried in this study, of which thirty-five were sampled (Fig. 4, 12). Spring discharge rates are generally low, less than 0.013 cfs (6 gallons per minute (gpm)), however, there are five that have discharge more than 0.22 cfs (100 gpm). Spring discharge rates were measured using a bucket and stopwatch method, or estimated by eye. Whereas on the eastern side of the Sacramento Mountains the vast majority of springs were confined to the high mountains (80% above 7400 ft), springs on the western side are more evenly dispersed (80% above 5200 ft). The majority of the springs are located in the high mountains and hilly plains regions; 40% in the NHM, 30% in the SHM, and 27% in the CHP (Fig. 21). The geologic unit with the highest density of springs is the volcanic rocks found in the NHM (29%); the Yeso Formation in the SHM has the next highest number of inventoried springs (19%). Twenty percent of the springs discharge from Quaternary alluvium and are evenly dispersed in the northern high mountains and Carrizozo hilly plains (Table 2).

Table 2—Number of wells and springs located in each hydrostratigraphic unit.

Hydrostratigraphic unit	Wells	Springs
Beeman/Holder Formations	3	2
Bursum Formation	0	0
Abo Formation	13	3
Yeso Formation	1	13
San Andres Formation	3	0
Clastic rocks (Permian, Triassic, Cretaceous Periods)	5	3
Late Cretaceous Marine Shales	5	1
Gallup Sandstone; Lower Crevasse Canyon Formation	24	0
Clastic rocks (Late Cretaceous Period; Eocene Epoch)	59	8
Sierra Blanca volcanics & intrusive units	48	20
Basin fill	79	5
Valley fill	22	14
Others	6	1

The emergence of springs is heavily controlled by the geology of the area, typically discharging above impervious units, or from fractures in bedrock. Springs in Sierra Blanca volcanic rocks typically have higher flow rates. Presumably the highly fractured nature of the volcanics contributes to the abundance and greater discharge rate of springs in this area.

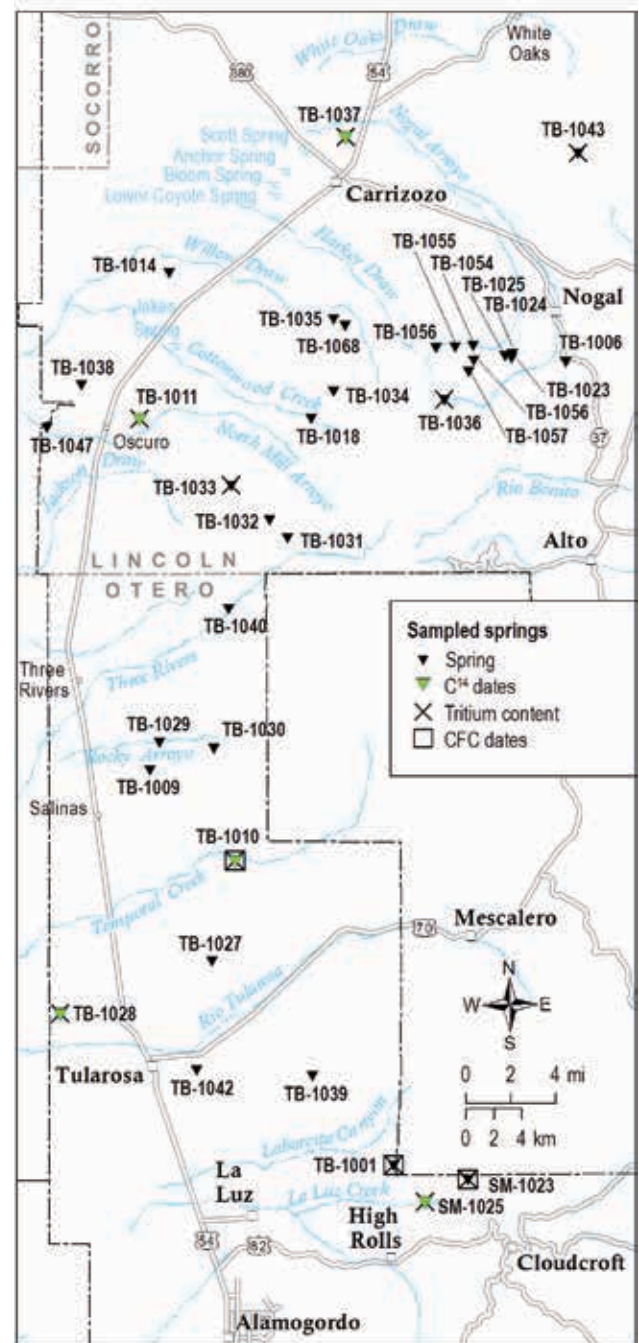


Figure 20—Location of springs inventoried in the study area, along with what sample analysis was performed.

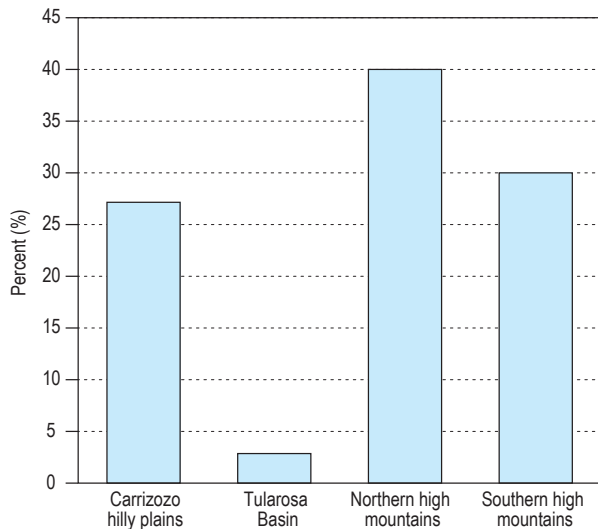


Figure 21—Percentage of total springs inventoried for study by topographic location.

Volcanic intrusions, where they are un-fractured, can also act as a barrier to groundwater flow. There are numerous seeps west of Carrizozo which are clearly controlled by the presence of a northwest-trending dike and discharge from the clastic rocks of the Late Cretaceous Period and Eocene epoch (Koning et al., 2014).

Fractures and faults in other lithologic units also play a key role in where springs emerge. These fractures allow groundwater to flow freely through the rock with little resistance. The largest spring in the area, Maxwell Spring (TB-1010), discharges near a fault in the Yeso Formation, which flows at roughly 6.7 cfs (3000 gpm) (E. Ranney, pers. commun., 2009).

Also of note is Carrizozo Spring (TB-1037), located just north of Carrizozo. This spring is unique in that it creates a local groundwater high point. Carrizozo spring discharges from Cenozoic basin-fill (QTBF), though it is likely flowing under artesian conditions from a deeper, older groundwater source.

Primary Aquifers

The primary source of groundwater varies greatly throughout the study area. In the Tularosa Basin, based on lithologic logs in water wells, the Cenozoic basin-fill (QTBF) is the primary source of groundwater (Fig. 9). This unit is made up of coarse unconsolidated streambed sediments and valley fill, mainly

cobbles, sand, and silt, making it a very productive aquifer where saturated. The average depth to water in wells sampled in the Tularosa Basin is 55 m (180 ft) on average. Basin-fill is 900–1200 m (3000–4000 ft) thick in the Tularosa area (Peterson and Roy, 2005; Healy et al., 1978; Orr and Myers, 1986). Aquifer tests show that values of transmissivity vary greatly throughout the unit, ranging from 50 to 3000 ft²/day (Garza and McLean, 1977; Orr and Myers, 1986; Morrison, 1989). As distance from the mountain front increases, the basin-fill is generally composed of finer grained, less permeable material. While it is generally treated as an unconfined aquifer, interbedded clay layers lead to partially confined conditions throughout the aquifer.

To the north in the Carrizozo hilly plains there are several available aquifers which are utilized, the most common being the Eocene-Cretaceous sediments (TKSCC), Gallup Sandstone (GLUP), Sierra Blanca volcanics (SBV), and Cenozoic basin-fill (QTBF) (Fig. 9). The average depth to water in the area is 22 m (71 ft). The majority of wells (34%) are screened in TKSCC relatively coarse-grained strata (Table 2). These include the Sanders Canyon Formation, Cub Mountain Formation, and the upper part of the Crevasse Canyon Formation. These strata are characterized by interbedded sandstone channel-fills and flood plain deposits, and are weakly to well cemented. Springs are common in sandstone intervals (e.g., Milagro (TB-1011), Jakes, and Shady Springs (TB-1034)) and field observations indicate that bedding plane, fracture, and interstitial groundwater flow occurs (Koning et al., 2014). We infer a relatively high transmissivity value of 90 ft²/day for this unit based pumping tests (Rau, 1986; Finch, 2001), the high proportion of channel-fills, thick intervals of weak cementation, and the relative abundance of springs.

The Sierra Blanca/Sacramento Mountain front to the east of the Tularosa Basin has the highest number of springs in the area, and the fewest wells. In this report the mountains are divided into two sections; the northern and southern high mountains. Sixty percent of wells in the NHM are screened in the Sierra Blanca volcanic rocks and sediment. The median depth

to water is relatively shallow, roughly 21 m (69 ft) deep. These igneous rocks are permeable only where they are fractured, and they generally yield only small amounts of water to wells. This makes it difficult to make estimations for flow from these volcanic aquifers to the basin floor. The main way in which this unit is believed to contribute to the basin is via springs which discharge into streams that flow to the valley floor.

The aquifers available west of the escarpment in the Sacramento Mountains are different from the eastern side studied by Newton et al. (2012). Wells in the southern high mountains (SHM) are primarily (47%) completed in the Abo Formation. The Abo formation is composed of fluvial deposits dominated by mudstone, as well as sandstone and conglomerate. The discontinuous sandstone and conglomerates in the Abo Formation form localized aquifers. The median depth to water in this area is 27 m (87 ft). While the Abo Formation is not the most productive aquifer, it is the most prevalent in the region west of the escarpment. This is in contrast to the Sacramento Mountain report (Newton et al., 2012), which found the Yeso Formation to be the primary aquifer east of the escarpment.

Groundwater Flow Conditions

To understand groundwater flow within and surrounding the northeastern Tularosa Basin region, a water elevation surface was developed (Fig. 22; Land et al., 2014). Contours of the regional water-level elevation in the study area were drawn by hand based on water-level measurements made between 2009 and 2011. Water-level elevations from wells were combined with spring elevations and valley floor elevations. Where these data were not available, static water levels were used from recent New Mexico Office of the State Engineer well records (Appendix 2). No attempt was made to distinguish between perched and regional aquifers. The hydrologic gradient was estimated by measuring the distance between the water-level contours. The general trend that can be seen from the water-level contours is that groundwater flow is driven by the topographic gradient from high to low elevation (Fig. 22), or from east to west.

The complex geology of the area plays a major role in groundwater flow patterns. In the southeastern portion of the study area, the SHM are composed of Paleozoic sedimentary rocks, while the NHM are dominated by younger Neogene volcanics. Running north-south, to the west of the mountains, is the Alamogordo fault. This is a normal fault and it is responsible for the down-dropped basin floor, which resulted in a steep mountain front compared with the more gently dipping strata on the eastern side of the southern Sacramento Mountains (Newton et al., 2012). These geologic conditions lead us to classify the western flank of the mountains as a Mountain-Front Recharge zone. Because of the steep slope the majority of the precipitation that falls on the western side of the mountains does not infiltrate into the aquifers, as it does on the eastern side. Instead, precipitation results in runoff that quickly drains into the Tularosa Basin, as Mountain-Front Recharge (MFR). MFR is a predominant source of recharge to basins in arid and semiarid regions, however it is also very difficult to quantify (Wilson and Guan, 2004). Uncertainty stems from climate variability, anthropogenic disturbances, and the geologic complexity often associated with these conditions.

Evidence of MFR can be seen by water table mounding near the mouths of drainage basins. This effect can be seen most clearly in the Three Rivers drainage and where it discharges into the Tularosa Basin. In the upper reaches of Three Rivers the water table is sloping toward the river, creating a “V” shape which points up gradient, indicating that water from the surrounding rocks drains into the river (Fig. 23). This section of the river is classified as a gaining system, which is reinforced by the springs which discharge along the incised river bed. As the river enters the basin, however, the water table is inverted and points down gradient, creating a mounding effect (also seen on Fig. 9). This change in gradient indicates that water from the stream is now infiltrating into the aquifer, and is identified as a losing system. The transition occurs just as the river crosses the Alamogordo fault and flows over the more conductive basin-fill sediments.

Groundwater flow in the NHM is heavily influenced by the volcanic intrusions. Volcanic

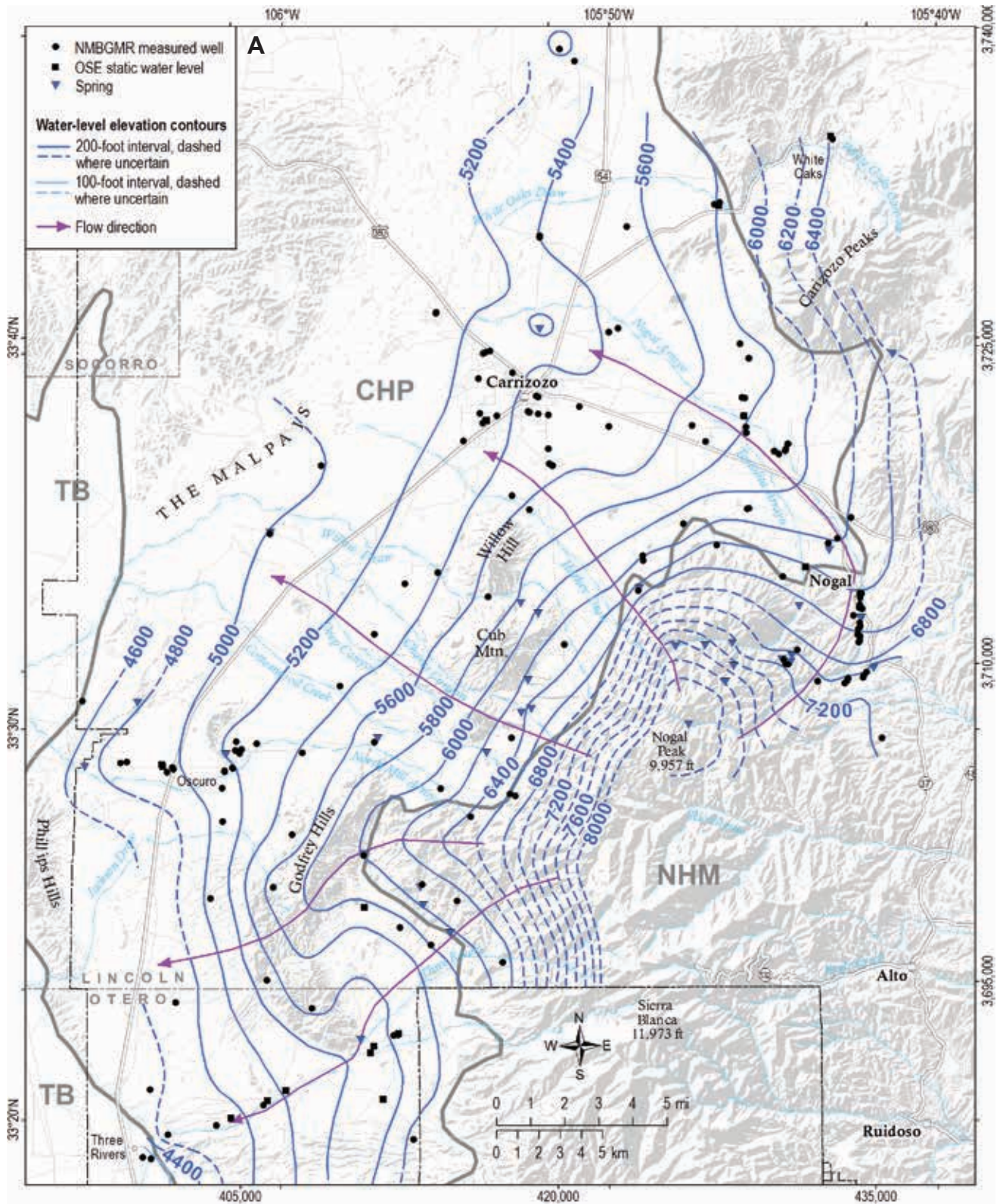


Figure 22A—Water table surface map for the northeastern region of the Tularosa Basin. Average water-level elevation contours (in feet) show the regional groundwater movement is controlled by topography. Groundwater flows from the eastern escarpment to the lower elevations to the west. Contours do not distinguish between perched and regional aquifers. The actual direction of groundwater flow at a local scale, particularly in the high mountains, may differ from that indicated by the regional elevation contours due to lithologic heterogeneities, the presence of regional faulting and intrusions, and variations in topographic relief. (Land et al., 2014).

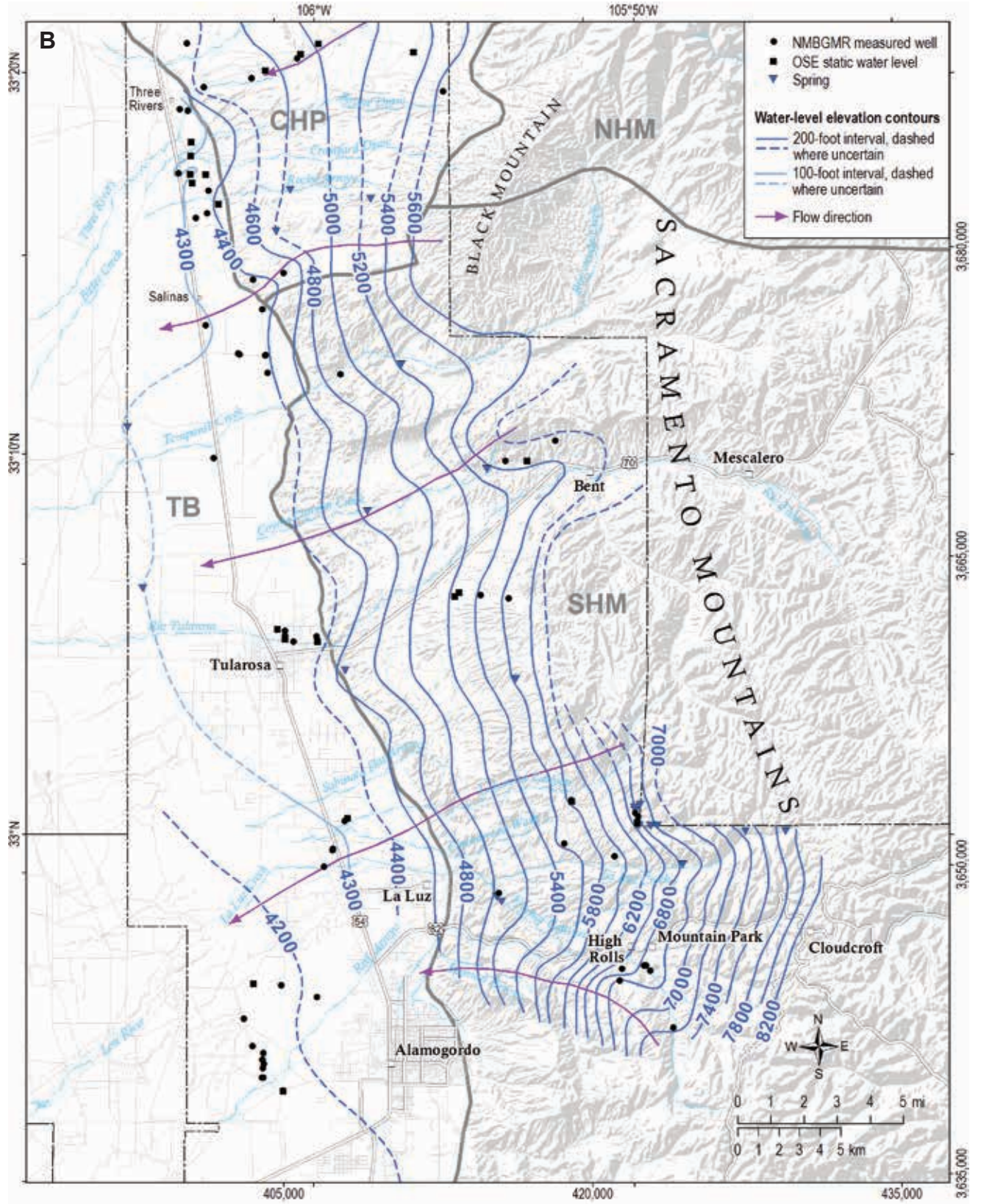


Figure 22B—Southern region water-level elevation contours.

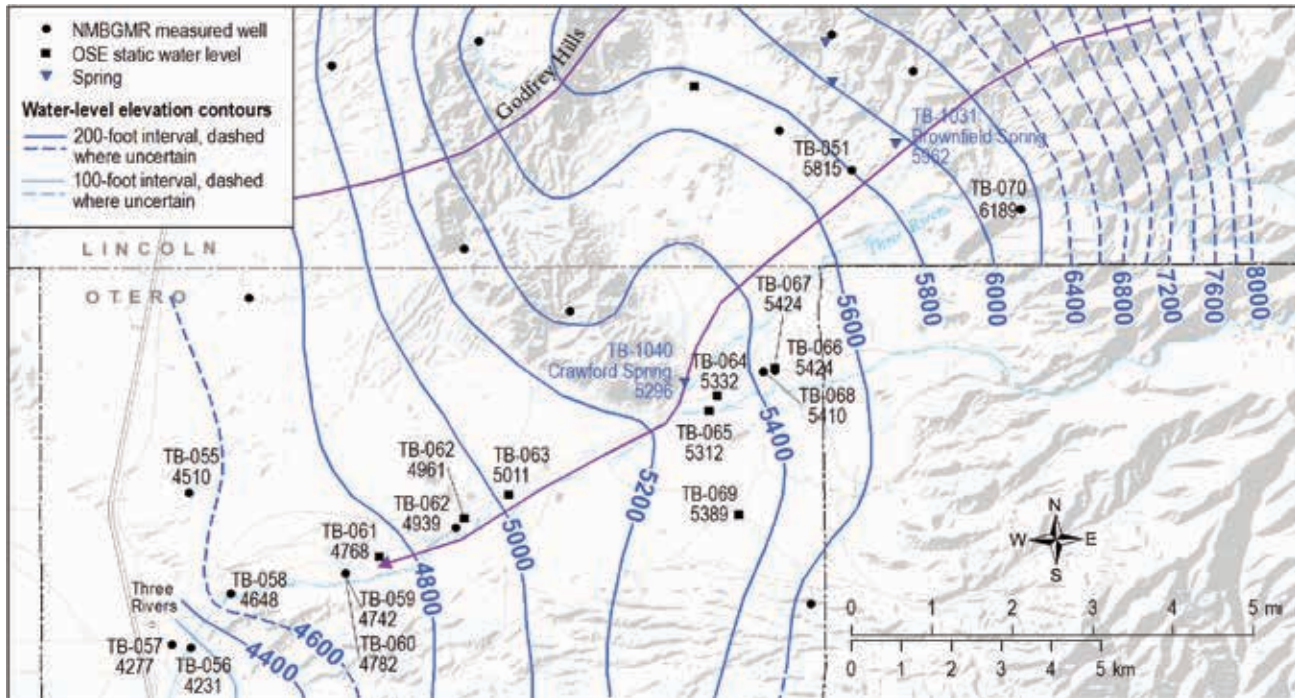


Figure 23—An expanded view of the water table in the Three Rivers drainage (Land et al., 2014).

rocks make very poor aquifers as spaces between the individual mineral crystals of igneous rocks are microscopically small, few, and generally unconnected; therefore, porosity is insignificant. These igneous rocks are permeable only where they are fractured, and they generally yield only small amounts of water to wells. Where wells intersect a fracture, however, they can be highly productive. Nogal Creek, which drains the igneous rocks of the Sierra Blanca highlands, is an ephemeral stream that flows into the CHP. To the east of Carrizozo there is a north-south trending normal fault that results in a sudden increase in depth of the permeable aquifer under Carrizozo. This permeable unit pinches out just west of Carrizozo as the less permeable aquifers slope up to the surface (Fig. 9a). As a result, this fault is responsible for a very shallow and flat water table at the mouth of the Nogal Creek drainage under Carrizozo (Fig. 22).

In SHM on the eastern side of the Sacramento Mountains escarpment, water flows eastward toward the Pecos Slope through the Permian age Yeso Formation (Newton et al., 2012). On the western escarpment, however, water flows through the Pennsylvanian and Permian age units (ABO, BRSM, HLDR, BEMN,

GBLR) (Fig. 9d). The water table slopes steeply to the west, with a hydraulic gradient of roughly 350 feet/mile at higher elevations. This steep gradient reflects the very low conductivity of the Paleozoic sedimentary rocks which make up the SHM. The fractured nature of these units coupled with very few hydraulic conductivity measurements makes it difficult to estimate groundwater flux through the mountain-block. The water table flattens out dramatically as it crosses the Alamogordo fault. On the western side of the down-dropped fault is the basin-fill aquifer, which has a significantly higher hydraulic conductivity. All of these factors contribute to the water table's low gradient of roughly 30 feet/mile in the basin (Fig. 22).

Water-Level Changes and Hydrographs

To better understand the hydrodynamics and physical properties of the various aquifers we looked for patterns in the changes in water levels in wells and how they relate to different aquifers and topographic settings. Records were collected with continuous data loggers in ten wells, and bimonthly from approximately 100 wells between August 2009 and July 2011. These records show

four main trends: pumping, recharge, decline and no change (Table 3, Figs. 24, 25, Appendix 6).

Pumping Trend

Tularosa and Alamogordo have experienced extensive groundwater pumping over the past 100 years. Hydrographs from pumping wells closely follow the agricultural cycle of the area. The wells that show a pumping signal are most often located in the Tularosa Basin, at an average elevation of 1387 m (4550 ft). Depth to water in these wells is on average 53 m (175 ft) below ground surface. The majority of pumping trend wells (80%) are screened in basin-fill (QTBF). When the growing season starts and farmers begin to water their fields, the water levels decrease from their highest point in March. Water levels decrease throughout the rest of the summer months, reaching their lowest point in September. The majority of the drawdown seems to occur in the spring. The monsoonal

rains begin in July, resulting in less groundwater pumping. As a result, the water levels decline more slowly with additional variation in the hydrographs near the end of the growing cycle. In September, when the growing season ends, the pumps are shut off and the water level quickly rebounds through December and begins to level out by March, before pumping resumes once again (Fig. 26). On average, there is 1.2 m (4 ft) of fluctuation between maximum drawdown and recovery, though the maximum rebound during the study period was 3.7 m (12 ft). Sixty-three percent of pumping hydrographs show groundwater depletion, meaning groundwater levels did not fully recover from 2009 to 2010, with an average deficit of 9 cm (0.3 ft).

Two wells that exhibit agricultural pumping records were instrumented with high precision pressure transducers, which accurately record water levels in the well on an hourly basis. Comparison of the water levels in these wells with

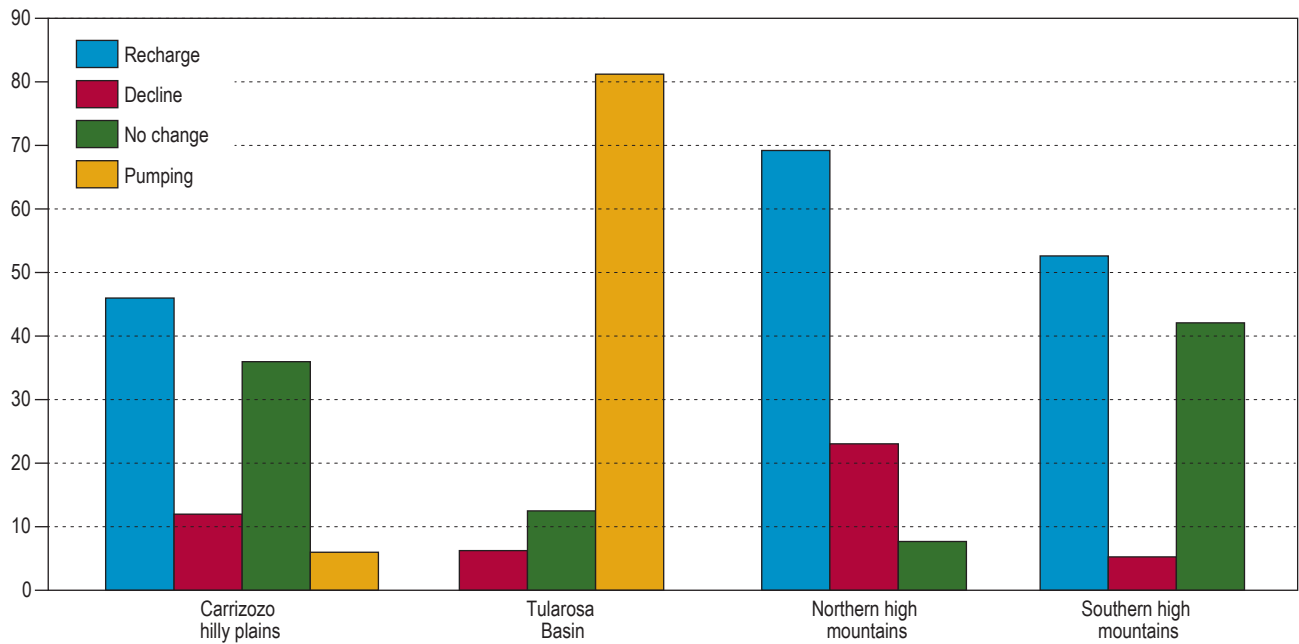


Figure 24—Bar graph showing the percent of wells within of each hydrograph trend by topographic location.

Table 3—Number of wells with distinct hydrograph trend in each hydrostratigraphic unit.

	QUAL	QTBF	SBV	TKSCC	GLP	MNCS	KTRP	SNAN	YESO	ABO	GBLR	HLDR	BEMN
Decline	1	4	2	2	0	1	0	0	0	0	1	0	0
No change	1	4	2	4	6	2	2	1	0	5	2	0	0
Pumping	1	13	0	0	1	0	0	1	0	0	0	0	0
Recharge	6	4	9	11	4	0	0	0	0	3	2	1	2

the atmospheric pressure recorded at the ground surface reveals an inverse relationship (i.e. when the atmospheric pressure rises, the water level in the well drops) (e.g. Fig. 27). In both wells the magnitude of the water level change is about two-thirds of the atmospheric changes. This indicates the aquifer in which these wells are screened is confined. An aquifer that is confined has a less permeable layer above and below it. As result, water cannot move up or down from the confined unit. Determining that the aquifer is confined tells us that recharge likely does not occur in the vicinity of the well. Water instead enters the aquifer some distance away in the high mountain recharge areas or at the alluvial fans in the foot of the mountain front.

Recharge Trend

Recharge trends are defined by hydrographs that show monsoonal precipitation or snowmelt (Fig. 26) entering the aquifer, leading to a rise in water levels. This can be very difficult to determine as the water level rise associated with recharge occurs at roughly the same time as the rebound period in pumping wells. Wells which show recharge are typically completed in hydrostratigraphic units TKSCC (22%) and SBV (26%). In general, wells that demonstrate recharge are at higher elevations, with 80% greater than 1830 m (6000 ft), and depth to water is relatively shallow, averaging 23 m (75 ft). Wells along the upper Nogal Creek responded strongly to the heavier snow fall during the winter of 2009–2010, with steep water level rises of approximately 3 m (10 ft) on average over a 3 month period (Fig. 26). The proximity of the wells to Nogal Creek suggests they are closely linked to the baseflow in the stream. The abrupt rise, coupled with the equally

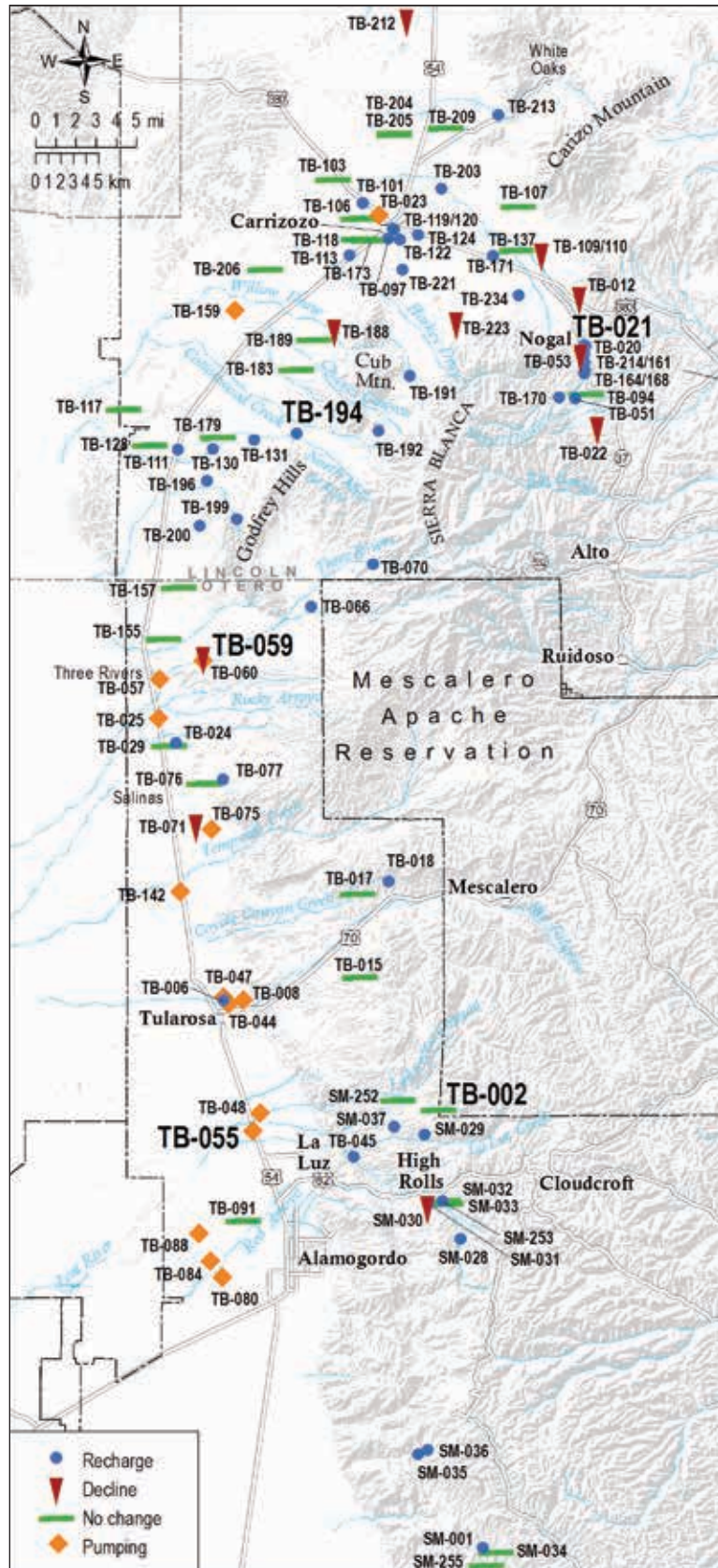


Figure 25—Map indicating the location of wells that were used in the hydrograph analysis, with corresponding trend. Locations of example hydrograph trends (Fig. 26) are enlarged.

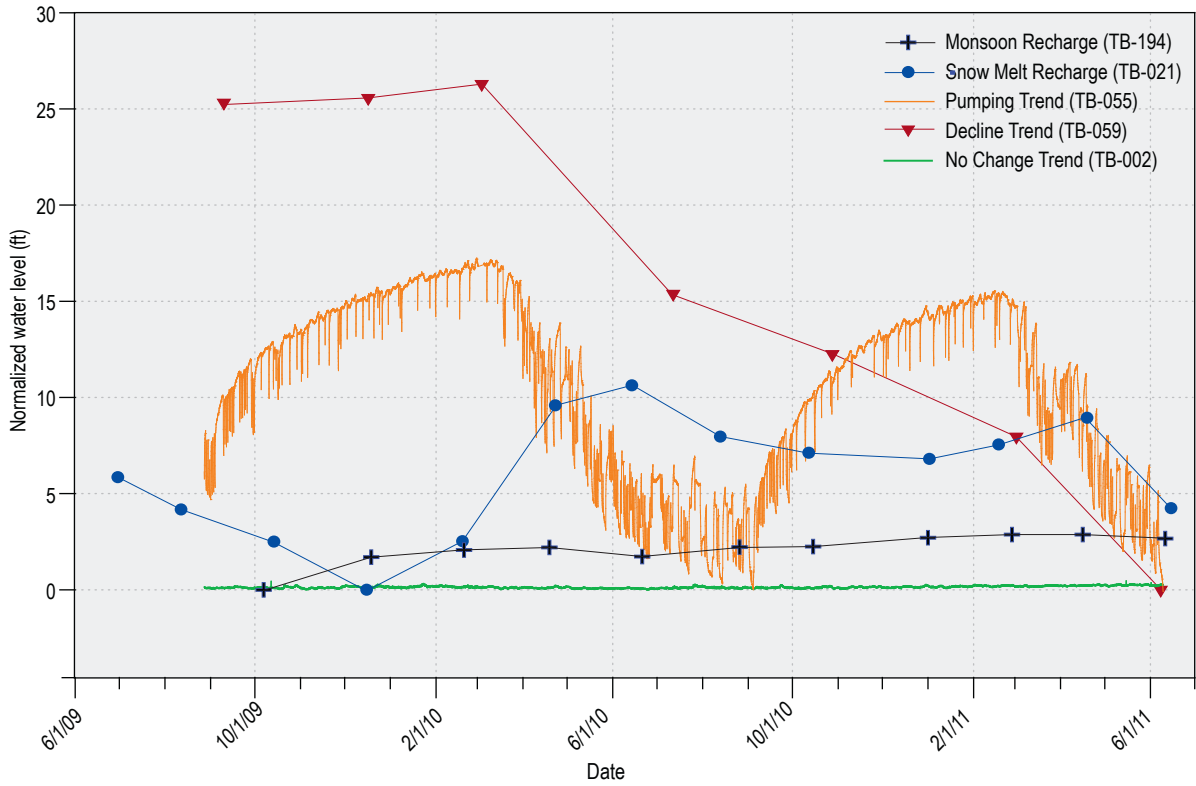


Figure 26—Examples of the four major trends seen in well water levels throughout the study period: recharge, pumping, decline, and no change.

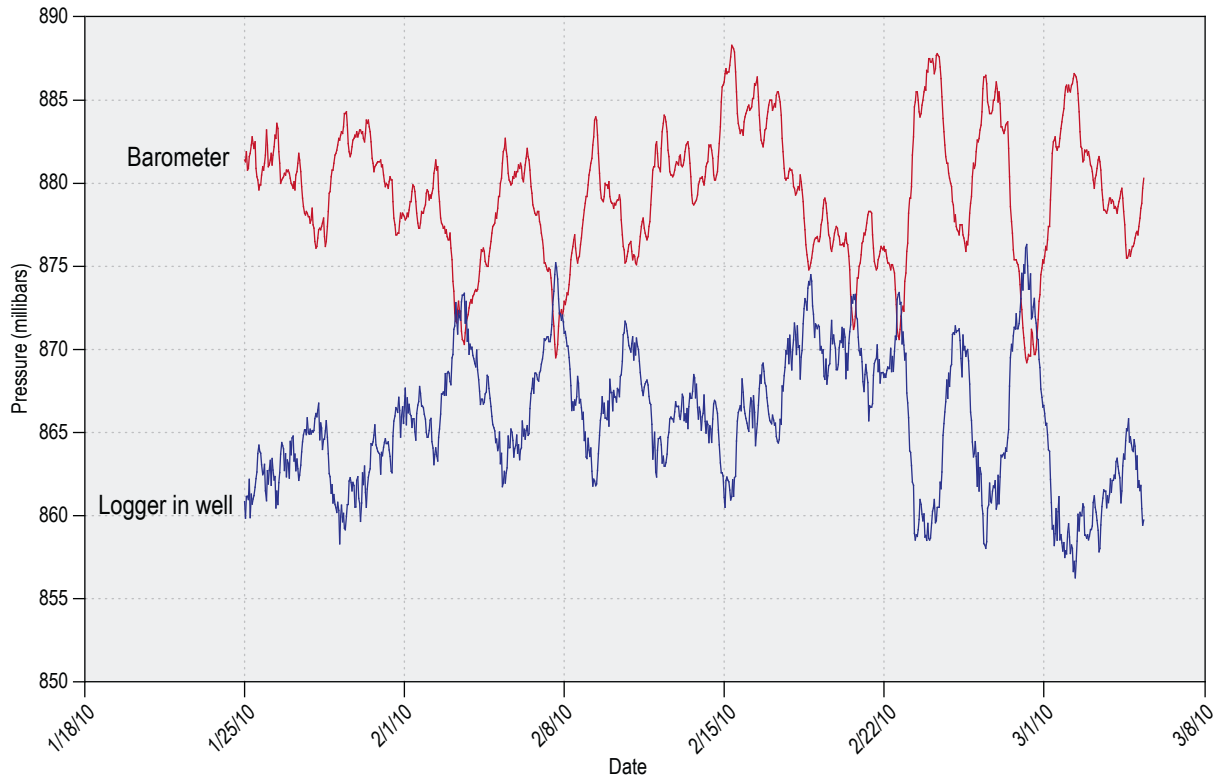


Figure 27—Comparison of the water levels with the atmospheric pressure recorded at some wells reveals an inverse relationship—when the atmospheric pressure rises, the water level in the well drops and vice versa. This is an example of well (TB-055) that is screened in a confined aquifer.

steep decline highlights the low porosity and highly fractured nature of the volcanic units. As opposed to the wells near Nogal that show snowmelt recharge, the well field in the vicinity of Carrizozo also has a significant number of recharge wells that react to monsoon precipitation (TB-097, 101, 113, etc) (Fig. 25). This is likely the result of runoff from the Nogal arroyo recharging the aquifer. These wells show a more attenuated recharge signal, generally no more than 0.6 m (2 ft) of rise.

No Change Trend

The hydrogeology of the Sierra Blanca mountain front is very complicated owing to the vast number of faults and heterogeneous lithologies throughout the area. As a result, water-level trends are quite varied, and do not always fluctuate in a predictable fashion. Wells that fluctuate less than 0.3 m (1 ft) per year are defined as “no change trend” (Fig. 26). This trend makes up 30% of the recorded hydrographs in the study area (Fig. 25). The majority of wells which show no change are completed in the

Gallup Sandstone (21%), and are located primarily in the Carrizozo hilly plains.

Decline Trend

Hydrographs with decline trends are characterized by greater than 0.3 m (1 ft) of decline per year (Fig. 26). The average water level drop per year in the decline wells is 1.3 m (4.3 ft), though there is one outlier that declined 21 m (68 ft) (TB-223, excluded from calculation). This trend makes up just 11% of the hydrographs. Wells that have a decline trend are scattered throughout the study area, though the highest density is in the north, around the Nogal drainage.

WATER CHEMISTRY

For this study, we examined several different chemical components of the groundwater, and performed several measurements in the field. The complete results are compiled in Appendix 7, and summarized in Table 4. Locations of samples collected are shown in Figure 3.

Table 4—Statistical summary for chemical parameters for springs, wells and streams. The standard deviations of the datasets are listed under “STD.” In the Parameter list, specific conductance (“SC field”) was measured in the field, and “TDS” represents the total dissolved solids calculation.

Parameter	Unit	SPRINGS				WELLS				STREAMS			
		Mean	Min	Max	STD	Mean	Min	Max	STD	Mean	Min	Max	STD
Temperature	°C	14.3	4.2	28.9	6.0	18.2	10.4	28.0	3.6	17.7	9.4	25.7	5.0
pH	pH units	7.5	6.4	8.0	0.4	7.3	7.0	7.9	0.2	8.1	7.9	8.3	0.2
SC field	µS/cm	1949.0	80.0	6164.0	1363.0	2383.0	834.0	5289.0	1084.0	1584.0	560.0	5325.0	1231.0
TDS	mg/L	1765.0	53.0	6170.0	1409.0	2140.0	536.0	6200.0	1223.0	1397.0	375.0	4208.0	1403.0
Calcium	mg/L	283.0	9.0	755.0	197.0	332.0	94.0	675.0	168.0	240.0	77.0	650.0	207.0
Magnesium	mg/L	87.9	1.2	380.0	85.7	103.4	25.0	260.0	60.7	68.5	12.0	195.0	64.2
Sodium	mg/L	165.8	3.1	710.0	166.6	188.2	21.0	870.0	153.7	115.2	28.0	445.0	162.2
Potassium	mg/L	2.80	0.36	12.0	2.96	3.35	0.19	12.0	2.74	2.69	0.86	7.3	2.43
Bicarbonate	mg/L	230.0	16.0	365.0	86.0	209.0	58.0	560.0	115.0	222.0	155.0	305.0	65.0
Sulfate	mg/L	797.0	16.0	2350.0	661.0	1040.0	180.0	2600.0	631.0	666.0	130.0	2090.0	716.0
Chloride	mg/L	280.0	3.0	1780.0	365.0	300.0	20.0	1600.0	296.0	167.0	19.0	715.0	269.0
Nitrate	mg/L	3.69	0.42	14.0	3.30	9.5	0.27	110.0	20.85	1.38	0.40	2.5	1.12
Bromide	mg/L	0.342	0.018	1.4	0.347	0.382	0.040	1.0	0.241	0.153	0.033	0.46	0.155
Silicon	mg/L	11.9	4.6	22.0	4.8	12.8	6.2	31.0	5.7	10.0	7.4	13.0	2.3
Fluoride	mg/L	0.65	0.10	1.80	0.40	0.85	0.18	2.20	0.55	0.47	0.36	0.69	0.13
Iron	mg/L	0.313	0.014	1.10	0.489	0.169	0.023	0.63	0.196	0.322	0.007	0.84	0.452
Boron	mg/L	0.0899	0.005	0.29	0.0763	0.1179	0.028	0.44	0.1095	0.0733	0.015	0.18	0.073
Barium	mg/L	0.034	0.008	0.12	0.032	0.024	0.02	0.03	0.004	0.052	0.027	0.1	0.033
Nickel	mg/L	0.0067	0.001	0.01	0.0041	0.0066	0.005	0.01	0.0024	0.007	0.001	0.013	0.0085
Strontium	mg/L	4.39	0.09	14.0	3.89	5.24	1.00	14.00	3.51	3.29	0.81	8.9	2.84
Zinc	mg/L	0.0347	0.001	0.39	0.0769	0.076	0.006	0.63	0.15	0.0187	0.008	0.039	0.0176

Field Measurements

Using field instruments, we measured parameters including pH, temperature, and specific conductance prior to collecting a water sample. As shown in Table 4, for all samples, the pH ranges from 6.4 to 8.3, residing in a fairly neutral pH range. The temperature of springs is generally cool, from 4.2 to 28.9°C (4.2–84°F) with a mean of 14.3°C (57.7°F). Well water samples ranged from 10.4 to 28°C (50.7–82.4°F), with a mean of 18.2°C (64.8°F). Streams range from 9.4 to 25.7°C (48.9–78.3°F), with a mean of 17.7°C (63.9°F). One simple way to examine the ion content of a water sample is with a measurement of the specific conductance (SC). SC measured in springs ranges from 80 to 6164 $\mu\text{S}/\text{cm}$, with an average of 1949 $\mu\text{S}/\text{cm}$. In well samples, we found SC values in the range of 834 to 5289 $\mu\text{S}/\text{cm}$, but with a higher mean of 2383 $\mu\text{S}/\text{cm}$. Streams range from 560 to 5325 $\mu\text{S}/\text{cm}$, with the lowest mean of 1584 $\mu\text{S}/\text{cm}$. Springs and wells (Fig. 28), in the high mountains generally have lower SC, and therefore lower ion content.

In general the water in this region, except for high in the mountains, has fairly high levels of ion content, making the water very mineralized. This is often observed as elevated “water hardness.” In this region, the water hardness (lab calc., summarized in Appendix 7) ranges from 28 mg/L in the high mountain springs, to 3451 mg/L in lower elevation locations. The average hardness in this region is 1163 mg/L, which is extremely hard.

Major Ion Chemistry and Water Type

The ion chemistry of groundwater in this region is variable. Calcium is the dominant cation in most of the water samples collected, followed by magnesium and then sodium, in various combinations. The dominant anion in this area is sulfate, with chloride to a lesser extent. The water chemistry can be summarized spatially with Stiff diagrams and with a Piper plot, as shown

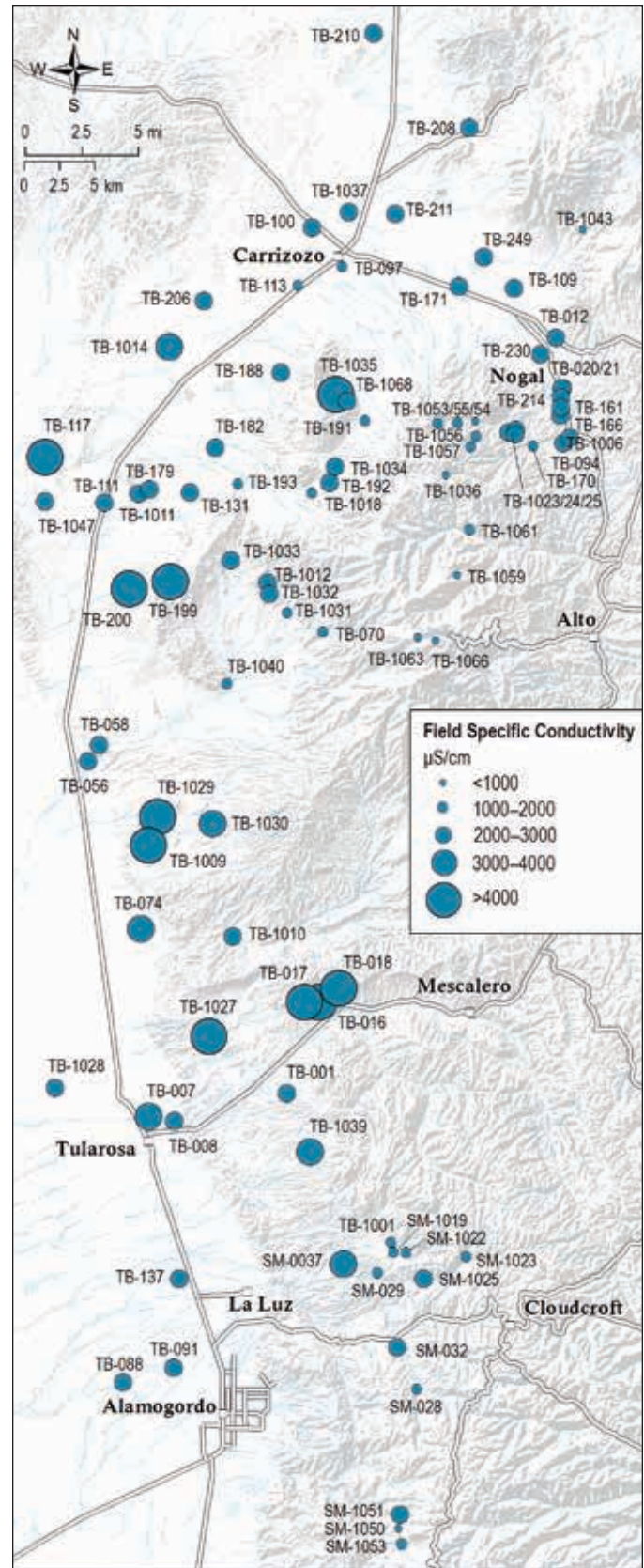
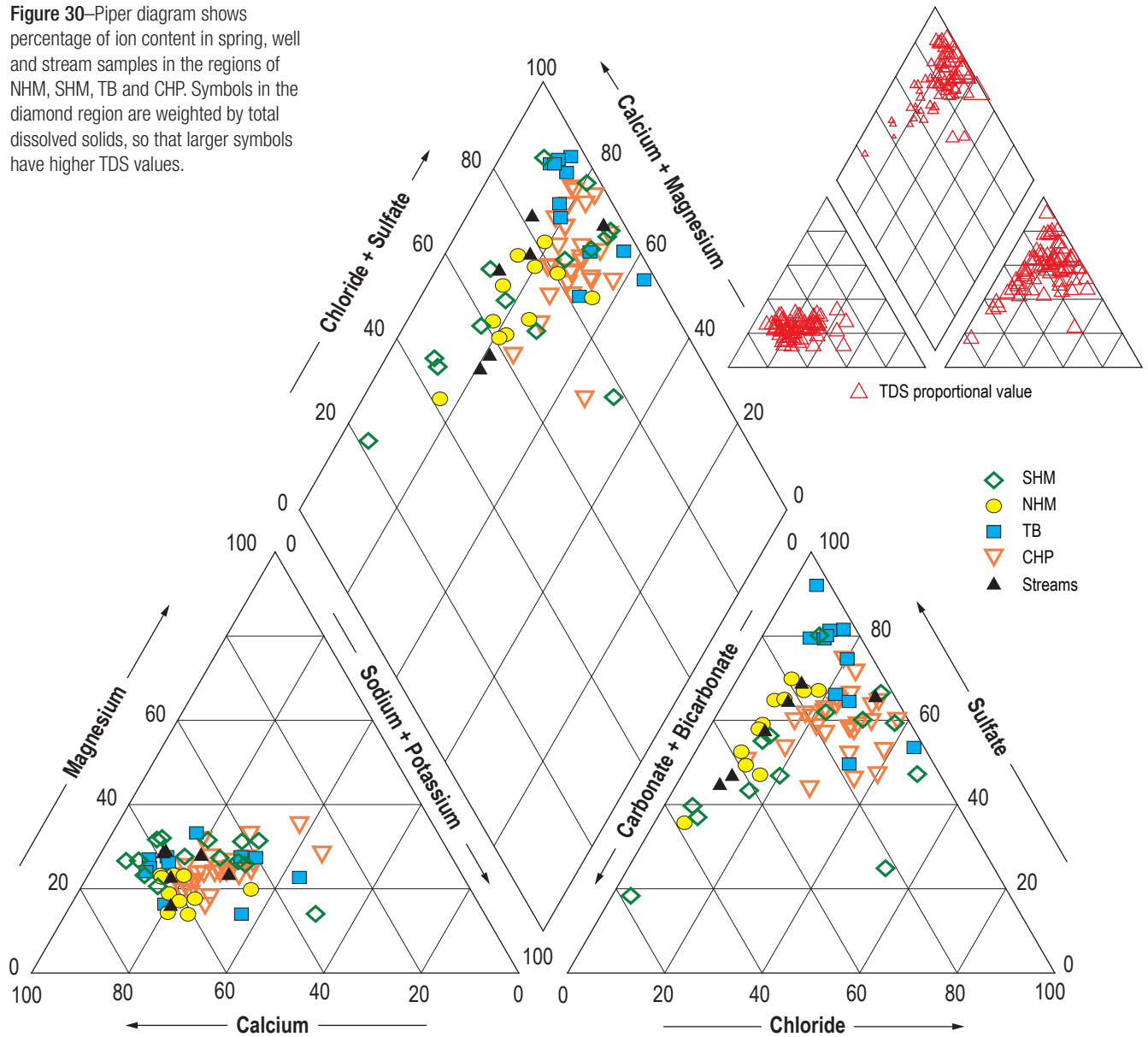


Figure 28—Map of specific conductivity measurements from field sampling locations, showing springs and wells.

Figure 30—Piper diagram shows percentage of ion content in spring, well and stream samples in the regions of NHM, SHM, TB and CHP. Symbols in the diamond region are weighted by total dissolved solids, so that larger symbols have higher TDS values.



carbonates is dominant, but silicate weathering is more common in some of the northern regions where volcanic material is more prevalent. If the molar ratio of bicarbonate to silica is greater than ten it implies that carbonate weathering predominates. However, if the ratio is less than five, then silicate weathering predominates (Hounslow, 1995). The observations of spatial trends in water chemistry are highly correlated to the geology and the flow path that the groundwater follows through the subsurface.

The chemistry data also indicates that many of the sampled waters have undergone cation exchange. We interpret Figure 33a, wherein data

largely plot along a line with a slope of negative 1, to suggest that ion exchange has occurred in these samples (Jankowski et al., 1998). Other plots, such as shown in Figure 33b, indicate dissolution of gypsum, calcite and dolomite, which indicates that carbonate dissolution from limestone is the dominant process influencing the water chemistry.

In order to assess the possibility of chloride-rich brines mixing with fresh groundwater, we examined the sodium (Na) to chloride (Cl) molar ratio in the groundwater samples. In Figure 34a, many samples have nearly a 1:1 ratio of Na/Cl dissolution of halite (salt). Samples with more

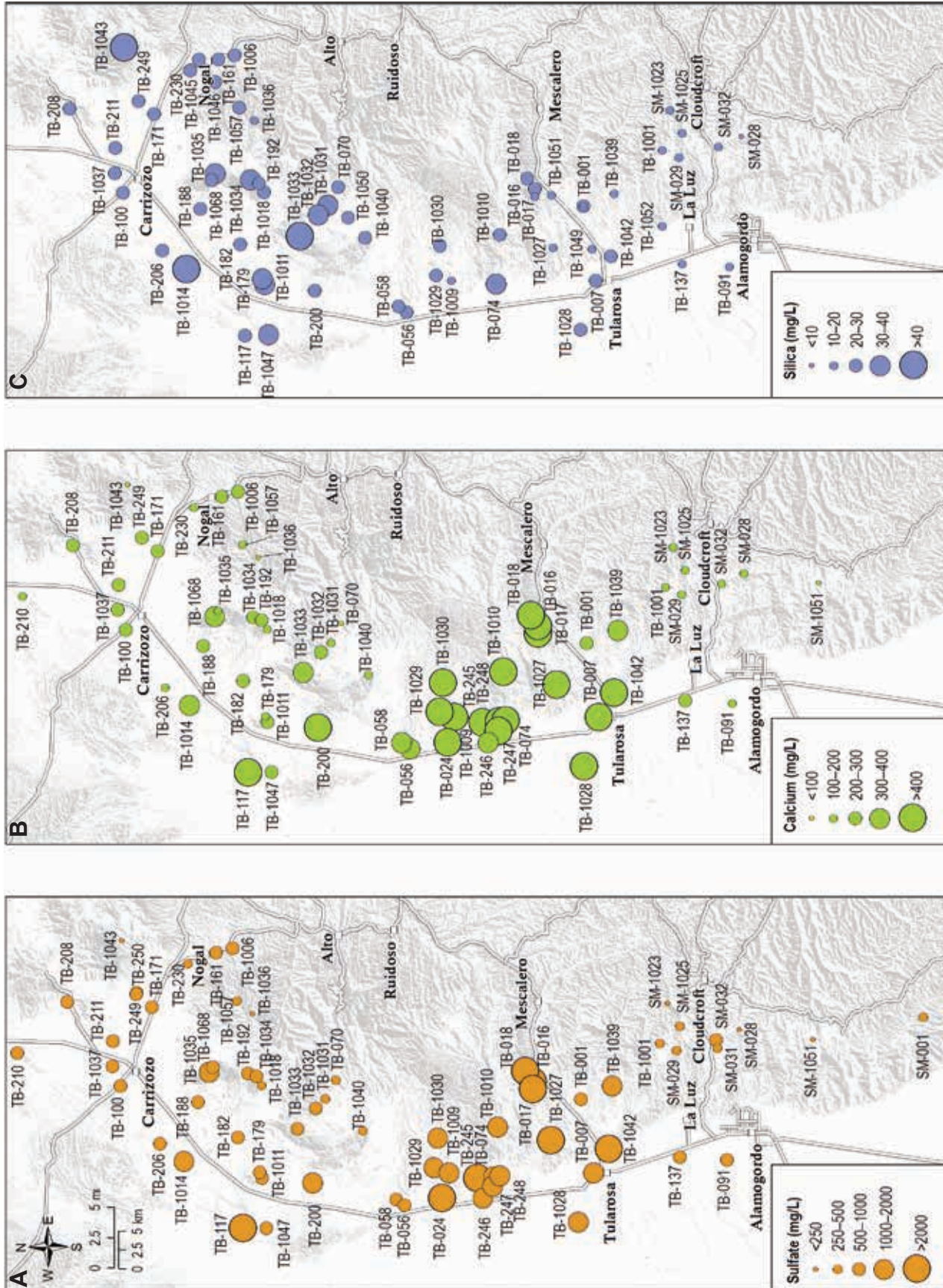


Figure 31—Map of A. sulfate, B. calcium and C. silica concentrations (in mg/L) from springs and wells in the study. The symbol sizes is proportional to concentration.

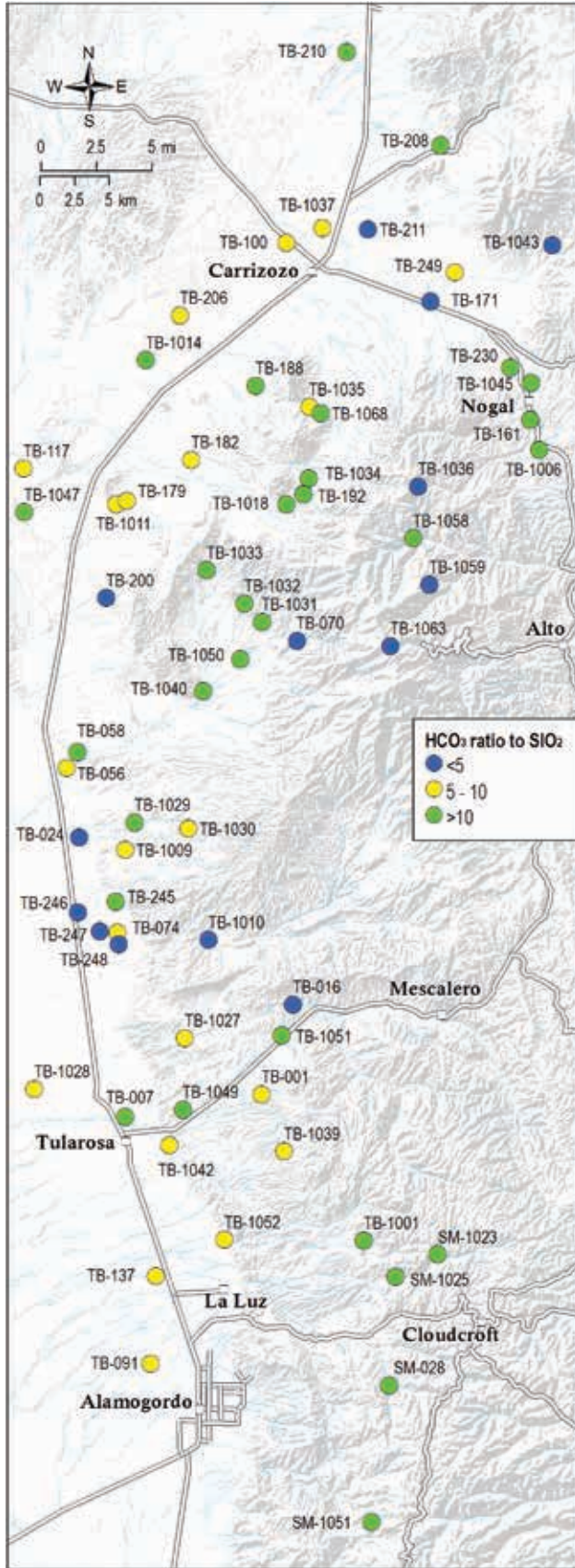


Figure 32—Map showing locations of samples color coded by the value of the molar ratios of bicarbonate/silica. Green symbols indicate the molar ratio of bicarbonate (HCO_3^-) to silica (SiO_2) is greater than 10, indicating a predominance of carbonate weathering reflected by the groundwater. Blue symbols are sites sampled where this molar ratio of $HCO_3^-:SiO_2$ is less than 5, suggesting that silicate weathering predominates (Hounslow, 1995). Beige symbols indicate locations where this ratio is between 5 and 10, which is ambiguous for either silicate or carbonate weathering.

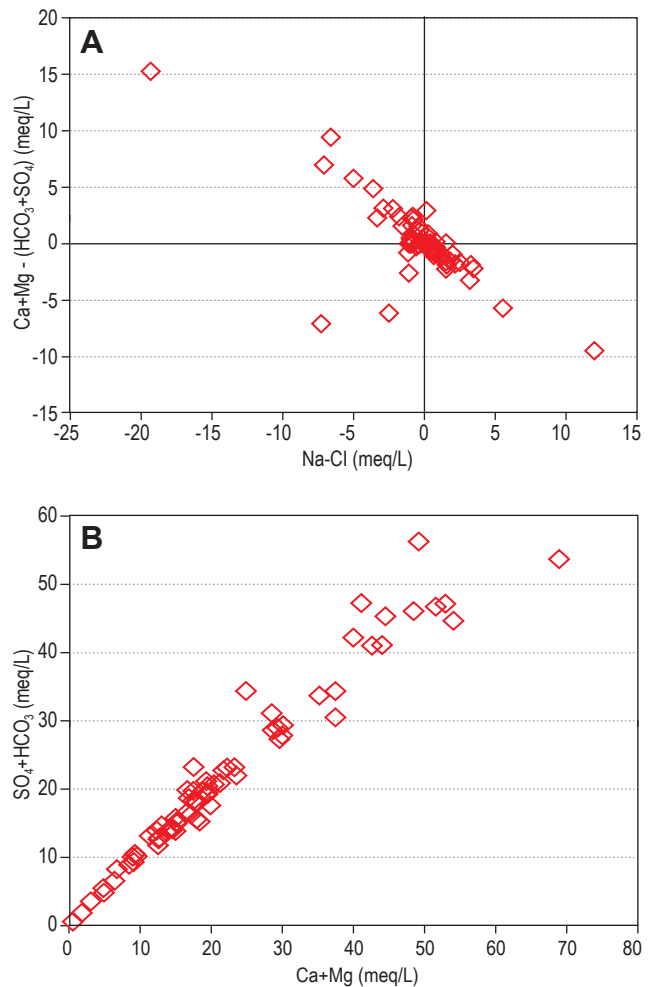
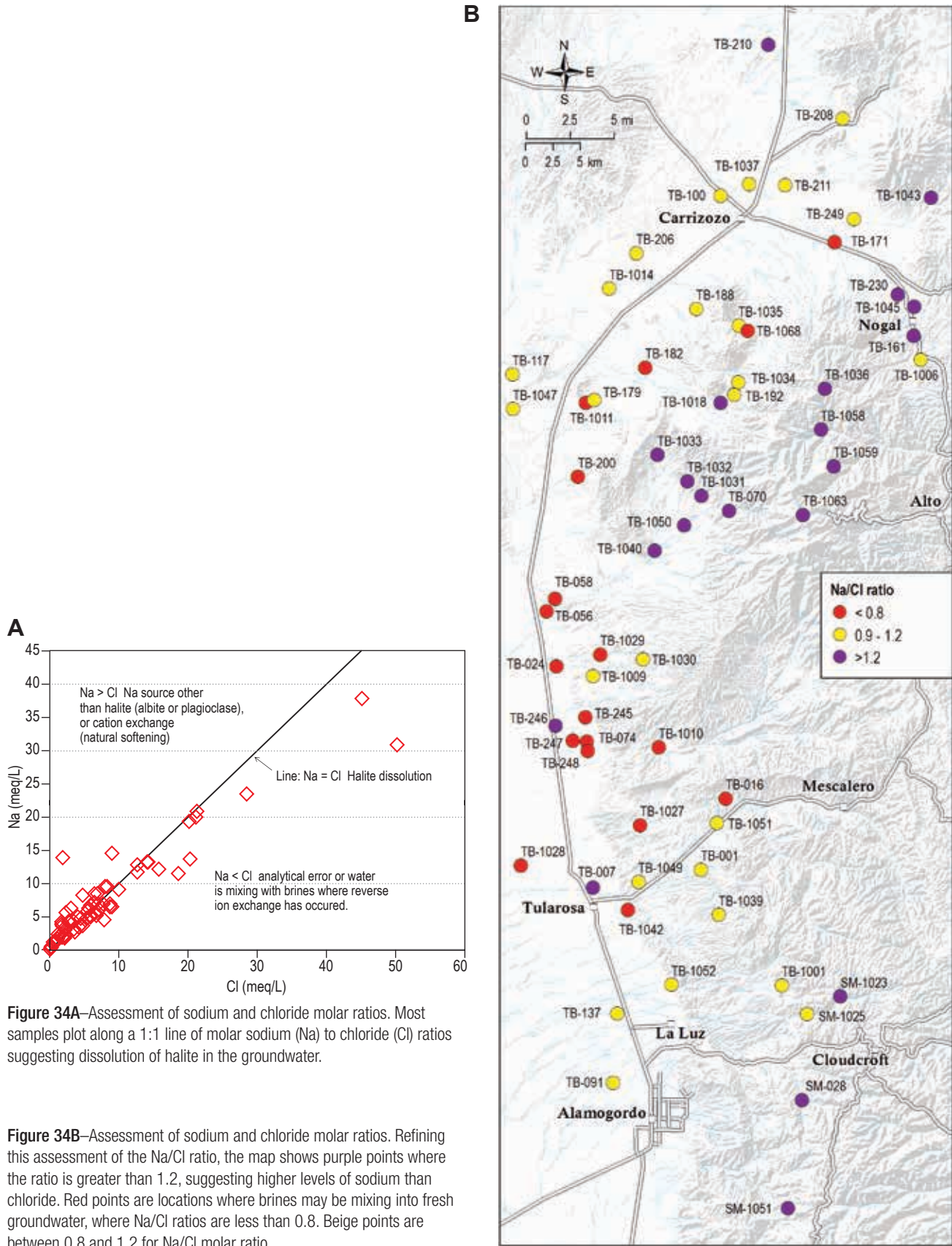


Figure 33—Water chemistry bivariate plots. **A.** Plot examining relationships for cation exchange. **B.** Plot of $Ca+Mg$ versus SO_4+HCO_3 , where the 1:1 linear relationship indicates that the dominant process is the dissolution of gypsum, calcite and dolomite is less than 5, suggesting that silicate weathering predominates.



than a 1:1 ratio (plotting above the line), with higher levels of sodium than chloride (Fig. 34b), may have undergone cation exchange or have dissolved plagioclase ($\text{NaAlSi}_3\text{O}_8$). On the other hand, samples with less than a 1:1 ratio (plotting below the line), with higher levels of chloride than sodium, likely have added chloride, a brine source. Mixing is indicated in the TB region along faults. Brines appear to be mixing into the groundwater system in regions where faults may provide a conduit for brines to rise from depth.

Stable Isotopes of Hydrogen and Oxygen

Because all groundwater and surface water in the study area is derived from precipitation in the Sacramento Mountains, it is important to characterize the stable isotopic composition of local precipitation. Figure 35 shows locations of precipitation collection sites, which were distributed throughout the study area at a range of elevations (Table 5). The linear regression of stable isotope data from precipitation defines a local meteoric water line (LMWL) for the western slopes of the Sacramento Mountains (Fig. 36) with an equation of:

$$\delta D = 7.9\delta^{18}\text{O} + 10.8$$

This equation is almost identical to the global meteoric water line defined by Craig (1961). It should be noted that the three points with positive $\delta^{18}\text{O}$ values were not used for the linear regression that defines the LMWL. These points represent samples collected in June 2011, and the isotopic compositions clearly indicate that this water has undergone significant evaporation, which likely occurred as rain drops descended through the atmosphere. Therefore, the observed isotopic compositions of these three samples do not represent the isotopic composition of atmospheric water at that time. The seasonal variability of the isotopic composition of precipitation is shown in the shaded areas of the LMWL (Fig. 36) as winter precipitation, which is a mixture of rain and snow that fell between December and March and summer precipitation, which is primarily monsoon rains that occur between June and September. Variations in the stable isotopic composition of precipitation are

probably due to two seasonal factors (Rozanski et al., 1993): 1) changing temperature and 2) changing source areas of vapor and/or different storm trajectories. In this area, the average temperature difference between summer and winter is approximately 15°C (59°F). The dominant source area of winter storms is the Pacific Ocean, while summer storms associated with the North American Monsoon originate from the

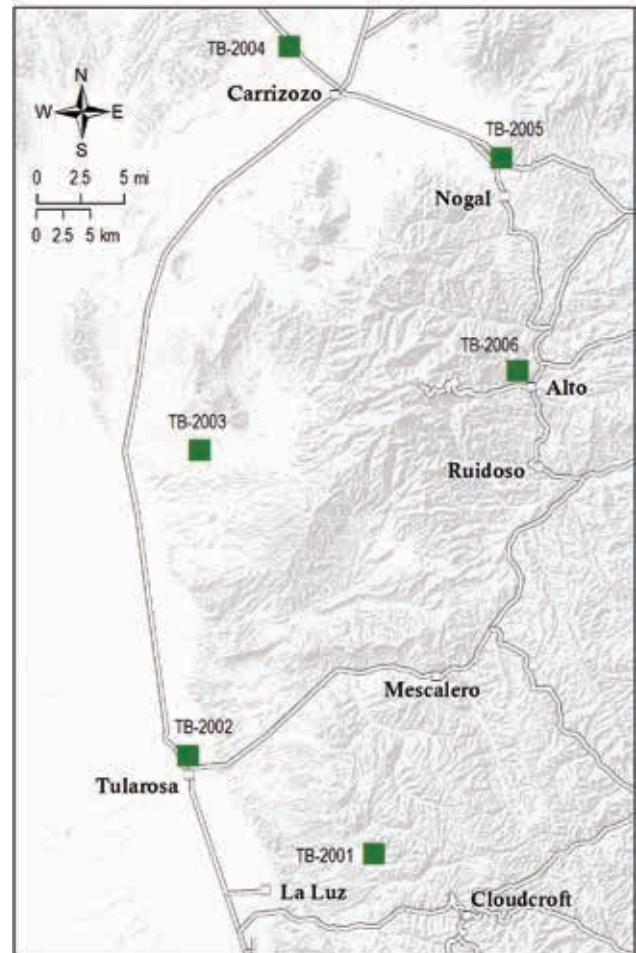
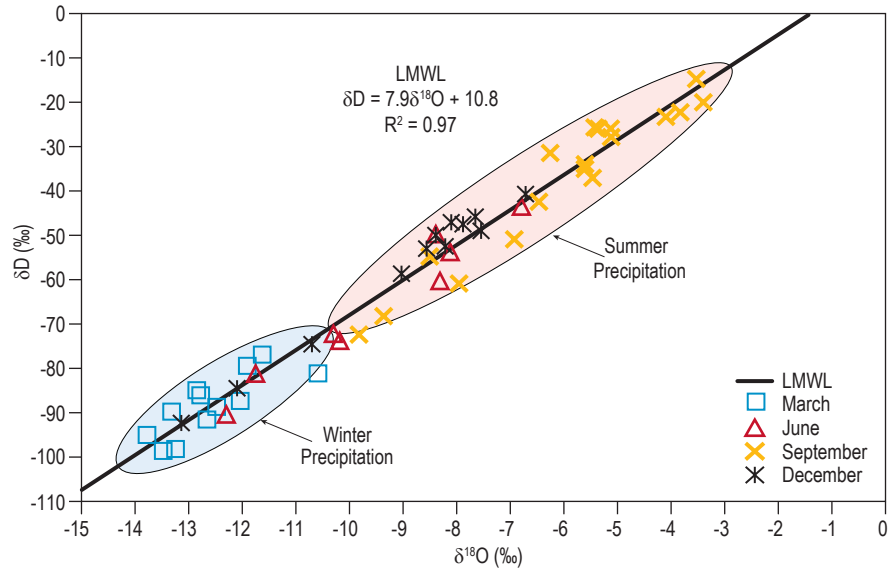


Figure 35—Locations of precipitation collection sites.

Table 5—Site elevations and periods of precipitation collection.

Point ID	Altitude (ft)	Date Installed	Date Removed
TB-2001	6565.84	6/12/2009	9/1/2011
TB-2002	4505.58	6/12/2009	9/1/2011
TB-2003	4982.00	6/11/2009	9/1/2011
TB-2004	5248.48	6/11/2009	9/1/2011
TB-2005	6300.60	6/11/2009	9/1/2011
TB-2006	7774.96	6/11/2009	9/1/2011

Figure 36—Local meteoric water line developed from stable isotope data for precipitation samples collected at five different locations over a wide range of elevations. Samples were collected quarterly over 3 years.



eastern Pacific and the Gulf of California. An elevation effect on the isotopic composition of precipitation was not observed. No other spatial trends were observed.

The stable isotopic compositions of well and spring samples collected in the study area can help to identify recharge areas, assess recharge mechanisms, and characterize groundwater flow paths. For this discussion, we will divide the study area into southern and northern regions (Similar to division on maps in Fig. 4). Figure 37 shows the stable isotopic compositions for wells, springs and streams in the southern region of the study area, which includes the TB and the SHM regions. It can be seen that most points plot below the LMWL, indicating that this water has undergone evaporation to some degree. However, the data are highly variable and do not indicate a single linear trend. It is likely that the isotopic compositions of most of these well, spring, and stream samples are due to evaporation of water with different initial isotopic compositions. The hypothetical evaporation line shown, which can explain some of the data, intersects the LMWL at the very top of the region where winter precipitation usually plots, indicating that this original water was winter precipitation. Most other data, which plot between this evaporation line and the LMWL, can be explained by other evaporation lines (not shown) with original isotopic compositions that are typical of summer precipitation. Other data points plot

on the LMWL in the range of values expected for summer precipitation. These data suggest that most groundwater recharge actually originates as summer precipitation. The observed high variability in isotopic compositions in groundwater indicates a complex system where recharge occurs at different rates in different areas. Additionally, it suggests that flow paths in different areas are isolated from each other. Although it appears that most water undergoes evaporation, either in the shallow soil or mountain streams before recharging the groundwater system, some water (whose isotopic composition plots along the LMWL) has made it into the hydrologic system quickly enough to avoid evaporation.

Stable isotopic data for springs, streams, and wells in the northern portion of the study area, which includes the NHM and the CHP, exhibit similar trends as those observed to the south (Fig. 38). Much of the data plots below the LMWL, and therefore indicate that these waters have undergone evaporation to some degree. Figure 38 shows two possible evaporation lines, one of which intersects the LMWL within the transition zone between areas where summer and winter precipitation usually plots. The other evaporation line intersects the LMWL in the region where summer precipitation generally plots. Many springs in the northern high mountains plot on the LMWL with summer precipitation values. Again, these data suggest that most, but not all water has undergone evaporation in the shallow

soil or mountain streams before recharging the groundwater system. The apparent presence of multiple evaporative trends indicates that individual groundwater flow paths are not interconnected on a large scale, thus waters are not well mixed. As observed in the stable isotope data in the southern portion of the study area, summer precipitation appears to be the primary source of groundwater recharge. However, there are several springs that plot near the LMWL with isotopically light values typical of winter precipitation. All of these springs are located at high elevations near Sierra Blanca. The isotopic composition of these springs indicate that they discharge from largely isolated perched groundwater systems that are recharged primarily by snowmelt.

Groundwater Age and Residence Time

The residence time of groundwater is often inferred from its “isotopic age,” based on interpretation of environmental tracers such as tritium (³H), chlorofluorocarbons (CFCs), or carbon-14 (¹⁴C). The isotopic age relates to the time elapsed between groundwater recharge and collection of a sample at a discharge point such as a well or spring (Mazor and Nativ, 1992). Tracer ages may also be influenced by mixing of groundwater from multiple sources, water-mineral interactions, and groundwater-atmosphere interactions. Therefore, it is advantageous to use several different environmental tracers to estimate groundwater residence time. In this

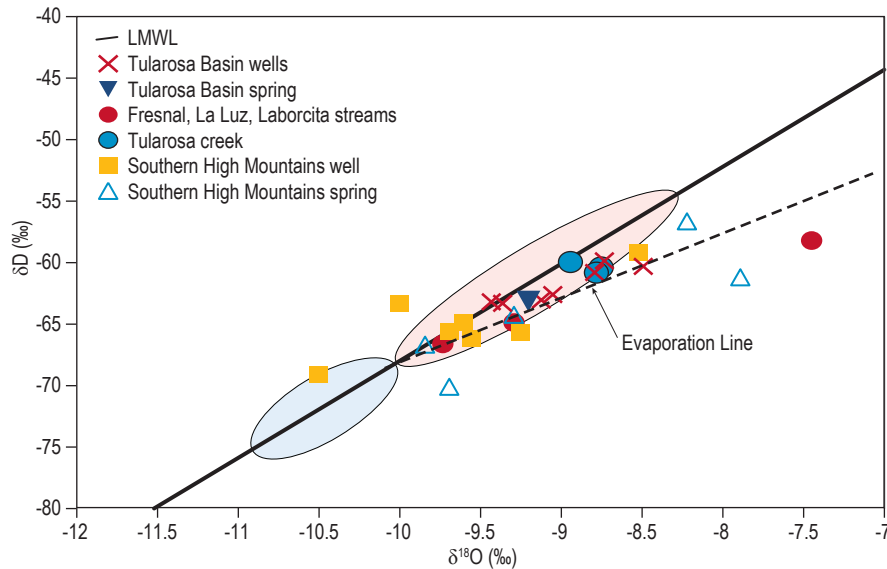


Figure 37—Stable isotopic compositions of water samples collected from wells, springs, and streams in the southern portion of the study area, which includes the Tularosa Basin, and the southern high mountains region. The isotopic compositions for most samples show an evaporative signature.

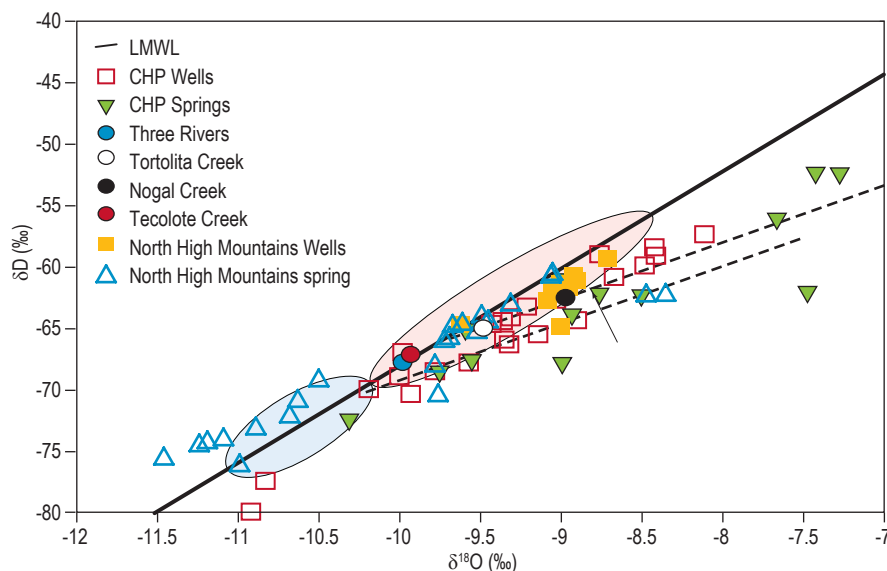


Figure 38—Stable isotopic compositions of water samples collected from wells, springs, and streams in the northern portion of the study area, which includes the Carrizozo hilly plains and the northern high mountains region. The isotopic compositions for most samples show an evaporative signature.

section, we present results and interpretations for environmental tracer analyses. Results are summarized in Table 6.

Tritium

Precipitation samples were not tested for tritium for this study. Newton et al. (2012) found tritium levels in precipitation in the southern Sacramento Mountains ranged from 3 to 10 tritium units (TU), reflecting typical seasonal variations and providing a range of values that represent “modern” precipitation. For a detailed explanation of tracer systematics, see Timmons et al. (2013).

In the current study area, tritium concentrations in well samples range from 0 to 3.8 TU, with an average value of 1 TU. Tritium concentrations in springs are slightly higher, ranging from 0 to 5 TU, with an average of 2 TU. Fifty percent of all well and spring samples exhibit tritium values less than 0.8 TU, indicating sub-modern recharge prior to 1952 (Clark and Fritz, 1997). The remaining well and spring water samples are a mixture of recent (5–10 years old) and sub-modern recharge.

Figure 39 shows the spatial variability of tritium values for samples collected from streams, springs, and wells. Tritium values appear to be spatially distributed randomly, with the exception of samples collected near the northern study area boundary, where all samples exhibit tritium concentrations less than 0.2 TU. Figure 40 shows tritium values as a function of elevation. Apart from the two highest tritium concentrations observed in the northern high mountains, there is no observed correlation between tritium concentrations and elevation. This apparently random spatial variability observed for tritium values suggests a complex hydrologic system, in which recharge occurs in different areas at different rates, and flow paths are relatively isolated from each other.

Tritium-Helium / Noble Gases

Noble gas analyses were performed on three well sample locations (TB-100, TB-192, and TB-070) within the study area and were used to derive tritium-helium (³H/³He) groundwater ages. The ³H/³He ages for TB-100 and TB-070 were both greater than 50 years, which indicates

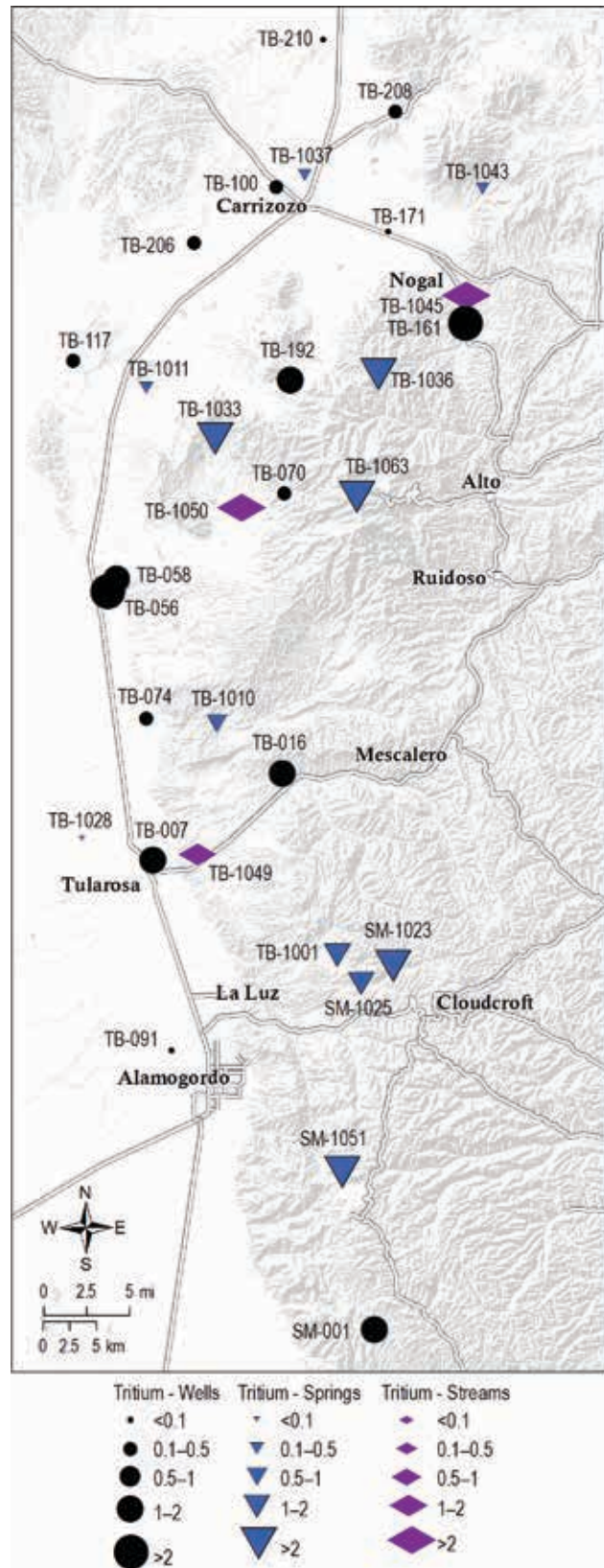


Figure 39—Tritium values for well, spring, and stream samples. Larger values indicate younger water. There are no obvious spatial trends observed.

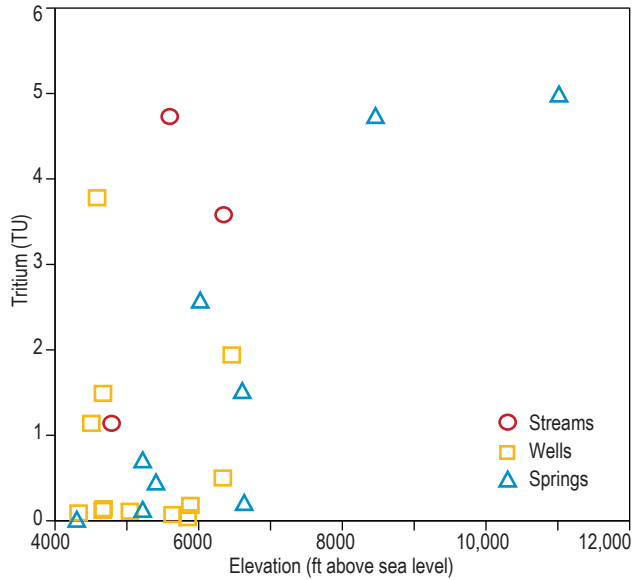


Figure 40—Tritium concentrations in well and spring samples as a function of elevation. There is no obvious correlation between tritium concentrations and elevation.

that the age is off the $^3\text{H}/^3\text{He}$ scale, and the true age of the groundwater sample is too old to be determined using noble gas systematics. TB-192 exhibits a $^3\text{H}/^3\text{He}$ age of 46.2 years, which is close to the upper age limit that can be accurately measured by this method. The old age of most water samples in the study area make this dating method not very useful.

Carbon-14

Carbon-14 (C-14) age estimates discussed in this section have been corrected to account for the dissolution of carbon-dead calcium carbonate and isotopic exchange between dissolved inorganic carbon and soil CO_2 , using the mixing model (Clark and Fritz, 1997) (See Appendix 7). It should be noted that this correction method is based on assumed recharge conditions and does not account for other processes such as matrix diffusion of C-14 and sulfate reduction. However, these values are an improvement over the uncorrected or apparent C-14 ages and are sufficient for comparing relative ages of groundwater in the study area.

It can be seen in Figure 41 that, as with the tritium data discussed above, C-14 age estimates do not correlate well with elevation. It should be noted that the four youngest age estimates (highlighted in blue) are likely in an open sys-

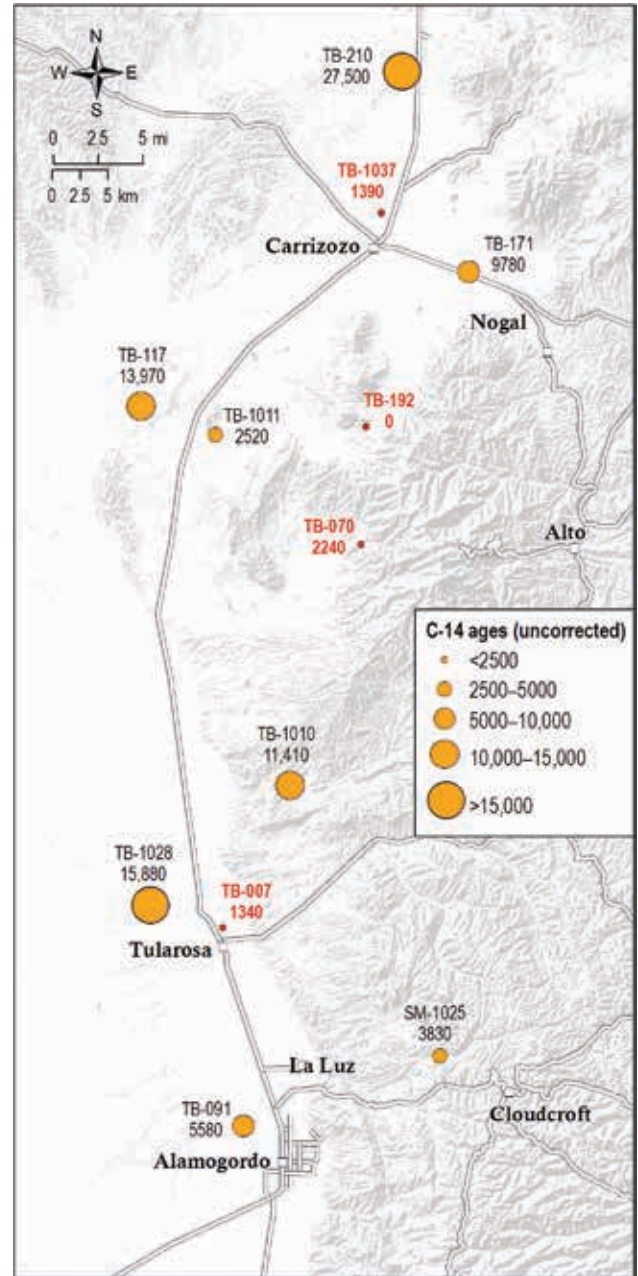


Figure 41—Map showing location of C-14 sampling and corresponding age. The highlighted samples in blue represent the four youngest ages sampled.

tem where isotopic exchange between dissolved inorganic carbon (DIC) and soil CO_2 occurs (See Appendix 7), resulting in complete or partial equilibration between C-14 in soil CO_2 and DIC. Therefore, the true ages of those four samples are likely significantly older than the age estimate shown. Excluding those four samples, the average C-14 age is about 7000 years before present for the springs and wells sampled. The oldest

groundwater sample was collected north of the study area, indicating that recharge to this particular aquifer occurred approximately 17,000 years ago.

Chlorofluorocarbons (CFCs)

Calculation of apparent age based on CFC concentrations in water samples depends on the recharge elevation and recharge temperature, with temperature being the more critical variable. For this study, we used a recharge elevation of 1828 m (6000 ft) above sea level, which represents an average elevation in the mountains where most recharge probably occurs. We used a recharge temperature of 10°C (50°F), which is the average annual temperature at Mescalero, NM according to the Western Regional Climate Center (<http://www.wrcc.dri.edu/>). These values are reasonable estimates for recharge elevation and temperature.

Samples analyzed for chlorofluorocarbons have CFC12 ages ranging from 26 to 56 years, with an average age of 40 years (Table 6). CFC113 ages are generally younger, with an average age of 33 years. Most of the different CFC species apparent ages are not concordant among each other, with discrepancies of 2 to 18 years between CFC12 and CFC113. CFC ratio ages were determined using CFC 2005–2a, a U.S. Geological Survey spreadsheet program for preliminary analysis of CFC data (Busenberg and Plummer, 2006). Groundwater apparent ages based on CFC113/CFC12 concentration ratios range from 0 to 49 years, with an average age of 25 years. For most water samples, the ratio ages are younger than apparent ages based on concentrations of CFC12 alone (Fig. 42). The relationship between these two age estimates is indicative of the mixing of waters of different ages (Han et al., 2001; Plummer et al., 2006).

In mountain hydrologic systems, mixing of different waters with different ages is a common process. To evaluate the CFC data, we used a simple binary mixing model that assumes that the observed CFC concentrations are a result of the mixing of a “young” CFC-bearing component and an “old” CFC-free component (recharged before 1950). Under such circumstances, the CFC ratio age represents the age of the young component, and the proportion of

young water in the mix can be calculated (Han et al., 2001; Plummer et al., 2006; Land and Huff, 2010; Newton et al., 2012). Mixing calculations indicate that young groundwater components in samples collected in the study area represent recharge that occurred between 1984 and 1991. The percentage of young water in well and spring samples ranges from 98% to 8% (Fig. 43). The strong correlation between the CFC12 apparent age and the fraction of young water in the mix, with the oldest samples containing the smallest percentage of young water, indicates that the assumptions associated with this binary mixing model are valid. This correlation also suggests that the percentage of young water is the principal factor influencing groundwater apparent age based on individual CFC species (e.g., Long et al., 2008). This assertion is also supported by the correlation between the estimated proportion of young CFC-bearing water and tritium concentrations (Fig. 44). Higher proportions of young CFC-bearing water correlate with higher tritium concentrations.

Figure 45 shows spatial distribution of CFC data in terms of the proportion of young water in the water sample. It should be noted that the number of data points is insufficient to accurately characterize the spatial variability of groundwater ages. However, it is apparent that, similar to the observed spatial variability of groundwater age estimated by other methods described above, there are no

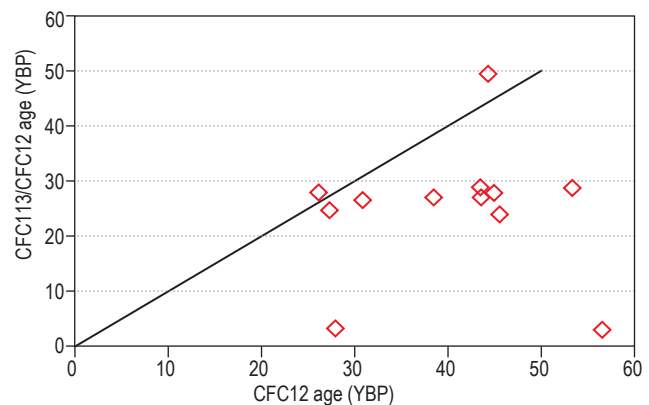


Figure 42—CFC113/CFC12 ratio ages as a function of CFC12 ages. Most ratio ages are younger than CFC12 ages, suggesting that waters of different ages are mixing.

Table 6—Groundwater age and residence time.

Point ID	Collection Date	Site Type*	Tritium (TU)	³ H- ³ He Age (yrs)	δ ¹³ C (‰)	¹⁴ C (pMC)	¹⁴ C (yrs)	C-14 (corrected)	CFC11 (yrs)	CFC113 (yrs)	CFC12 (yrs)	CFC113/12 ratio (yrs)	Avg % young in mix from CFC113/12
SM-0001	7/10/2007	GW	1.32	0						20			
SM-0032	8/13/2008	GW								27	31	24	
SM-1023	11/13/2006	SP	2.99							21	22	21	
SM-1025	11/6/2006	SP	1.63		-9.6	62.05	3830						
SM-1051	11/6/2006	SP	2.91							21	22	20	
TB-001	8/3/2010	GW							0	21	25	0.1	67.09
TB-007	8/2/2010	GW	1.14		-13.4	84.64	1340		0	24	23	24.89	98.19
TB-016	12/3/2010	GW	1.51					1213	37	29	35	24.03	47.96
TB-056	9/8/2010	GW	3.78										
TB-058	8/12/2010	GW	1.49										
TB-070	8/12/2010	GW	0.50	>60	-14.8	75.67	2240	2240	44	33	41	24.12	27.75
TB-074	8/2/2010	GW	0.12						49	41	50	25.69	7.78
TB-091	8/3/2010	GW	0.09		-8.6	49.93	5580	3242	46	34	42	24.7	22.66
TB-100	12/3/2010	GW	0.21	>60					40	34	40	25.83	30.54
TB-1001	5/11/2010	SP	1.52						24	23	24	21.67	75.88
TB-1010	5/11/2010	SP	0.71		-9.9	24.16	11,410	7632	42	44	41	46.27	
TB-1011	8/31/2010	SP	0.13		-10.2	73.07	2520	1737					
TB-1028	5/11/2010	SP	-0.02		-11.5	13.85	15,880	12,339					
TB-1033	5/13/2010	SP	2.58										
TB-1036	6/14/2010	SP	4.74										
TB-1037	6/9/2010	SP	0.45		-13.8	84.11	1390	1296					
TB-1043	7/31/2010	SP	0.21										
TB-1045	7/30/2010	ES	3.58										
TB-1049	8/10/2010	ES	1.14										
TB-1050	8/12/2010	ES	4.73										
TB-1063	10/14/2010	SP	4.99										
TB-117	8/5/2010	GW	0.14		-6.5	17.57	13,970	6136	52	35	54	0.1	
TB-161	8/9/2010	GW	3.25						49	25			
TB-171	8/9/2010	GW	-0.10		-8.9	29.6	9780	5881	44	33	43	20.91	17.83
TB-179	8/5/2010	GW							38	29			
TB-192	8/11/2010	GW	1.94	46.2	-12.9	102.39	0	0	32	25	28	23.52	72.71
TB-206	8/2/2010	GW	0.11										
TB-208	9/7/2010	GW	0.18										
TB-210	9/7/2010	GW	0.07		-9.4	3.26	27,500	25,099					

* GW=well SP=spring ES=streams

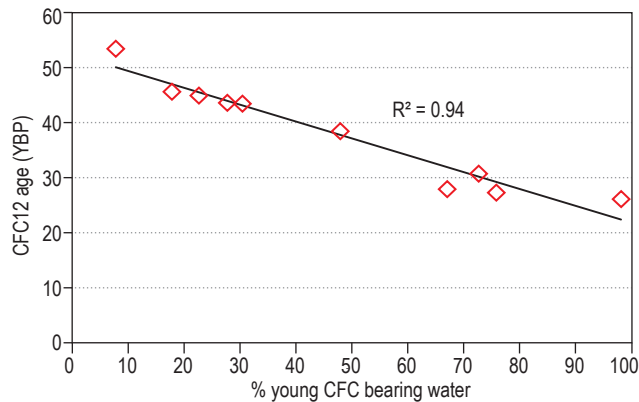


Figure 43—CFC12 apparent age as a function of the proportion of young CFC-bearing water that represents recharge that occurred between 1984 and 1991.

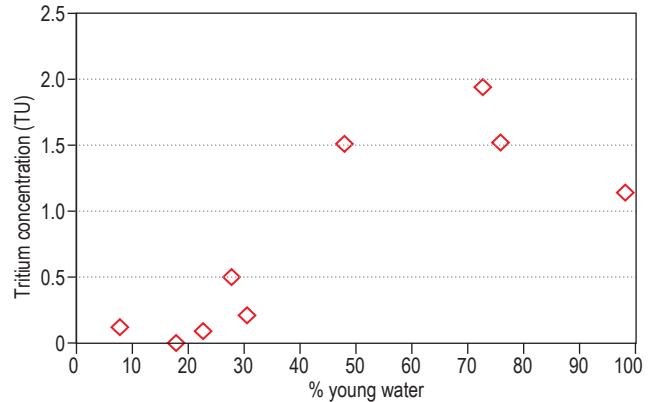


Figure 44—Tritium concentrations as a function of the proportion of young water, calculated based on CFC data. Higher tritium concentrations correlate with higher proportions of young recharge.

obvious spatial trends, indicating a complex system where recharge occurs at various regions at different rates.

Groundwater Residence Time

From the groundwater age data described above, it is apparent that most samples collected in the study area contain water that is hundreds

to thousands years old. This old water is observed at high elevations in the mountains as well as lower elevations in the basin. The presence of this old water in sedimentary and volcanic rocks in the mountains with relatively high hydraulic gradients suggests that this groundwater is moving very slowly, likely as a result of barriers that effectively restrict groundwater in the mountains from flowing directly into the basin-fill aquifer to the west as mountain block recharge. This interpretation is in agreement with most other researchers (Garza and McLean, 1977; Orr and Myers, 1986; Waltemeyer, 2001; Huff, 2004, Livingston and Shomaker, 2006) who assume that most recharge to the basin-fill aquifer occurs as mountain-front recharge as a result of runoff in the different drainage basins. Water that makes it into mountain streams can potentially recharge the basin-fill aquifer at and west of the Alamogordo Fault.

Tritium and CFC data indicate that although much of the groundwater is very old, there is young water (less than 50 years old), that makes its way into the system and mixes with the older water. This young water, according to CFC analyses, generally represents recharge that occurred between 1984 and 1991. Again, there is no obvious correlation between the occurrence of this young water and topography. It should be noted that the mixing of young and old waters likely occurs by two mechanisms: 1) macrodispersion, and 2) multiple recharge areas along a flow path. Macrodispersion is mixing of a substance, in this case environmental tracers, due to spatial variations in the flow velocity of groundwater along a flow path. The tortuous flow paths through different lithologies and structures in this mountain hydrologic system likely result in a large range of velocities that cause the mixing of waters of different ages. It is also very likely that along flow paths in the different drainages, water enters the system at different points along a flow path, thereby mixing younger water with older water. The high spatial variability in the groundwater ages discussed above is consistent with stable isotope results that suggest that flow paths in different areas, the locations of which are controlled by the location of the large drainages coming off the mountains, are isolated from each other.

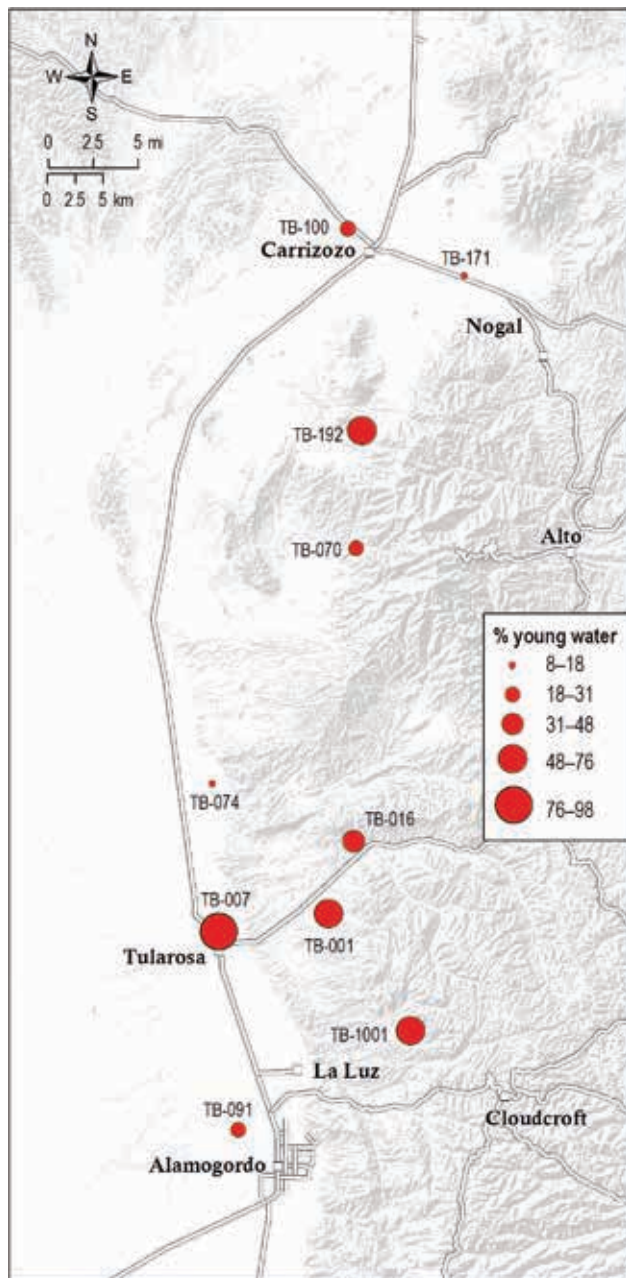


Figure 45—Spatial distribution of young groundwater. The larger the data point, the larger the proportion of young CFC-bearing water is present. This young water represents recharge that occurred between 1984 and 1991.

V. CONCLUSIONS

In this section we draw conclusions from the data set we have described so far. Integrating results from geologic mapping, hydrograph analysis, water chemistry and age dating analysis, we can identify recharge areas for this region, quantify the groundwater recharge, assess the flow directions and rates of groundwater movement, and examine the interactions between different aquifers, as well as groundwater-surface water interactions. We compare our results and previous studies, identify the location and mechanism for recharge, and then suggest future work to be done.

ESTIMATING DARCY CALCULATION VALUES

To quantify how much groundwater is recharging the basin we performed a basic Darcy Flow calculation to estimate volumetric flow rate (Q) of groundwater across three transects (Fig. 46) perpendicular to the mountain front. Thanks to our robust data set we are able to calculate the total flow into the basin with more certainty than previous studies which used similar methods (Rau, 1986). The Darcy Flow equation used to quantify volumetric flux is described as:

$$Q = -K * \frac{\Delta h}{\Delta s} * A$$

where A is the saturated cross sectional area of the aquifers, and K is the average hydraulic conductivity of the aquifers. The gradient of the water table ($\frac{\Delta h}{\Delta s}$) is defined as the change in head (Δh), divided by the change in distance (Δs). Estimating saturated aquifer area is necessary to calculate the quantity of water that can move through each aquifer. The three cross sections that run perpendicular to flow directions into the basin were created for the purpose of determining the aquifers present, and estimating the cross

sectional area of the saturated aquifers. The northern cross section trends northeast near Carrizozo to the Bald Hills running approximately 10.6 km (6.6 mi) (E-E'). The central section trends northeast from Three Rivers to Carrizozo and stretches 27.7 km (17.2 mi) (F-F'). This section runs parallel to the Godfrey Hills. The southern cross section extends 37.2 km (23.1 mi) southeast from Three Rivers, parallels Highway 54 along the mountain front to Alamogordo (G-G'). In this way, all water that enters the aquifers, either from stream infiltration east of the cross sections, or through deeper flow paths in the mountain block is calculated.

Estimating the hydraulic properties of the aquifers present in each cross section is necessary to calculate how quickly groundwater can flow through them. Basin-fill is present in the northern section, though very little of it is saturated near Carrizozo and as a result does not contribute much to the groundwater flow. Using hydrostratigraphic unit descriptions from the geologic mapping efforts, we are able to make educated estimations of hydraulic properties of the other aquifers. The primary aquifer in the northern section is the TKSCC. Hydraulic conductivity is difficult to estimate for this unit as there have been only a few aquifer tests with highly variable results. Based on the unit description of channel fill, weaker cementation, and the existence of numerous springs, we assign a fairly high conductivity value to this unit: 0.61 meters/day (2 ft/day). Beneath the TKSCC we find the GLUP hydrostratigraphic unit. We assume a very low hydraulic conductivity as it is made up of highly cemented sandstone, and no springs emerge from this unit: 0.003 meters/day (0.01 ft/day). The central cross section has many of the same aquifers that are present in the northern cross section. The southern cross section is different in that the primary aquifer present is basin-fill. Numerous previous studies (Morrison, 1989) in

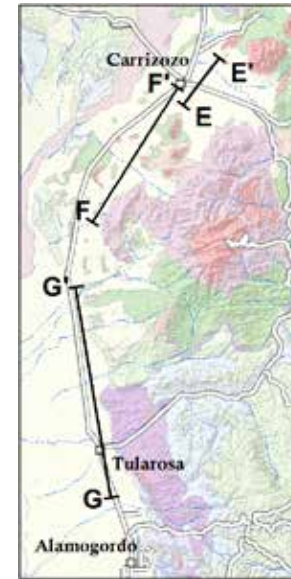
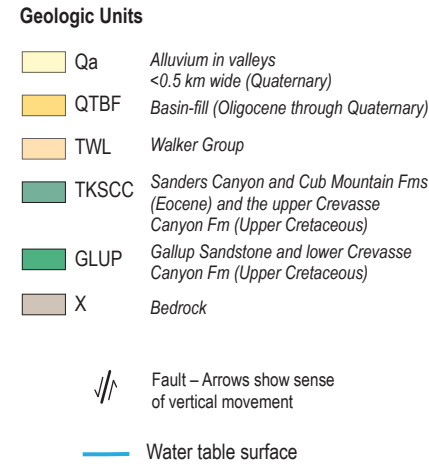
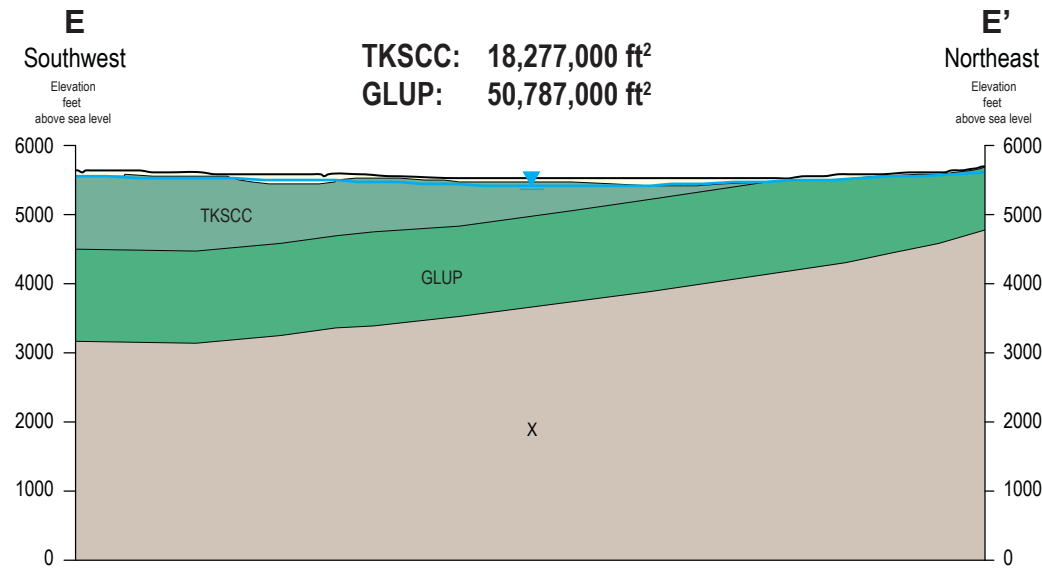
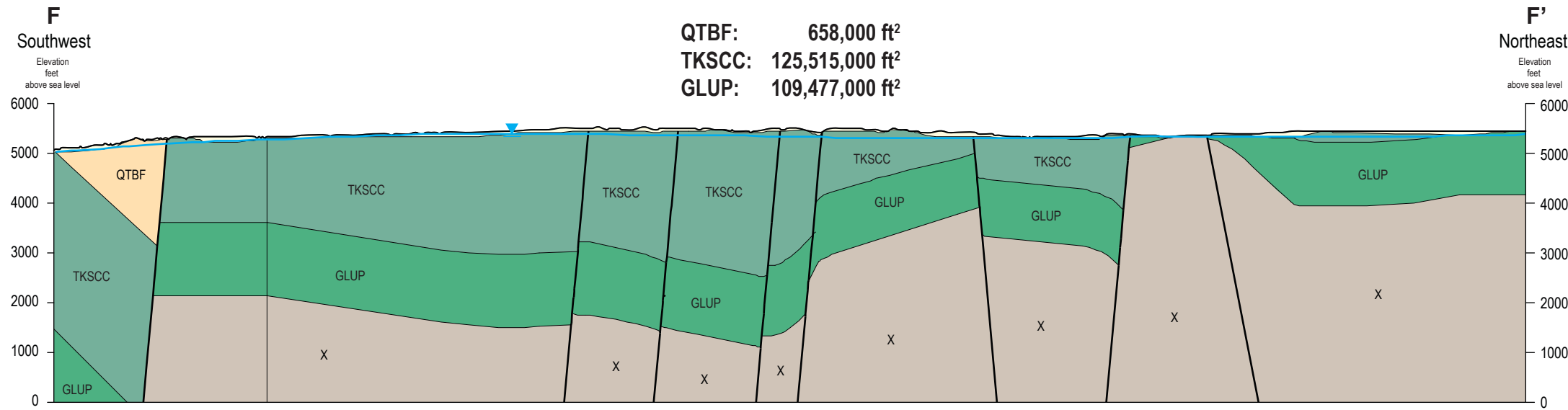


Figure 46—Cross sections used to estimate area of available aquifer for Darcy Flow calculation.

the Tularosa Basin have conducted aquifer tests in the basin-fill aquifer, and as a result we have a much better estimate of conductivity. We assign a hydraulic conductivity of 1.8 meters/day (6 ft/day) to this unit.

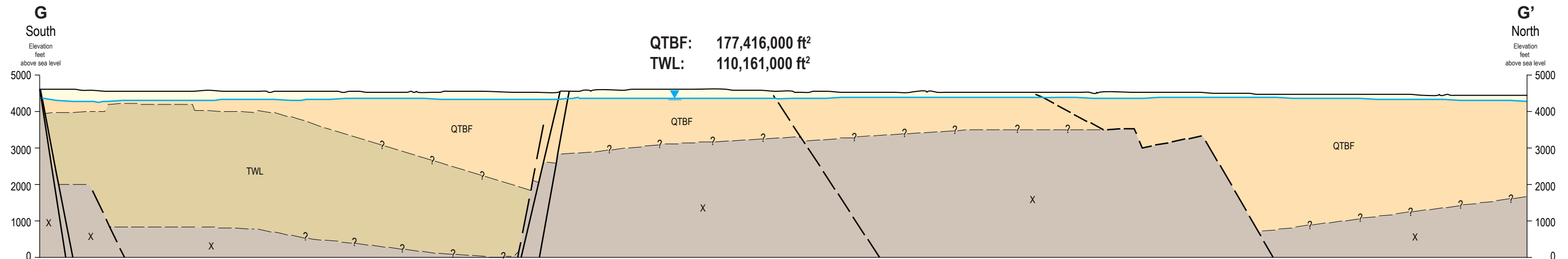
One of the major controls of how much water moves through an aquifer is the gradient of the water table. To calculate this we used the water table map which was compiled for this study using over 250 well water-level measurements spread throughout the area (Land et al., 2014). In the northern area, near Carrizozo, the water table gradient is relatively shallow, dipping west at approximately 22.5 meters/mile (74 ft/mile). West of the Godfrey Hills, where the central cross section is located, the water table is moderately steep, dipping 32 meters/mile (105 ft/mile). Across the southern cross section, in the Tularosa Basin, the water table gradient is quite shallow, dipping only 9.8 meters/mile (32 ft/mile).



RECHARGE ESTIMATES

North

Using the Darcy Law equation we were able to estimate the total recharge to the basin. In the north, we estimate 4600 AFY moves through the cross section, recharging the basin. This can be normalized to be approximately 650 AFY per mile. The majority of the flow is believed to pass through the TKSCC aquifer. Rau (1986) estimated 3000 AFY of recharge. This estimate



only accounted for flow through the basin-fill aquifer, and assumed 30 m (98 ft) of saturated basin-fill sediment at the mouth of the drainage basin. From our more rigorous aquifer cross section area estimation we find that the majority of the basin-fill in the area of the cross section, at present day, is unsaturated. As the depth of the aquifer was not well constrained in the Rau (1986) recharge calculation, our estimate is likely a more accurate approximation. The USGS study (Waltemeyer, 2001) did not extend north to this portion of the mountain front. Applying the same methods we calculated that approximately 4300 AFY of recharge results from runoff. The Livingston and Shomaker (2006) surplus precipitation calculation for the drainage basins that drain through the northern cross section are estimated to total 8300 AFY of recharge.

Central

Through the central transect, west of the Godfrey Hills, we estimate approximately 4300 AFY of recharge, or 350 AFY per mile. Hydraulic conductivity in this area is believed to be significantly less than in other areas due to the heavy faulting and volcanic intrusions associated with the Godfrey Hills. These faults and intrusions impede groundwater movement and as a result we reduce the conductivity of the aquifers in the area by an order of magnitude. The USGS (Waltemeyer, 2001) estimates only 640 AFY of stream runoff recharging through this transect. This small value of surface runoff is due largely to the lack of significant drainage basins in the area. Additionally, the Godfrey Hills intrusion acts as a barrier, and as a result, precipitation that falls to the east of these hills drains south before entering the Three Rivers drainage. Livingston and Shomaker (2006) estimate 5800 AFY of recharge.

South

Recharge through the southern transect is where we see the majority of flow entering the basin. In this area, which is dominated by thick basin-fill deposits, we estimate approximately 60,000 AFY of recharge. That is approximately 2600 AFY of recharge per mile. The stream runoff

estimation calculated 40,300 AFY of recharge entering the basin in this area (Waltemeyer, 2001). The Livingston and Shomaker (2006) report estimate was very close to our approximation of recharge, calculating 60,500 AFY of recharge through this transect.

Totals

In total, the Darcy Flow calculations estimate approximately 67,900 AFY of annual recharge to the basin for the entire study area (Table 7). The average annual volume of precipitation that falls on the study area is roughly 761,500 AFY. (This volume is calculated by taking the mean elevation of each drainage basin and multiplying it by the average annual rainfall which falls at that elevation). Our estimate of groundwater recharge to the basin is roughly 8.9% of the total precipitation. This compares well with the Maxey-Eakin estimates of mountain-front recharge for Nevada (Watson et al., 1976), and Utah (Hood and Waddell, 1968). The Darcy Flow recharge value is similar to the surplus precipitation estimate of 75,000 AFY by Livingston and Shomaker (2006). Our Darcy Flow calculation is 22,500 AFY more than the 45,300 AFY estimate of surface water runoff using the Basin-Climatic Characteristic Method for the area.

Each flow calculation methods has its own assumptions, uncertainties, and limitations. Darcy’s Law functions under the assumption that the aquifers are isotropic and homogeneous, and the hydraulic conductivities are well defined. As a result, there is a degree of uncertainty associated with these calculations. However, despite the complexity of the aquifer system, our Darcy Law calculation is perhaps the most informed

Table 7—Flow volume estimates through each section, broken down to estimate mountain-front recharge, and mountain-block recharge component.

	DARCY (AFY) Flow Equ.	MFR* (AFY)	MBR (AFY)
North	4553	4322	232
Central	4291	641	3650
South	59,056	40,361	18,695
Total	67,901	45,324	22,577

*Basin-Climatic Characteristic Method

recharge calculation conducted for this section of the basin. We have a more accurate understanding of the aquifer interactions than previous reports as result of rigorous geologic mapping, and the broad suite of water chemistry analysis conducted for this study.

LOCATION AND MECHANISMS CONTROLLING RECHARGE

Direct infiltration of precipitation to the basin floor in arid climates is typically negligible, due to limited precipitation volumes, high evaporation rates, and deep water table. Instead, precipitation that falls on the neighboring mountains is typically the source of recharge for aquifers in the adjacent basins. There are two mechanisms that facilitate recharge from mountain precipitation to these basin aquifers; mountain-front recharge (MFR), and mountain-block recharge (MBR).

Mouths of Drainage Basins: Mountain-Front Recharge (MFR)

The mouths of drainage basins, where perennial and ephemeral streams enter the basin and infiltrate into porous alluvial fans, are considered to be one of the primary locations of groundwater recharge, as first observed by Meinzer and Hare (1915). This type of recharge is classified as “mountain-front-recharge” (MFR), and is typically found in arid and semiarid climates. MFR helps to describe the contribution of mountain regions to the recharge of aquifers in adjacent basins (Wilson and Guan, 2004). Water table mounding in the alluvium at the mouths of some drainages supports recharge in these locations. The most prominent example of this can be seen at the mouth of the Three River drainage, and near Carrizozo (Fig. 22). In the upper reaches of most rivers the water table is sloping toward the river, creating a “V” shape which points up gradient (Fig. 23). This indicates that water from the surrounding rocks in the mountains drains into the incised river channel. As the river enters the basin, however, the water table is inverted and points down gradient, creating a mounding effect. This change in

gradient indicates that water from the stream is now infiltrating into the aquifer. The transition generally occurs just as the river crosses the Alamogordo fault and flows over the highly conductive basin-fill sediments. Recharge hydrographs are also prevalent in these locations, particularly near Carrizozo.

Further evidence of MFR is substantiated by determining the residence time/ age of groundwater. Groundwater that enters the basin-fill aquifer via MFR can have a very young age. This is because MFR mainly consists of runoff from storms that is quickly flushed into the basin, where it recharges quickly. The presence of young groundwater in the Tularosa Basin supports this mechanism for providing recharge to the basin (Figs. 39, 41, 45). Groundwater that enters the basin via MFR does not necessarily have to be young however. Water in the streams that lead to MFR can mix with older water discharging from springs at higher elevations. Additionally, older water in the basin mixes with the younger water and confounds the estimated date.

Other evidence of MFR is shown by evaporation signatures. Groundwater that originated as runoff or streamflow generally has an evaporative isotopic signature. Samples collected in the Tularosa Basin commonly show an evaporative isotopic signature (Figs. 37, 38).

Estimating the rate of MFR can be fairly straightforward. Recharge can easily be estimated by gauging streams or calculating runoff from a watershed. While the majority of the recharge entering the basin from MFR is from precipitation runoff, perennial streams receive additional flow via groundwater/ surface water interactions and springs. The exact volume that is contributed to streamflow in this way is difficult to determine and was not the focus of this report. To get a rough estimate of MFR we used the results presented by Waltemeyer (2001), which calculated stream runoff to the basin. Sixty-six percent of total recharge to the basin is believed to be derived from streamflow/ MFR.

High Mountains: Mountain-Block Recharge (MBR)

The mountain regions on the eastern border of the study area, which extend from Carrizo

Mountain in the north to Cloudcroft in the south, are at significantly higher elevations than the rest of the area. With more precipitation falling at high elevations (Fig. 7), recharge is certain to enter the mountain aquifers. The higher elevation also allows for the development of a snow pack in the winter months. Even though the winter precipitation only accounts for a quarter of total precipitation, it provides a slower, more sustained, source of recharge. The water that recharges here slowly flows through the mountain-block, flowing down gradient through the aquifers present, before entering the basin-fill aquifer. This is defined as mountain-block recharge (MBR).

While it is difficult to delineate flow paths, we believe the flow generally follows the most direct path down the mountain. Assumed flow paths are from east to west, perpendicular to the water table contours (Fig. 47). Preferential flow can occur along faults. Faults in bedrock create a fracture network that may enhance permeability and direct groundwater flow parallel to the fault. Offset along faults may juxtapose a high-permeability unit, such as porous sandstone, against a low-permeability unit like mudstone, creating fault barriers and potentially blocking groundwater flow. As the western side of the Sacramento Mountains is the result of faulting determining flow through these rocks is very difficult.

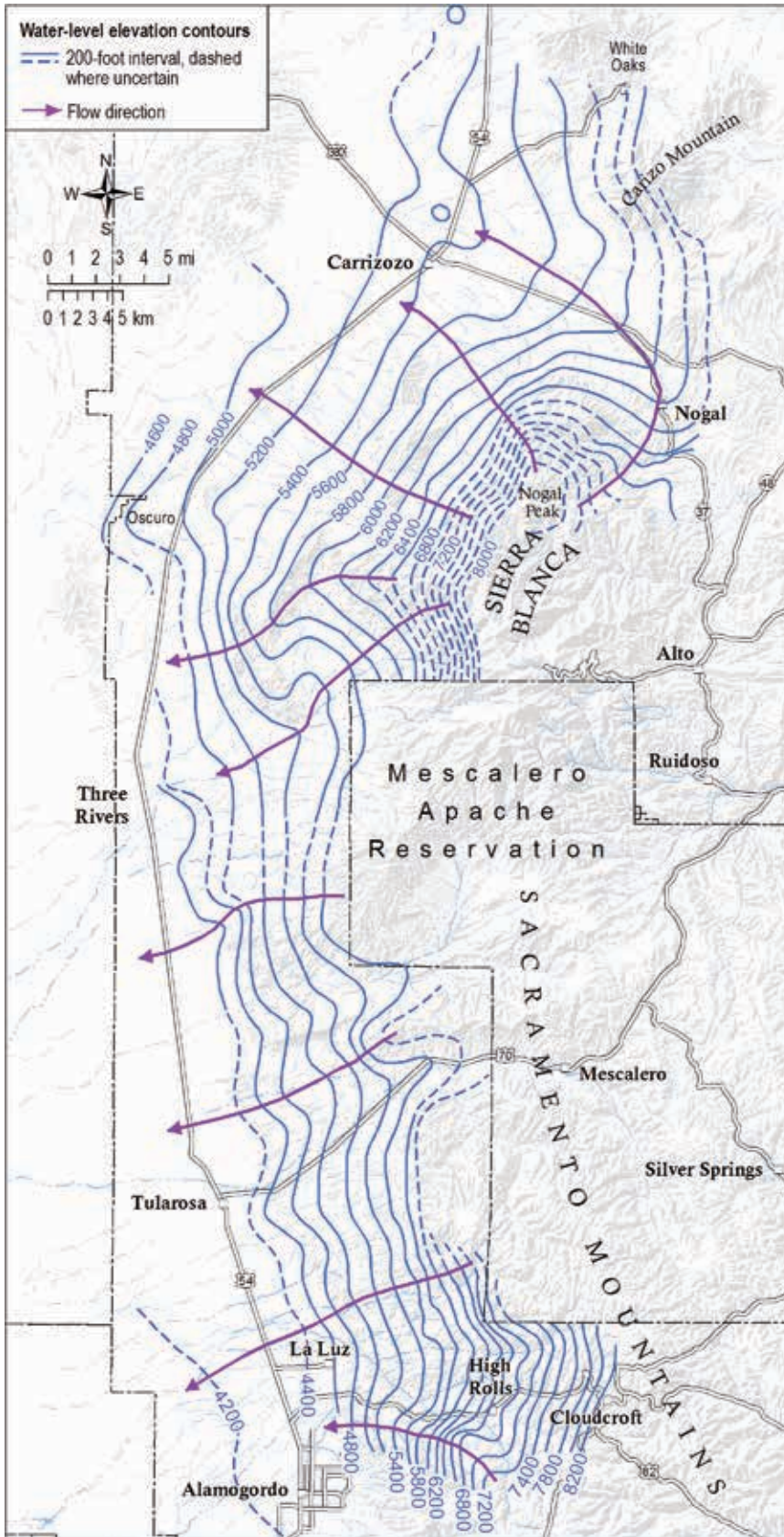
Evidence of recharge occurring in the high mountains is supported by well hydrograph analysis. Sixty percent of wells located in the HM regions show recharge trends, which correlate with monsoonal precipitation, or spring melt recharge (Figs. 24, 25, 26).

Chemistry data in the basin points to recharge from the high mountains. In the north, well and spring data show high silica values, and in the south there are high values of carbonate and evaporite elements (Ca, SO₄, Cl). These chemical signatures are the result of groundwater being in prolonged contact with the rocks present in the high mountains. Silica concentration found in the northern portion of the basin tells us that the groundwater passed through the igneous materials in the Sierra Blanca Mountains. Higher carbonate levels in the groundwater in the southern basin suggest

that it drained through the sedimentary rocks in the southern Sacramento Mountains. This means that some of the groundwater originated in the HM before slowly moving through the mountain rocks and finally into the basin. We call this mountain-block recharge. Another indicator of mountain-block recharge is samples with a high chloride to sodium ratio. Higher ratios of chloride indicate contact with a brine source. Samples that indicate brine mixing are associated with faults, which may provide a conduit for bringing up brines from depth, through longer flow paths (Figs. 31, 32, 34).

Stable isotope chemistry was conducted to shed more light on mountain-block flow paths in the area, and to answer questions of when, where and how fast recharge occurs. This data set served to reiterate how complicated the groundwater system is. In the NHM we see a wide range of values that demonstrate distinct summer and winter precipitation. Additionally we see distinct summer and winter evaporation trends. This broad range of values indicates a non-mixed system, showing that individual groundwater flow paths are not interconnected on a large scale. Groundwater age, estimated with tritium, CFC, and C-14, shows that while the individual flow paths are not mixed, water within the flow paths is. The presence of young and old water within the flow paths likely occurs as result of spatial variability in the flow velocity as result of different lithologies and structures, and multiple recharge zones. The SHM stable isotope data suggest that the majority of the groundwater recharge originates as summer precipitation, with a smaller percent derived from winter precipitation. The wide range of values again indicates that this is not a well-mixed system, and that recharge in the high mountains occurs at different rates in different areas. Flow paths in different areas appear to be isolated from each other. Spatial distribution of groundwater age supports this slow, non-mixed model of mountain-block recharge we see throughout the mountains.

To estimate the volume of recharge to the basin via MBR we looked at the difference between the Darcy Flow calculations and the



Basin-Climatic Characteristic stream flow estimates (Waltemeyer, 2001). If the Waltemeyer study accounts for all surface runoff entering the basin via MFR, and the Darcy calculation accounts for both infiltrated surface water (MFR) and deeper flow paths (MBR), then we estimate that on average 33% comes from deeper flow paths, or mountain-block recharge. Our findings agree with the conclusions of Eastoe and Rodney (2014) that both MBR and MFR play a role in recharging the Tularosa Basin in this study area.

Groundwater-Surface Water Interactions

As streams flow down the mountain front a certain amount of mixing of water from different origins occurs. Adding to the complexity are springs, which generally occur at breaks in slope, changes in lithologies, and faults. Alternatively, streams can also lose water as they flow down the mountain. Stream water typically is young and has an evaporative signature. When this water infiltrates into the mountain aquifers it can be incorporated into the deeper flow paths and lead to the appearance of groundwater from a mixture of different sources. Water-levels in wells in the vicinity of streams are closely linked to stream flow. These wells often respond more rapidly to precipitation or snowmelt events, and have larger fluctuations.

Figure 47—Estimated flow paths, based on water table contours.

IMPLICATIONS AND FUTURE WORK

The results of this study have significantly increased our knowledge about the hydrologic system responsible for recharging the Tularosa Basin from the east. Surface water and groundwater, which originate from the western side of the Sacramento Mountains, is crucial for sustaining water levels in the basin aquifers. Previous studies in the area suggested that runoff infiltrating to the basin from streams is the primary source of water entering the basin, or MFR. With the help of groundwater-level records, chemical analysis, age dating of water, detailed geologic mapping and the construction of detailed cross sections we were able to evaluate the potential input from deeper flow paths entering the basin through MBR. Our work suggests that deep flow paths do exist, however flow is highly variable due to the fractured and faulted mountain-block geology. Environmental tracer data suggests that the individual flow paths are isolated from each other. Within the flow paths, however, mixing occurs due to heavily fractured aquifer systems. As a result of the different lithologies and structures in the mountain hydrologic system, a large range of velocities exist that cause mixing of waters of different ages. Comparing existing MFR approximation with our Darcy Flow calculations we were able to estimate that roughly 22,500 AFY replenishes the basin through MBR.

Our results suggest approximately 68,000 AFY of water enters the basin along this stretch of mountains. A total of 66% is estimated to enter the basin via streams and runoff at the mountain front, while 33% is believed to derive from deeper mountain-block flow paths. While the portion represented by MFR is considered to be potable water, the portion entering the basin via MBR may not be. Groundwater that recharges the basin via the deep flow paths is typically very old water, and has been in contact with the mountain aquifers for an extended period. The longer water is in contact with the aquifers the more dissolution occurs, and as a result, the potability of the water is diminished. While the quality of the MBR is not ideal it is

a fairly reliable source. Additionally, the long tortuous flow paths associated with MBR makes it less susceptible to drought.

While recharge derived from MFR is a good source of fresh, potable water, it is not a very reliable source of recharge. MFR is highly dependent upon precipitation, and as a result is heavily impacted by periods of drought. Many of the streams whose flow was estimated to account for MFR are ephemeral, and rely on runoff from storm events. This has important implications on how this hydrologic system may respond to variability in precipitation. Future research on the effects of global climate change on the North American monsoon and hurricane systems will help to predict how climatic controls on groundwater recharge may change in the near future.

An additional line of research for future work is the creation of a detailed 3D groundwater flow model of the area. Models of groundwater flow in the basin already exist, however flow through the mountain-block has not yet been attempted. Previously a study modeling the flow through the mountain-block would not have been feasible, however, with the help of the detailed geologic mapping that was conducted for this study a comprehensive groundwater flow model of the basin and adjacent mountains is possible.

Not included in this report is the potential impact of the closure of Bonito Lake in 2012. Prior to the Little Bear Fire that led to its closure, Alamogordo was receiving 20% of its water from the lake. An increased dependence (albeit temporarily) on groundwater, as a result of the closure of Bonito Lake, will likely lead to a decline in the water table. As result, continued water level monitoring will be crucial to observe future groundwater depletion. With the city's increased dependence on local groundwater, community outreach relating to water conservation is highly encouraged.

PROJECT PERSONNEL AND ACKNOWLEDGEMENTS

PROJECT PERSONNEL

Stacy Timmons, M.S., Interim Aquifer Mapping Program Manager, NMBGMR, stacyt@nmbg.nmt.edu
Talon Newton, Ph.D., Hydrogeologist, NMBGMR, talon@nmbg.nmt.edu
Ethan Mamer, M.S., Hydrogeologist, NMBGMR, emamer@nmbg.nmt.edu
Geoffrey Rawling, Ph.D., Field geologist, NMBGMR, geoff@nmbg.nmt.edu
J. Michael Timmons, Ph.D., Deputy Director for Mapping Programs, NMBGMR, mtimmons@nmbg.nmt.edu

GEOLOGIC MAPPERS

Dan Koning, M.S., Field Geologist, NMBGMR, dkoning@nmbg.nmt.edu
Shari Kelley, Ph.D., Sr. Geophysicist, Field Geologist, NMBGMR, sakelley@nmbg.nmt.edu
Bruce Allen, Ph.D., Sr. Field Geologist NMBGMR, allenb@nmbg.nmt.edu
Colin Cicoski, M.S., Field geologist, NMBGMR, Brown and Caldwell, Boise, ID
Fraser Goff, Ph.D., Department of Earth and Environmental Science, New Mexico Tech, candf@swcp.com
Kate Zeigler, Ph.D., Field geologist, Zeigler Geologic Consulting, LLC., zeiglergeo@gmail.com

SUPPORT PERSONNEL

Brigitte Felix, Report Production Coordinator/GIS Specialist, NMBGMR, bfk@nmbg.nmt.edu
Bonnie Frey, M.S., Chemistry Lab Manager, Geochemist, NMBGMR, bfrey@nmbg.nmt.edu
Cathie Eisen, Hydrologic Technician

ACKNOWLEDGMENTS

Within the southern Sacramento Mountains, Sierra Blanca region and Tularosa Basin area, we have had the opportunity to work with many kind residents who have graciously provided access to their property, wells and springs. These locations provided crucial data for our study and interpretations, and without naming names, we would like to thank each of them. Support on multiple levels (i.e., funding, outreach, interest) from the Otero Soil and Water Conservation District, especially with help from Vicky Milne, greatly furthered the dataset and products of this study.

The many fine products from this study were supported by the New Mexico Bureau of Geology and Mineral Resources, at New Mexico Tech, through the Aquifer Mapping Program and the National Cooperative Geologic Mapping Program (STATEMAP). Reviews of this particular report provided by Geoff Rawling and Lewis Land were useful and appreciated. We also wish to acknowledge and thank Bonnie Frey and Dustin Baca for the water chemistry analysis at the NM Bureau of Geology. Andrew Campbell and his stable isotope laboratory provided high quality data used in this report, as well as the University of Miami Tritium Laboratory, Beta Analytic, Inc., and the University of Utah Dissolved and Noble Gas Laboratory.

RELATED PRODUCTS

- Allen, B.; Koning, D.; Frechette, J.; Kelley, S., 2008, Preliminary geologic map of the Sabinata Flat quadrangle, Otero County, New Mexico, New Mexico Bureau Geology Mineral Resources, Open-file Geologic Map, v. OF-GM 184, pp. 1:24,000.
- Cikoski, Colin T.; Koning, Daniel J.; Kelley, Shari A.; Zeigler, Kate E., 2011, Geologic map of the Church Mountain quadrangle, Sandoval County, New Mexico, New Mexico Bureau Geology Mineral Resources, Open-file Geologic Map, v. OF-GM 215
- Goff, Fraser; Kelley, Shari A.; Lawrence, John R.; Cikoski, Colin T.; Krier, Donothan; Goff, Cathy J.; McLemore, Virginia T., 2011, Geologic map of the Nogal Peak quadrangle, Lincoln and Otero counties, New Mexico, New Mexico Bureau Geology Mineral Resources, Open-file Geologic Map, v. OF-GM 134
- Kelley, Shari; Kempter, Kirt, 2008, Geologic map of the Cat Mountain quadrangle, Otero County, New Mexico, New Mexico Bureau Geology Mineral Resources, Open-file Geologic Map, v. OF-GM 183, pp. 1:24,000.
- Kelley, S.A., Koning, D.J., and Allen, B., 2014, Preliminary Geologic Map of the Tularosa and Bent Region, northeastern Tularosa Basin, Otero County, New Mexico: New Mexico Bureau of Geology and Mineral Resources, Open-file Report 563.
- Koning, Daniel J., 2009, Preliminary geologic map of the Three Rivers quadrangle, Otero County, New Mexico, New Mexico Bureau Geology Mineral Resources, Open-file Geologic Map, v. OF-GM 187, pp. 1:24000.
- Koning, D.J., 2010, Comparison of alluvial fan geomorphology, sedimentation, and erosion along the eastern margin of the Tularosa Basin, New Mexico (abs.), in: New Mexico Geological Society, 2010 Annual Spring Meeting, April 16, Abstracts with Programs, New Mexico Institute Mining and Technology, Socorro, New Mexico, New Mexico Geology, v. 32, no. 2, pp. 60.
- Koning, Daniel J., 2010, Preliminary geologic map of the Carrizozo East quadrangle, Lincoln County, New Mexico, New Mexico Bureau Geology Mineral Resources, Open-file Geologic Map, v. OF-GM 211
- Koning, Daniel J., 2010, Preliminary geologic map of the Oscura quadrangle, Lincoln and Otero Counties, New Mexico, New Mexico Bureau Geology Mineral Resources, Open-file Geologic Map, v. OF-GM 198, pp. 1:24000.
- Koning, Daniel J.; Frechette, Jed, 2008, Geologic map of the Tularosa quadrangle, Otero County, New Mexico, New Mexico Bureau Geology Mineral Resources, Open-file Geologic Map, v. OF-GM 179, pp. 1:24000.
- Koning, Daniel J.; Kelley, Shari A., 2008, Preliminary geologic map of the Tularosa NE quadrangle, Otero County, New Mexico, New Mexico Bureau Geology Mineral Resources, Open-file Geologic Map, v. OF-GM 185, pp. 1:24,000.
- Koning, Daniel J.; Kempter, Kurt A.; Zeigler, Kate E.; Cikoski, Colin, 2011, Geologic map of the Cub Mountain quadrangle, Lincoln County, New Mexico, New Mexico Bureau Geology Mineral Resources, Open-file Geologic Map, v. OF-GM 138
- Koning, Daniel; Cikoski, Colin; Kempter, Kirt, 2012, Preliminary geologic map of the Carrizozo area, Lincoln County, NM, New Mexico Bureau Geology Mineral Resources, Open-file Report, v. 0548, pp. 3.
- Koning, D.J., Kelley, S.A., and Goff, F., 2014, Preliminary Geologic Map of the Northeastern Tularosa Basin and Western Sierra Blanca Basin, Lincoln and Otero Counties, New Mexico: New Mexico Bureau of Geology and Mineral Resources, Open-file Report 564.
- Mamer, Ethan A.; Newton, B. Talon; Timmons, Stacy; Koning, Daniel J.; Land, Lewis A., 2014, Recharging the Tularosa Basin, in: New Mexico Geological Society, Annual Spring Meeting, April 11, 2014, Macey Center, New Mexico Institute Mining Technology, Socorro, NM,
- Rawling, Geoffrey C., 2011, Geology of the Capitan and Nogal quadrangles, Lincoln County, New Mexico, New Mexico Bureau Geology Mineral Resources, Open-file Report, v. 0538
- Rawling, Geoffrey, 2010, Geologic map of the Nogal quadrangle, Lincoln County, New Mexico, New Mexico Bureau Geology Mineral Resources, Open-file Geologic Map, v. OF-GM 195, pp. 1:24000.
- Rawling, Geoffrey; Koning, Daniel, 2011, Geologic map of the White Oaks South quadrangle, Lincoln County, New Mexico, New Mexico Bureau Geology Mineral Resources, Open-file Geologic Map, v. OF-GM 216, pp. 1:24000.
- Zeigler, Kate; Allen, Bruce, 2010, Geologic map of the Bull Gap quadrangle, Lincoln County, New Mexico, New Mexico Bureau Geology Mineral Resources, Open-file Geologic Map, v. OF-GM 210
- Zeigler, K. E.; Allen, B. D., 2012, A preliminary geologic map of the Bull Gap quadrangle, Lincoln County, southeastern New Mexico, in: New Mexico Geological Society, 2012 Annual Spring Meeting, April 27th, Socorro, NM, New Mexico Geology, v. 34, no. 2, pp. 57.

REFERENCES

- Ahrens, and C. Donald, 2003, An introduction to Weather, Climate, and the Environment, Meteorology Today, 7th Edition, Thompson Learning, Inc.
- Allen, M.S. and Foord, E.E., 1991, Geological, geochemical and isotopic characteristics of the Lincoln County porphyry belt, New Mexico: Implications for regional tectonics and mineral deposits, *in* Barker, J.M., Kues, B.S., Austin, G.S., and Lucas, S.G., eds., *Geology of the Sierra Blanca, Sacramento and Capitan Ranges, New Mexico*: New Mexico Geological Society, 42nd Annual Field Conference Guidebook, p. 97–113.
- Arkell, B.W., 1983, *Geology and coal resources of the Cub Mountain area, Sierra Blanca coal field, New Mexico* [Masters Thesis]: Socorro, NM, New Mexico Institute of Mining and Technology, 104 p.
- Bodine, M.W., Jr., 1956, *Geology of Capitan coal field, Lincoln County, New Mexico*: New Mexico Bureau of Mines and Mineral Resources, Circular 35, 27 p.
- Busenberg, E., and Plummer, L.N., 2006, Potential use of other atmospheric gases. In *Use of chlorofluorocarbons in hydrology: A guidebook*.
- Cather, S.M., 1991, Stratigraphy and provenance of Upper Cretaceous and Paleogene strata of the western Sierra Blanca basin, New Mexico, *in* Barker, J.M., Kues, B.S., Austin, G.S., Lucas, S.G., eds., *Geology of the Sierra Blanca, Sacramento and Capitan Ranges, New Mexico*: New Mexico Geological Society, 42nd Annual Field Conference Guidebook, p. 265–275.
- Clark, I., and Fritz, P., 1997, *Environmental Isotopes in Hydrogeology*, Lewis Publishers, New York
- Craig, H., 1961, Isotopic Variations in Meteoric Waters, *Science*, Vol. 133, p. 3702–3703.
- Darton, N.H., 1922, *Geologic structure of parts of New Mexico*: U.S. Geological Survey, Bulletin 726-E, p. 173–275.
- Eastoe, C.J., and Rodney, R., 2014, Isotopes as tracers of water origin in and near a regional carbonate aquifer: The Southern Sacramento Mountains, New Mexico. *Water*, 6(2), 301–323.
- Embid, E.H., and Finch, S.T., 2011. *White Sands National Monument Inventory of Water Rights and groundwater Evaluation Data*. John Shomaker & Associates, Inc. Report prepared for White Sands National Monument.
- Finch, S.T., 2001, Hydrogeologic evaluation of T-255 et al., near Carrizozo, NM: JSAI.
- Garza, S., and McLean, J.S., 1977, *Fresh-water resources, southeastern part Tularosa Basin*: New Mexico State Engineer Technical Report 40
- Gochis, D.J., and Higgins, W.R., 2007, The Path to Improving Predictions of the North American Monsoon: *U.S. Clivar*, v. 5, no. 1.
- Han, L.F., Pang, Z. and Groening, M., 2001, Study of groundwater mixing using CFC data: *Science in China* 44: 21–28
- Harrington, M.W., 1885, *Lost Rivers*: Science, New Series, vol. 6, No. 138, p. 265–266.
- Healy, D.L., Wahl, R.R., and Currey, F.E., 1978, *Gravity survey of the Tularosa Valley and adjacent areas, New Mexico*: U.S. Geological Survey, Open-file Report 78–209, 37 p. and 4 plates.
- Herrick, C.L., 1900, The geology of the White Sands of New Mexico: *Journal of Geology*, vol. 8, p. 112–128.
- Herrick, C.L., 1904, Lake Otero, an ancient salt lake basin in southeastern New Mexico: *American Geologist*, vol. 34, p. 174–189.
- Hood, J. W., and Waddell, K.M., 1968, Hydrologic reconnaissance of Skull Valley, Tooele County, Utah: State of Utah Department of Natural Resources, Technical Publication 18: p. 57
- Hounslow, A.W., 1995, *Water quality data analysis and interpretation*, Lewis Publishers, Boca Raton.
- Huff, G.F., 2004, Simulation of ground-water flow in the basin-fill aquifer of the Tularosa Basin, South-Central New Mexico, predevelopment through 2040: U.S. Geological survey, Scientific Investigations Report 2004–5197.
- Jankowski, J., Acworth, R.I., and Shekarforoush, S., 1998, Reverse ion-exchange in deeply weathered porphyritic dacite fractured aquifer system, Yass. In New South Wales Australia. In: Arehart GB, Hulston JR (eds) *Proceedings of 9th international symposium on water-rock interaction, Taupo, New Zealand* (Vol. 30, pp. 243–246).
- Kelley, V.C., and Thompson, T.B., 1964, Tectonics and general geology of the Ruidoso-Carrizozo region, central New Mexico, *in* Ash, S.R., and Davis, L.V., eds., *Ruidoso Country: New Mexico Geological Society, 15th Annual Field Conference Guidebook*, p. 110–121 NO REF (p. 6, l. 22) Thompson, 1964
- Kelley, V.C., 1971, *Geology of the Pecos country, southeastern New Mexico*: New Mexico Bureau of Mines and Mineral Resources, Memoir 24, 77 p. and 7 plates.
- Kelley, S., Koning, D.J., and Allen, B., 2014, Preliminary geologic map of the Tularosa and Bent region, northeastern Tularosa Basin, Otero County, New Mexico: NMBGMR, Open-file report 564
- Kelley, S.A., Koning, D.J., Goff, F., Cikoski, C., Peters, L., and McIntosh, W., in press, Stratigraphy of the northwestern Sierra Blanca volcanic field: *New Mexico Geological Society Guidebook, 65th Annual Field Conference*.
- Koning, D.J., 1999, Fault segmentation and paleoseismicity of the southern Alamogordo fault, southern Rio Grande rift, New Mexico: Albuquerque, University of New Mexico, 286 p.
- Koning, D.J., Grauch, V.J.S., Connell, S.D., Ferguson, J., McIntosh, W., Slate, J.L., Wan, E., and Baldrige, W.S., 2013, Structure and tectonic evolution of the eastern Española Basin, Rio Grande rift, north-central New Mexico, *in* Hudson, M., and Grauch, V.J.S., eds., *New Perspectives on the Rio Grande rift: From Tectonics to Groundwater*: Geological Society of America, Special Paper 494, p. 185–219, doi:10.1130/2013.2494(08).
- Koning, D.J., Kelly, S., and Goff, F., 2014, Preliminary geologic map of the northeastern Tularosa Basin and western Sierra Blanca Basin, Lincoln and Otero Counties, New Mexico: NMBGMR, Open-file report 563
- Land, L., Felix, B., and Newton, B.T., 2014, *Regional Water Table Map of the Northeastern Tularosa Basin region, Otero and Lincoln Counties, New Mexico*: NMBGMR, Open-file report 561, scale 1:100,000.

- Liebmann, B., Blade, I., Bond, N.A., Gochis, D., Allured, D., and Bates, G. T., 2008, Characteristics of North American Summer-time Rainfall with Emphasis on the Monsoon: *Journal of Climate* v. 21, p.1277–1294
- Livingston and Shomaker, 2006, City of Alamogordo 40-Year Water Development Plan 2005– 2045: Consultant's Report prepared for the City of Alamogordo, 56 pp.
- Long, A., Sawyer, J. and Putnam, L., 2008, Environmental tracers as indicators of karst conduits in groundwater in South Dakota, USA, *Hydrogeology Journal*, v. 16, p. 263–280.
- Lozinsky, R.P., and Bauer, P.W., 1991, Structure and basin-fill units of the Tularosa Basin: *New Mexico Geological Society Guidebook* 42.
- Lucas, S.G., Cather, S.M., Sealey, P., and Hutchison, J.H., 1989, Stratigraphy, paleontology, and depositional systems of the Eocene Cub Mountain Formation, Lincoln County, New Mexico—a preliminary report: *New Mexico Geology*, v. 11, p. 11–17.
- Lucas, S.G., 1991, Triassic stratigraphy, paleontology and correlation, south-central New Mexico, *in* Barker, J.M., Kues, B.S., Austin, G.S., Lucas, S.G., eds., *Geology of the Sierra Blanca, Sacramento and Capitan Ranges, New Mexico*: New Mexico Geological Society, 42nd Annual Field Conference Guidebook, p. 243–259.
- MacBride, T.H., 1905, *The Alamogordo Desert: Science*, New Series, vol. 21, no. 525, p. 90–97
- Malm, N. R., 2003, *Climate Guide Las Cruces, 1892–2000*, New Mexico Agricultural Experimental Station Research Report 749.
- Mazor, E. and Nativ, R., 1992, Hydraulic calculation of groundwater flow velocity and age: Examination of the basic premises: *Journal of Hydrology* 138: 211–222
- McLean, J.S., 1970, Saline Ground-water resources of the Tularosa Basin, New Mexico, USGS OSW Report No. 561.
- Meinzer, O.E., and Hare, R.E., 1915, Geology and water resources of the Tularosa Basin, New Mexico: U.S. Geological Survey Water-Supply Paper 489, 317 p.
- Moore, S.L., Foord, E.E., Meyer, G.A., and Smith, G.W., 1988a, Geologic map of the northwestern part of the Mescalero Apache Indian Reservation, Otero County, New Mexico: U.S. Geological Survey, Miscellaneous Investigations Map I-1895, 1:24,000 scale, color.
- Moore, S.L., Foord, E.E., and Meyer, G.A., 1988b, Geologic and aeromagnetic map of a part of the Mescalero Apache Indian Reservation, Otero County, New Mexico: U.S. Geological Survey, Miscellaneous Investigations Series Map I-1775, scale 1:50,000.
- Moore, S.L., Thompson, T.B., and Foord, E.E., 1991, Structure and igneous rocks of the Ruidoso region, New Mexico, *in* Barker, J.M., Kues, B.S., Austin, G.S., Lucas, S.G., eds., *Geology of the Sierra Blanca, Sacramento and Capitan Ranges, New Mexico*: New Mexico Geological Society, 42nd Annual Field Conference Guidebook, p. 137–145 NO REF (p. 7, l. 7) Allen and Foord (1991)
- Morrison, T.D., 1989, A regional model of the basin-fill aquifer near Tularosa and Alamogordo, New Mexico: New Mexico State Engineer Office Technical Division Hydrology Report 89–3, 71 p. plus app.
- National Weather Service Forecast Office, n.d. a, The North American Monsoon: http://www.wrh.noaa.gov/twc/monsoon/monsoon_info.php (May 2010).
- National Weather Service Climate Prediction Center, 2003, “Reports to the Nation: The North American Monsoon”, http://www.cpc.noaa.gov/products/outreach/Report-to-the-Nation-Monsoon_aug04.pdf
- National Weather Service Southern Region Headquarters, 2006, Special Feature: The North American Monsoon. <http://www.srh.noaa.gov/abq/climate/Monthlyreports/July/nams.htm>.
- Newton, B.T., Rawling, G. C., Timmons, S. S., Land, L., Johnson, P.S., Kludt, T. J., and Timmons, J. M., 2012, Sacramento Mountains hydrogeology study: NMBGMR, Open-file report 543
- Orr, B.R., and Meyers, R.G., 1986, Water resources in basin-fill deposits in the Tularosa basin, New Mexico: U.S. Geological Survey, Water Resources Investigations Report 85–4219, 94 p.
- Otte, C., 1959, Late Pennsylvanian and early Permian stratigraphy of the northern Sacramento Mountains, Otero County, New Mexico: NMBGMR, Bulletin 50, 111 p. and 14 plates.
- Pertl, D.J., and Cepeda, J.C., 1991, The Carrizo Mountain stock and associated intrusions, Lincoln County, New Mexico, *in* Barker, J.M., Kues, B.S., Austin, G.S., Lucas, S.G., eds., *Geology of the Sierra Blanca, Sacramento and Capitan Ranges, New Mexico*: New Mexico Geological Society, 42nd Annual Field Conference Guidebook, p. 147–152.
- Peterson, C., and Roy, M., 2005, Gravity and flexure models of the San Luis, Albuquerque, and Tularosa basins in the Rio Grande rift, New Mexico, and southern Colorado, *in* Lucas, S.G., Zeigler, K.E., Lueth, V.W., and Owen, D.E., eds., *Geology of the Chama Basin*: New Mexico Geological Society, 56th Annual Field Conference, p. 105–114.
- Plummer, L. N., Busenberg, E., and Han, L., 2006, CFCs in binary mixtures of young and old groundwater, in *Use of Chlorofluorocarbons in Hydrology: A Guidebook*, International Atomic Energy Agency, Vienna, p. 59–72.
- Pray, L.C., 1952, Stratigraphy of the escarpment of the Sacramento Mountains, Otero County, New Mexico [unpublished dissertation]: Pasadena, California Institute of Technology, 370 p.
- Pray, L.C., 1961, Geology of the Sacramento Mountains escarpment, Otero County, New Mexico: New Mexico Bureau of Mines and Mineral Resources, Bulletin 35, 144 p. and 3 plates.
- Rau, B., 1986, Ground-water resources in the Carrizozo Area, NM: New Mexico Geological Society Guidebook, 37th Field Conference, Truth or Consequences, pp 315.
- Rawling, G.C., 2012, Geology of the southern Sacramento Mountains, Otero and Chaves Counties, New Mexico, Geological Society of America Abstracts with Programs, Vol. 44, No. 6, p. 12.
- Rawling, G.C., 2009, Geology of the Ruidoso area, Lincoln and Otero Counties, New Mexico: NMBGMR, Open-file Report 507, scale 1:24,000.
- Rawling, G.C., 2011, Geology of the Capitan and Nogal quadrangles, Lincoln County, New Mexico: NMBGMR, Open-file Report 538, scale 1:24,000.
- Ritchie, E., Wood, K., White, S., and Gutzler, D., 2007, The Impact of Tropical Cyclone Remnants on the Rainfall of the North American Southwest Region, Paper presented at the 28th Conference on Hurricanes and Tropical Meteorology, Orlando, FL.
- Ritchie, E. and Szenasi, D., 2006, The Impact of Tropical Cyclone Remnants on the Rainfall of the North American Southwest Region, Paper presented at the 27th Conference on Hurricanes and Tropical Meteorology, Monterey, CA.
- Rozanski, K., Araguas, L., and Gonfiantini, R., 1993, Isotopic Patterns in Modern Global Precipitation, *in* Swart, P. K., Lohmann, K. C., McKenzie, J., Savin, S. (eds.), *Climate Change in Continental Isotopic Records*: American Geophysical Union, Geophysical Monograph 78, p.1–36.
- Speer, S.W., 1983, Abo Formation, north-central Sacramento Mountains: An onlapping fluvial clastic wedge, in *Guidebook for file trip to the Abo red beds (Permian), central and south-central New Mexico*: Roswell Geological Society and the New Mexico Bureau of Mines and Mineral Resources, p. 54–72.

- Stensrud, D.J., Gall, R.L., Mullen, S.L., and Howard, K.W., 1995, Model Climatology of the Mexican Monsoon: *Journal of Climate* v. 8, p.1775–1794.
- Tarr, R.W., 1891, A recent lava flow in New Mexico: *American Naturalist*, vol. 25, p. 524–527.
- Tight, W.G., 1905, Boslon plains of the Southwest: *American Geologist*, vol. 36, p. 271–284.
- Timmons, S.S., Land, L., Newton, B. T., Frey, B., 2013, Aquifer Mapping Program technical documents: water sampling procedures, analysis and systematics: NMBGMR, Open-file Report 558.
- Thompson, T.B., 1966, Geology of the Sierra Blanca, Lincoln and Otero Counties, New Mexico [Ph.D. dissertation]: Albuquerque, University of New Mexico, 146 p.
- Thompson, T.B., 1972, Sierra Blanca Igneous Complex: *Geological Society of America Bulletin*, v. 83, p. 2341–2356.
- Thompson, T.B., 1973. Mineral deposits of Nogal and Bonito mining districts, New Mexico: NMBGMR, Circular 123, 29 p w/color geologic map.
- Thompson, T.B., 1974, Geology and mineral deposits—Sierra Blanca igneous complex: *New Mexico Geological Society Silver Anniversary Guidebook*, 25th Fall Field Conference, p. 379–380.
- Waltemeyer, S.D., 2001, Estimates of mountain-front streamflow available for potential recharge to the Tularosa Basin, New Mexico: U.S. Geological Survey, Water-Resources Investigations Report 01–4013.
- Watson, P., Sinclair, P., and Waggoner, R., 1976, Quantitative evaluation of method for estimating recharge to desert basins of Nevada: *Journal of Hydrology*, 31 (3/4): 335–357
- Weber, R.H., 1964, Geology of the Carrizozo quadrangle, New Mexico, *in* Ash, S.R., and Davis, L.V., eds., *Ruidoso Country: New Mexico Geological Society, 15th Annual Field Conference Guidebook*, p. 100–109.
- Weber, R.H., 1971, K/Ar ages of Tertiary igneous rocks in central and western New Mexico: *Isochron West*, no. 71–1, p. 33–42.
- Wilson, J.L., Guan, H., 2004, Mountain-block hydrology and mountain-front recharge: *Water Science and Application*, 9, 113–137.
- Wegemann, C.H., 1914, Geology and coal resources of the Sierra Blanca coal field, Lincoln and Otero Counties, New Mexico: U.S. Geological Survey, Bulletin 541, p. 419–542.



New Mexico Bureau of Geology and Mineral Resources
A Division of New Mexico Institute of Mining and Technology

Socorro, NM 87801
(575) 835-5490
Fax (575) 835-6333
www.geoinfo.nmt.edu